2011

Guiding Electric Fields for Electroporation Applications

Jose Rey
University of South Florida, jirey@mail.usf.edu

Guiding Electric Fields for Electroporation Applications

by

José I. Rey

A dissertation submitted in partial fulfillment
of the requirements for the degree of
Doctor of Philosophy
Department of Chemical & Biomedical Engineering
College of Engineering
University of South Florida

Major Professor: Richard Gilbert, Ph.D.
Francis Moussy, Ph.D.
J. Anthony Llewellyn, Ph.D.
Mark Jaroszeski, Ph.D.
Richard Heller, Ph.D.
Andrew Hoff, Ph.D.

Date of Approval:
March 25, 2011

Keywords: Implantable Biosensors, Focusing Electric Fields, Biosensor Implantation, Tumor Electrochemistry

Dedication

I entirely dedicate this new achievement to my beloved: mother, father, sister, brother, and wife, for their support, love, advice and words of encouragement.

Acknowledgments

The culmination of this work would not be possible without the guidance, support, and encouraging bestowed by my adviser Dr. Richard Gilbert and main collaborators to the project Dr. Francis Moussy, Dr. Mark J. Jaroszeski, Dr. Andrew Hoff, and Dr. J. Anthony Llewellyn.

I also would like to express my gratitude to:

(a) The National Science Foundation - Integrative Graduate Education and Research Training (NSF-IGERT, DGE-0221681) program. Special gratitude goes to Dr. Shekar Bhansali and Mr. Bernard Batson

(b) Alfred P. Sloan Foundation

(c) Florida Center of Excellence for Biomolecular Identification and Targeted Therapeutics (FCoE-BITT) Seed Grant

(d) My research group and peer graduate students, specially Dr. Richard J. Connolly

(e) Dr. Karl Muffly and his group at the USF College of Medicine.

(f) Dr. Richard Heller, Dr. Loree Heller and their group.

(g) Dr. Francis Moussy and his group, specially Dr. Bazhang Yu and Mr. Leigh West

(h) All Faculty, Staff and Minority programs of USF

(i) To my parents Rodolfo Rey and Martha Rey, my brother, David E. Rey, and my sister Diana A. Rey

(j) And last but not least, to my wife Dr. Jeffy Jiménez

Table of Contents

List of Tables

List of Figures

Abstract

Electroporation is the critical step in an electric field mediated drug or gene delivery protocol. Electroporation based protocols have been successfully demonstrated in cancer clinical trials, however, its impact in other applications is still under investigation. A significant roadblock to long term functioning of implantable biosensors *in vivo* is the tissue reaction in the form of fibrous encapsulation that results in reduced transport to the sensing element of the biosensor. *In vivo* gene electroporation has a great potential as a means to modify the transport properties of tissues in the proximity of the sensing element of implantable biosensors.

This dissertation examines two postulated electroporation based strategies to modify tissue for enhanced performance of an implantable biosensor. In the first, the implantation protocol is modified to accommodate *in vivo* electroporation. In the second strategy, the the modification is applied post implantation. This post-implantation *in vivo* electroporation application requires that electric energy be delivered at the site of electroporation close to the biosensor while minimizing effects far from such site. A novel method, focusing electric fields, developed for this purpose is presented. A theoretical framework as well as *in vitro* and *in vivo* experiments are provided as the introduction to the method and in support of its potential as the basis of a viable technology.

Chapter 1. Prelude

The manuscript before you summarizes my research on the problem presented to me at the start of my doctoral studies. This challenge represents the convergence of two different technologies that were being developed at the University of South Florida (USF, Tampa, FL). The first technology consists of a subcutaneous implantable glucose biosensor being developed at the time by the USF Biosensors and Biomaterials Laboratory, an interdisciplinary team under the direction of Dr. Francis Moussy (currently at the World Health Organization, Switzerland). The second technology, *in vivo* electric field mediated drug and gene delivery, is part of the ongoing technology development work at the USF Center for Molecular Delivery which is led by Dr. Richard Gilbert.

The proposed work was to define requirements for an *in vivo* electroporation protocol capable of delivering therapeutic molecules to tissue surrounding the sensing element of the implantable glucose biosensor. The appropriate therapeutic molecule candidates to be delivered would then be selected to solve a roadblock which is common to many implantable sensing devices: the development of collagenous fibrous encapsulation of the sensing element that impedes the transport of molecules, hence, hindering the functionality of such biosensor, shortening its performance life cycle. In the case of the implantable biosensor, the candidate molecules could be DNA coding for

neovascularization factors such as Vascular Endothelial Growth Factor (VEGF), which have the potential of increasing the transport properties of tissues.

From the early stages of this research project, two research pathways were evident. These pathways originated from the inability to predict the timing of the sequence for biological tissue response events following the implantation of the glucose biosensor. One pathway is to investigate the delivery of therapeutic molecules at the time of implantation of the biosensor. The other approach is to develop a method that increases the effectiveness of delivery of therapeutic molecules in deep tissue that is not in direct contact with the electrodes used to deliver the electric fields.

The body of the work represented in this dissertation advances the knowledgebase needed to solve the interdisciplinary problem associated with the fibrous encapsulation at the glucose biosensor. It demonstrates how electric field mediated gene delivery brings the solution to that problem a step closer by defining a viable tissue engineering application. In addition, the research results provide a wealth of potential technological advancement in the study of *in vivo* electroporation itself, as well as modeling tools and techniques to develop applicable electric field mediated drug and gene delivery protocols to tissue engineering.

Part I

Chapter 2. Literature Review

This review begins with an overview of implantable glucose biosensors to accent the current state of the technology as it relates to this work. Biosensor design, implantation procedure, and tissue reactions to implanted biosensors are presented. Electric field mediated drug and gene delivery is then introduced from a historical perspective with its applications. Finally, tissue engineering applications as they relate to this project are presented.

2.1. Implantable Glucose Biosensor

2.1.1. Glucose Biosensor Design

The implantable glucose biosensor at the core of this project [1] was the subject of intensive development by the "USF Biosensors and Biomaterials Laboratory." The laboratory has led several efforts to improve the function and reliability of the sensor under implanted conditions. This micro-implantable glucose sensor is an amperometric enzyme biosensor that includes a reference electrode and a sensing element. The sensing element is loaded with glucose oxidase and protected by several layers of porous polymeric materials that improve the biosensor's biocompatibility, durability, and sensitivity. The biosensor's sensing element is made of a 0.125 mm diameter platinum-iridium wire coiled around a cotton fiber with glucose oxidase, surrounded by an enzyme layer within a

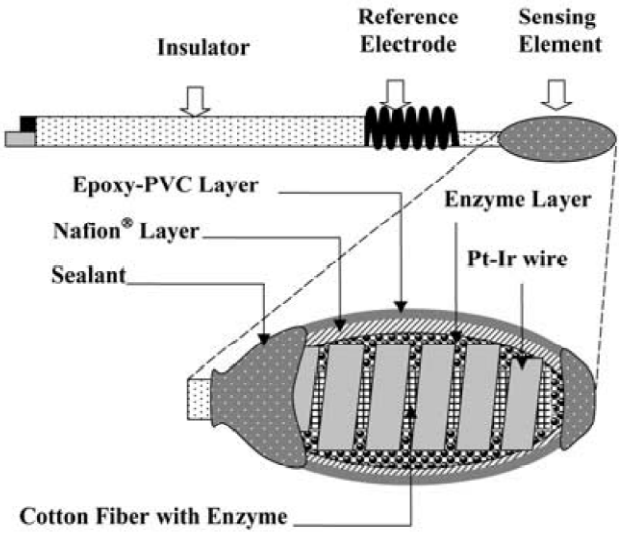

Figure 2.1. Implantable glucose biosensor [2]. Reproduced with permission from Wiley.

Nafion® layer coated with an external Epoxy-PVC layer. This forms a cylindrical element roughly 0.5 mm in diameter by 1 mm long. The reference electrode is 0.125 diameter silver wire coated with Teflon which is about 2 to 4 mm away from the sensing element [2, 3]. Figure 2.1 shows a diagram of the glucose biosensor with a detail of the reference electrode, sensing element, enzyme loaded volume, and protective layers. In this biosensor design, the immobilized glucose oxidase enzyme catalyzes the oxidation of glucose using oxygen to produce gluconoloctone and hydrogen peroxide; the hydrogen peroxide is then measured at the electrode when it oxidizes and produces an electrical current proportional to the oxidized glucose concentration [4].

2.1.2. Implantation Procedure

Preclinical testing of such biosensors has required development of implantation techniques that are adequate to improve sensor survival in animal models, and can potentially be translated to humans when the biosensors are ready for clinical testing [5]. Current efforts to improve the long term function and bio-stability of the implanted biosensor include cross-linked porous scaffolds that surround the sensing element of the biosensor by potentially minimizing tissue reactions while stimulating angiogenesis around the sensing element of the biosensor [6]. The current pre-clinical glucose sensor implantation procedure is designed to test biosensor reliability *in vivo* using Sprague-Dawley (SD) rats. The biosensor is implanted subcutaneously leaving two contacts for electrodes

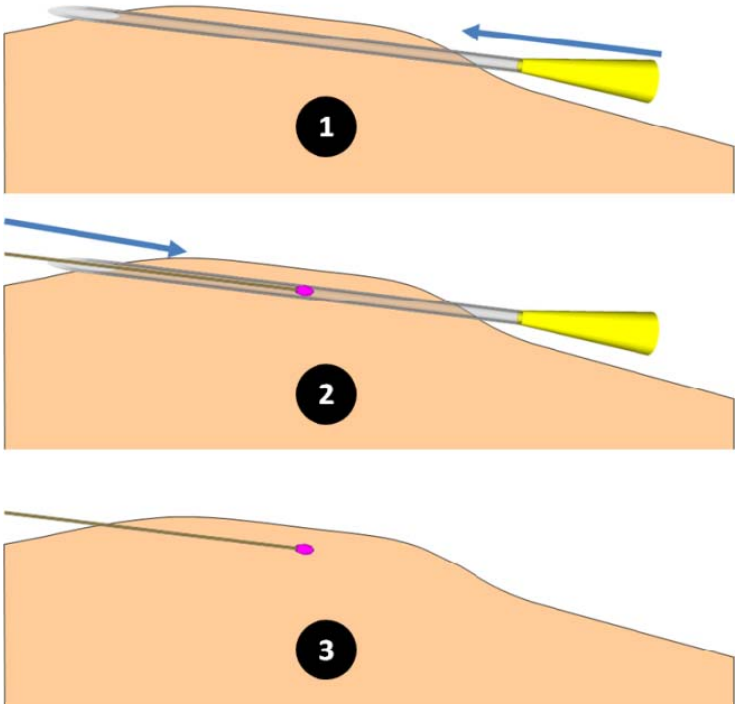

Figure 2.2. Preclinical glucose biosensor implantation procedure.

protruding from the back of the animal. It was designed to simulate a potential clinical use of the biosensor while keeping the practicality of animal testing. The experimental design allows that periodic measurements be made using an external commercial potentiometer.

In the case of the glucose biosensor of interest, the implantation protocol involves the use of a 16 gauge punch needle inserted subcutaneously in which the biosensor is inserted and left in place when the needle is then removed; the technique is designed to immobilize the sensor and reduce complications related to the procedure and post-procedure recuperation [7]. Figure 2.2 shows the initial implantation procedure in which the needle cannula is inserted (1), followed by the insertion of the implantable biosensor in the exiting end of the cannula (2), and removal of the cannula to leave the implantable biosensor in place. The biosensor can be affixed to the tissue using sutures. In clinical applications, the biosensor would not protrude to the exterior, but would use wireless protocols to provide real time glucose data.

2.1.3. Tissue Reactions to Implantable Biosensor

Tissue reactions to implants are dependent on a myriad of factors. These factors include but are not limited to the extent of the injury created at the time of the implantation procedure, characteristics of the animal model, tissues affected, geometry of the implant, materials of the implant, and other characteristics of the implant [8]. In the case of biosensors, such as the glucose biosensor, the tissue reactions have an added complexity that is attributed to the applied potential for

amperometric measurements and production of hydrogen peroxide as a result of the reduction-oxidation reaction.

Chronologically, the response to the implantable glucose sensor starts with the injury caused by the implantation procedure and is followed by blood-material interactions [10]. These responses include a provisional matrix formation, inflammation, granulation of tissue, foreign body reaction, and finally, fibrous encapsulation and loss of vasculature that decreases the transport of glucose and oxygen to the sensing element of the biosensor, resulting in loss of function [9, 11-13]. Figure 2.3 shows a generalization of the temporal variation of such processes including the type of cells and tissue reactions. The migration of neutrophils starts with the inflammation process, and is followed by macrophage migration. Neovascularization allows further migration of foreign body giant cells

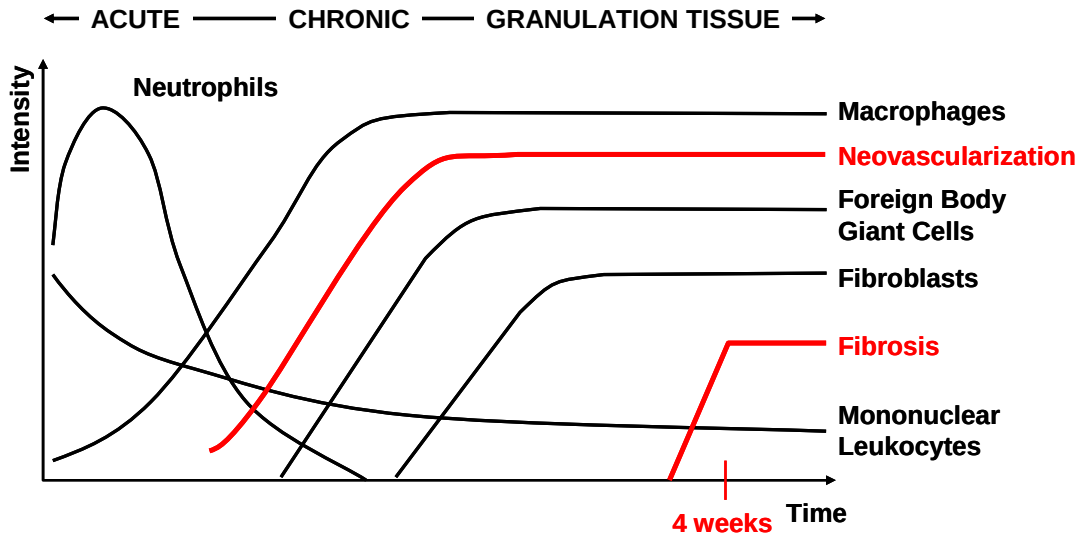

Figure 2.3. Temporal variation in the acute and chronic inflammatory, granulation tissue development, and foreign body response to implanted biosensor. Adapted from Anderson, 2001 [9].

and fibroblasts which are responsible for the fibrous encapsulation. Of particular interest for this project is the fibrosis process, which has an adverse effect in the transport of glucose and oxygen to the sensing element of the implantable biosensor in a matter of weeks. A study by Bazhang Yu et al., performed in 2006 in the former Biosensors and Biomaterials Laboratory at the University of South Florida confirmed that while the glucose biosensor can properly function for 3 to 4 months continuously *in vitro*, when implanted *in vivo*. It generates tissue reactions, as those shown in Figure 2.3, that make it unreliable after 4 weeks post implantation [14].

2.2 Historic Perspective of Electroporation

Historically, electric field mediated drug and gene delivery has been used as an effective method for altering the behavior of targeted biological systems. The developments in the field of electroporation have been achieved gradually, and by different groups working on several applications in parallel. This section introduces a perspective of this technology reflecting its applications, challenges and successes in living systems.

2.2.1. Electroporation as a Transport Mediating Process

Electroporation as a transport enhancement process in biological systems has its beginnings in the early 1960's with the use of electric fields to irreversibly break down cellular components and to extract materials from animal and plant tissues [15]. The direct effect of electric fields on cell membrane permeabilization was characterized in the later years of the 1960's decade in unicellular biological

systems (bacteria, yeast, protoplasts, and suspended mammalian cells) by Hamilton and Sale [16-18]. In the beginning of the 1970's, Neumann et al. [19] proved that cell membranes could be permeabilized reversibly by the application of electric fields to facilitate molecular transport. Nevertheless, the reversibility of the electric field induced permeabilization of the cell membrane was a phenomenon already implicitly understood from experiments in the early 1950's by Hodgkin [20, 21].

2.2.2. Plant Applications

The early research on plant gene electroporation was first reported in protoplasts in 1985 by Fromm et al. [22] and later on intact plant cells by Hiromichi et al. in 1986 [23], directly into leaf tissue of rice plants by Dekeyser et al. in 1990 [24]; and in pollen by Matthews et al. in 1990 [25]. The main application of plant gene electroporation is to produce genetically modified plants by stably transferring genes that confer desired qualities such as disease or pesticide resistance to the next generation of plants [26]. Several strategies with different complexities exist to modify the genome of such plants. In the case of plant cells and tissues, the strategy is to isolate transformed cells and regenerate a complete genetically modified plant from such cells. In a second strategy which circumvents many problems of plant regeneration from pollen, germinating pollen can be genetically modified producing genetically modified plants, or pollen can be transformed before fertilization and then transferred to the stigma of a plant for germination [27].

2.2.3. Animal and Human Cancer Applications

Intensive interest on *in vitro* electric field mediated gene transfer research began in the 1980's with the application of electroporation to mammalian cells by Wong [28], Neumann [29], and Potter [30]. These studies use multiple exponential decay high field pulses (4,000 V/cm to 8,000 V/cm) with relative short duration (5 μs to 25 μs). Such early work in conjunction with the investigations on cell electropermeation by Crowley et al. [31] on electrical breakdown of synthetic lipid membranes, Zimmerman et al. [32] on reversible membrane permeabilization as it applies to electrofusion, and Tessie et al. [33] on bilayer lipid vesicle electroporation, opened the discussion for the first time to the biophysical aspects of gene transfer in cells. Neumann et al. [29] proposed that the mechanism of transmembrane transfer of DNA would be due to either electric field activated transmembrane transport protein, or an unspecified electrobiophysical aspect related to membrane 'defects'.

In humans, electroporation protocols are mainly used for two different types of applications. In one, cell membrane impermeable small molecules such as chemotherapy agents are delivered in cancer applications. In the second application, electroporation is used to deliver genes packaged in plasmid DNA with the purpose of having tissues produce proteins of therapeutic value; most prominent of such application are cancer DNA electroporation. Electrochemotherapy, or the use of anticancer drugs in combination with electroporation was first used in solid tumors and reported animal preclinical trials [34], and human trials [35-39] in the 1990s. In this cancer application of

electroporation, the tumor anticancer effects of chemotherapeutic agents such as bleomycin [34-36, 39] and cisplatin [38] can be greatly increased. Several animal models have been explored including hepatoma of the liver [40, 41], and melanoma among others [42, 43]. *In vivo* gene delivery via an electroporation mechanism holds promising applications in cancer treatment, as it is an effective way to deliver therapeutic genes to accessible tumors with the purpose of producing a therapeutic proteins such as those in the Interleukin family [41, 44]. The culmination of these investigations has resulted in Phase I clinical trials that demonstrated its safety and generated data paving the way for the use of electric field mediated gene delivery as a potential treatment for metastatic melanoma [45].

2.2.4. Tissue Engineering Applications

Tissue engineering via gene delivery to functionalize tissues has been used for a variety of applications that involve transplanted and host cells. Applications that use transplanted cells are divided into three classes. The first one, called autografts, involve the same individual's cells from a different site. The second, allografts involve cells from the same species but a different individual. The third class of transplant is xenografts, which involve cells or tissues from a different species. Additionally, applications that use host cells can involve tissue scaffolds that allow migration, or can involve the cells within tissue that are modified *in situ*.

Specifically in the case of implantable biosensors, two studies that use neovascularization genes are worth highlighting. In the first, the use of *ex vivo*

gene therapy showed encouraging results by allowing the improvement of the functioning of a glucose biosensor in a chicken embryo model by the introduction of a gene coding for vascular endothelial growth factor (VEGF), into chicken fibroblast cells, which then were transplanted into a chicken embryo chorioallantoic membrane (CAM) [46]. This approach used retroviral gene delivery, which might not be the optimal method for the demands of the biosensor application due to safety reasons among others. In another application, a micro osmotic infusion pump was used to deliver VEGF protein during 28 days to create neovascularization with the purpose of improving a glucose biosensor's function [47].

Electroporation is an effective method in any of these strategies, on either cells or tissues, and at any step of the processes. Cells in tissues are functionalized by electroinserting DNA coding for biologically relevant proteins, or directly functional RNA such as messanger RNA (mRNA) [48] and interference RNA (iRNA) [49]. *In vivo* electroporation has been used effectively in several tissue engineering applications to modify tissue function. In one, Kishimoto et al. 2002 [50] generated ectopic bone formation in mouse muscle tissue using bone morphogenetic proteins (BMP) in specific, electroporating a plasmid coding for BMP-4 gene. In another tissue engineering application, this time relevant to wound healing, Ferraro et al. 2009 delivered a plasmid coding for VEGF to rat skin flaps promoting neovascularization and thus improving wound healing by reducing ischemia and tissue necrosis [51].

Chapter 3. Materials and Methods

3.1. Gene Electroporation Experiments

3.1.1. *In Vivo* Gene Electroporation Protocol

This protocol effectively modifies the implantation procedure developed by the USF Biosensors and Biomaterials Laboratory [3]. It adapts the procedure to add *in vivo* gene electroporation. Electric field parameters were selected based on previous experience and simulation results (COMSOL Multiphysics, Comsol Inc., Los Angeles, CA). The cannula used in the implantation protocol is also used as one of the electrodes to apply the electric field.

Figure 3.1 shows a photograph of the surface electrode and the cannula electrode. The photograph shown in Figure 3.1a is a close-up of the two electrodes positioned in proximity one to the other in a similar fashion as they were positioned *in vivo*. The image in Figure 3.1b shows the two electrodes separately. The cannula electrode consists of a 14 gauge 2" long commercially available Surflo® I.V. catheter (Terumo Medical Products, Somerset, NJ) attached to a handle providing an electrical contact. The curvature of the surface electrode was derived from measurements performed on animal cadavers using the same cannula electrode below the animal skin at the same anatomical location of the implantation site. From these measurements, the thickness of the

skin from the cannula location to the surface was determined to be 1.7 mm at the site of implantation.

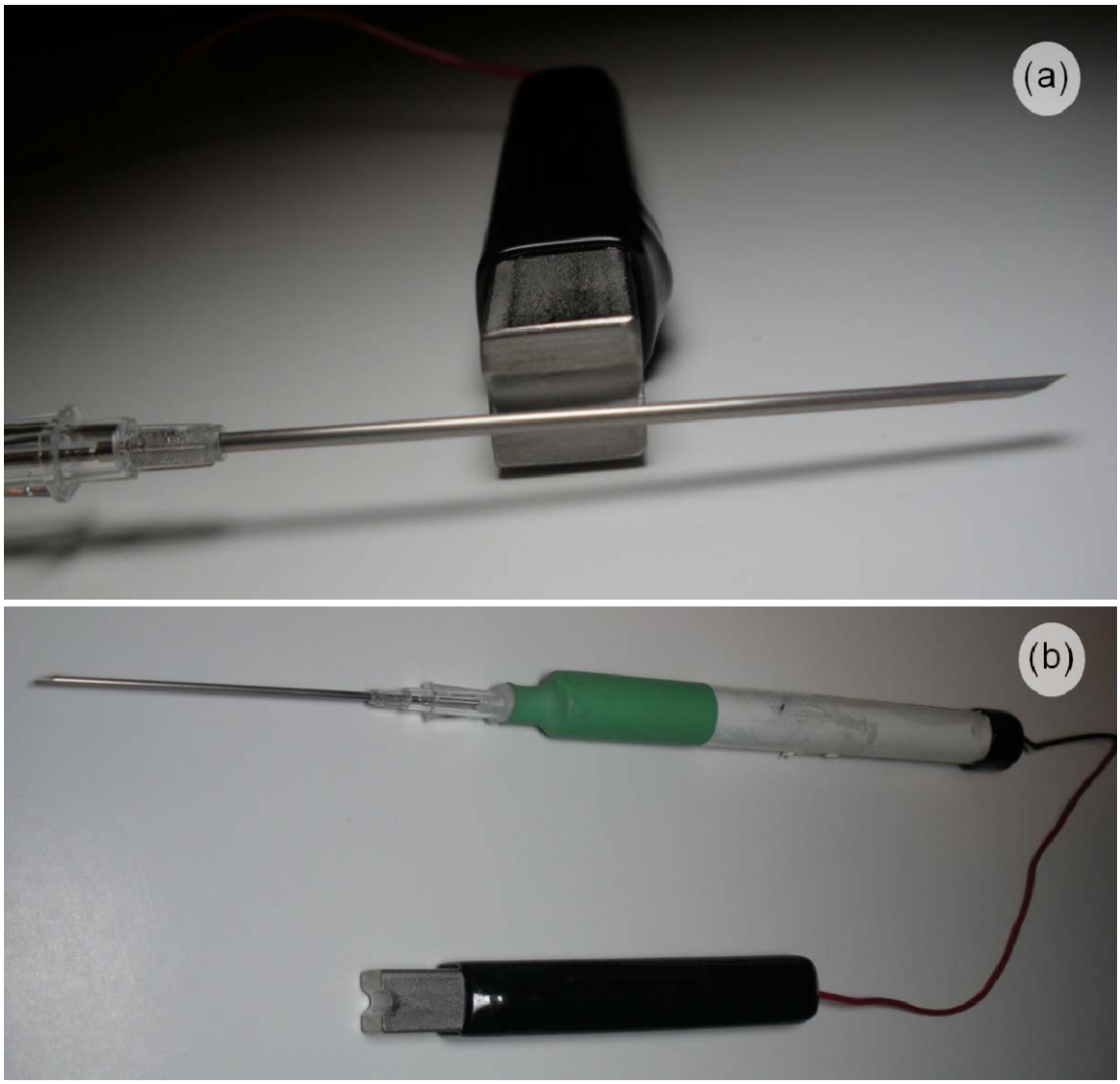

Figure 3.1. Cannula electrode and surface electrode applicators used in implantable biosensor electroporation. Permission from the Center for Molecular Delivery.

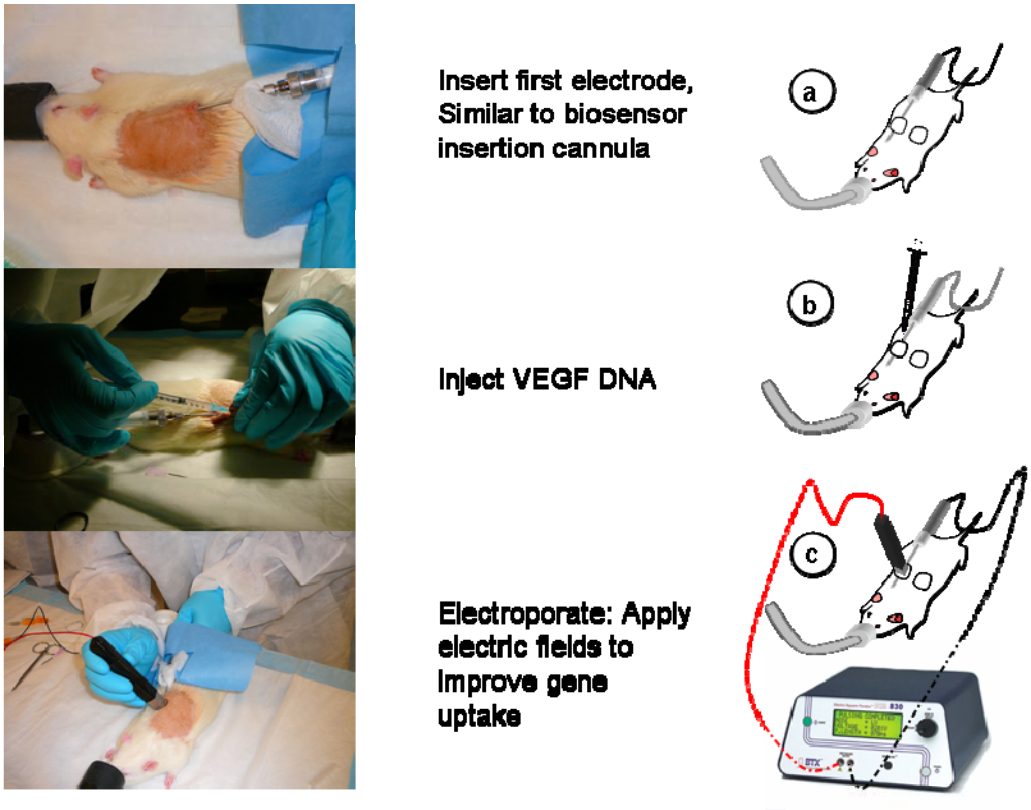

Figure 3.2. *In vivo* gene electroporation procedure. Permission from the Center for Molecular Delivery.

The plasmid construct selected for this study was gWIZ Luciferase (Aldevron, Fargo, ND). The map for this plasmid is shown in Figure 3.3. The construct contains a modified human cytomegalovirus virus (CMV) promoter for increased protein expression in mammalian systems. The promoter site is located between the NdeI-183 and SalI-1874 restriction endonuclease cutting sites. The coding region of the plasmid contains a firefly gene that expresses luciferase protein and is located between the SalI-1874 and BamHI-3590 restriction enzyme cutting sites. When used in this protocol, and if expressed *in*

vivo, the gene results in firefly luciferase protein. The detection of this expression is explained in detail in the next subsection.

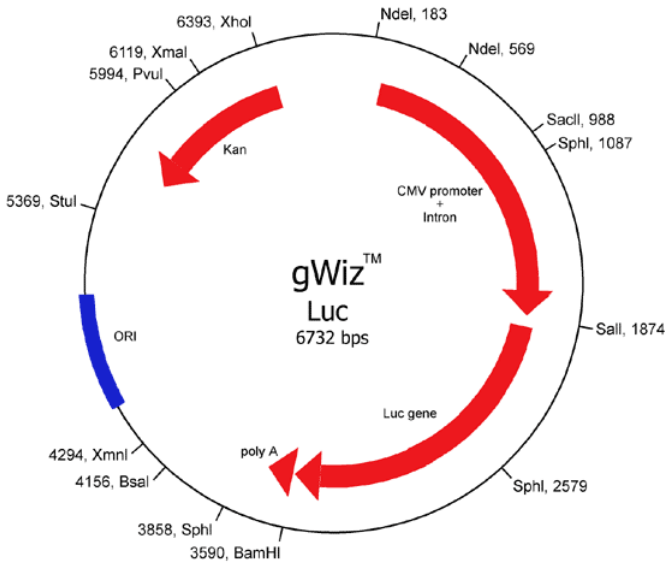

Figure 3.3. Luciferase plasmid used to deliver tracer gene, gWIZ Luc. Source Aldevron, Fargo, ND.

3.1.2. *In Vivo* Bioluminescent Imaging

In vivo biolumninescent imaging was used as a tool to measure Luciferase gene expression from the tracer gene study. This method was first reported as used for *in vivo* electroporation in 2001 by Honigman et al. using *in vivo* bioluminescent detection by charge coupled device (CCD) camera to detect Luciferase expression [52]. The imaging procedure follows. At 0 (before electroporation), 1, 4, 8, 15, and 22 days, animals were injected with 150 µg of D-luciferin (Xenogen Corporation, Hopkinton, MA) per gram of body weight in saline solution and images were acquired using a cooled CCD camera (IVIS 200,

Xenogen Corporation). Images were analyzed and bioluminescence quantified using photonics information based analysis software (Living Image, Xenogen Corporation). The quantification was executed using circular regions of interest. Results were then statistically analyzed using Student's t-test.

Figure 3.4 shows a representation of the *in vivo* imaging protocol. The top panel shows the reaction in which luciferase expressing protein oxidizes the luciferin substrate producing oxyluciferin and a photon. The photograph below is a superposition of the light image of a rat with two electroporated sites producing light. The pseudocoloring represents the photon flux with red being the highest emission and blue the lowest level. The panel to the right shows the

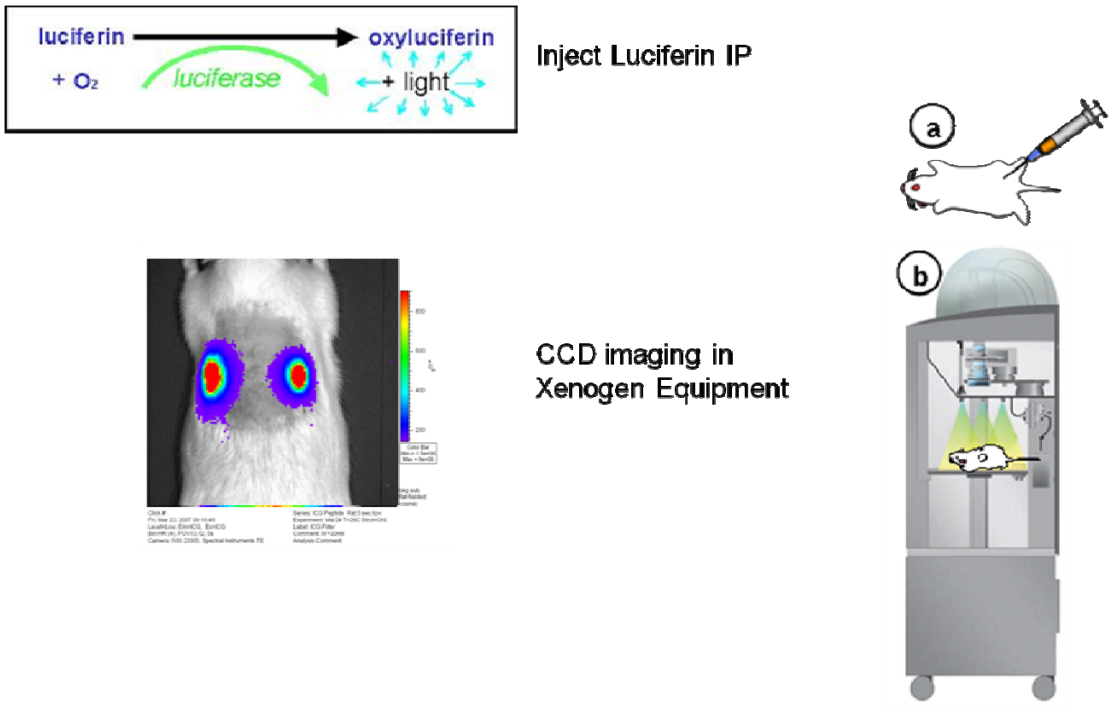

Figure 3.4. *In vivo* imaging protocol. Permission from the Center for Molecular Delivery.

intraperitonial injection of luciferin substrate (Figure 3.4a), and a representation of the rat imaging within the Xenogen IVIS system.

3.2. Electric Field Focusing Experiments

3.2.1. *In Vitro* Electric Field Focusing Experiments

Cells cultured for *in vitro* experiments were B16F10 adherent murine melanoma cells (ATCC CRL6475, American Type Culture Collection, Manassas, VA). The culture medium used for B16F10 cells is McCoy's 5A (Mediatech, Manassas, VA) medium with 10% fetal calf serum and 90 μg/ml of gentamicin sufate (Mediatech) as antibiotic. Culture previous to experiments is done in an incubator at 37ºC and 5% CO_2. The cells were detached from culture flasks using trypsin EDTA (Mediatech) and placed in 60mm culture dishes (Culture surface of 20cm^2). The cell density used for *in vitro* experiments was of 204,000 cells/cm^2, which corresponds to about 4 million cells per each 60mm culture dish. Cells are cultured for 18 hours in dishes and wells to assure cell attachment to the bottom of the culture dish. Calcein ($C_{30}H_{26}N_2O_{13}$, Sigma-Aldrich, Inc., St. Louis, MO) was used as a fluorescent tracer molecule. Calcein is a membrane impermeable molecule that will effectively enter cells after the cells have been exposed to an electric field.

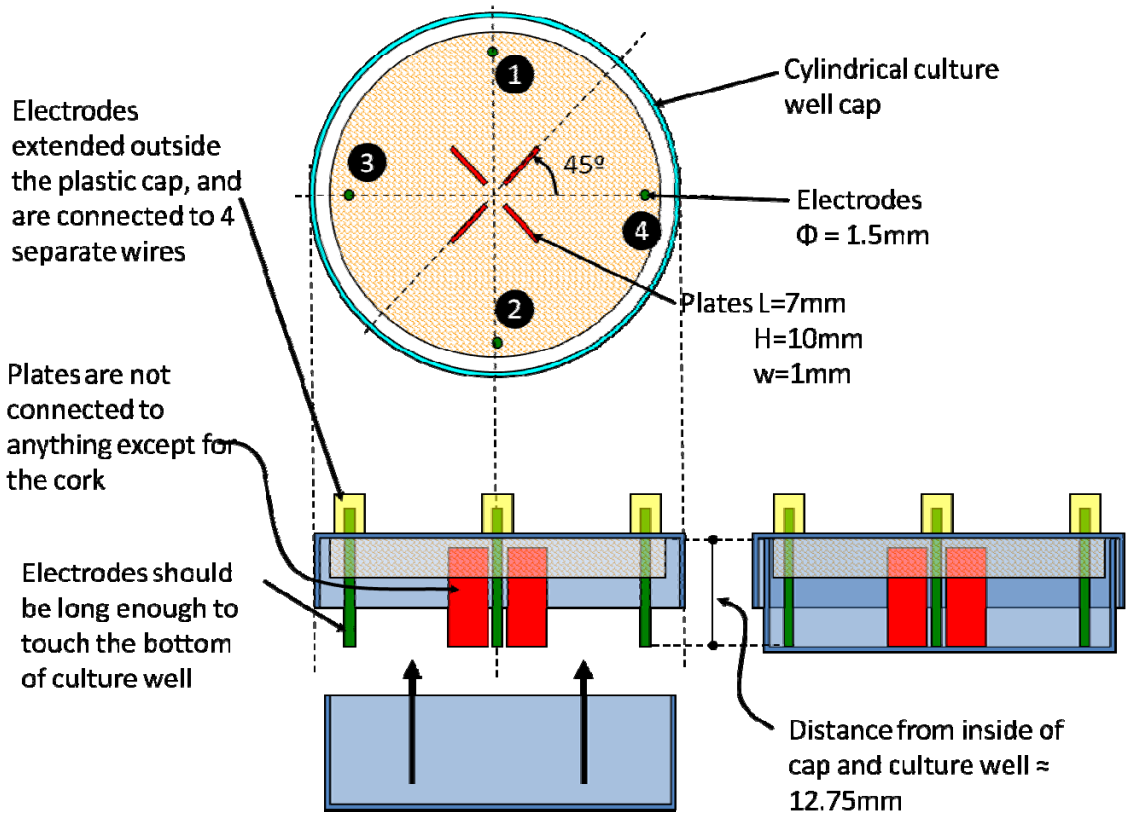

Figure 3.5. Design of electrodes and floating rectangular inserts. [53].

For the purpose of electric field focusing, a customized *in vitro* applicator was required. The primary design constraint for this unique electroporation applicator was the need to deliver electric fields on the bottom of a 60 mm culture dish containing adherent B16F10 cells. A diagram for this applicator superimposed on a 60 mm cell culture dish is illustrated in Figure 3.5. The figure shows the 4 stainless steel needle electrodes symmetrically placed near the circumference of the applicator as a vertically positioned electrode pair, electrodes 1 and 2, and a horizontal electrode pair, electrode 3 and 4. The diagram also indicates four rectangular elements at the center of the culture dish. These 4 plates work as “floating electrodes” since they are non-grounded. They

are placed in a “cross” configuration at the center of the dish. These elements are held in place on top of the cell culture dish using a Teflon™ (Small Parts, Miami, FL) rod which guarantees they are electrically insulated. The electric fields were applied through pairs of opposing electrodes at the time using an Electro Square Porator™ ECM 830 (BTX – Harvard Apparatus, Inc., Holliston, MA) pulse power generator.

Previous to exposure to electroporation, the media in the culture dish was removed, and the surface of the dish was covered with 2 ml of a 120 μM calcein phosphate buffer solution (PBS, Mediatech). The applicator's electrodes and 4 rectangular “floating electrodes” were brought into contact with the surface of the of culture dish where the B16F10 cells were cultured. Each pair of electrodes (1-2, or 3-4) was used to apply four pulses in each direction with a potential differential of 1,500 V (equivalent to a nominal electric field of 375 V/cm) for a total of 16 pulses, pulse duration was of 150 μs and the interval between pulses was of 500 ms. The calcein treated cells were rinsed three times with PBS following a 30 minute incubation time but prior to cell florescence intensity detection. The control experiments were also analogous to the *in vitro* parameter optimization experiments except for the placement of the four plates in the center of the dish.

3.2.2. *In Vivo* Fluorescent Dye Uptake by Electric Field Focusing

C57BL/6J mice were injected in a single flank with one million B16F10 mouse melanoma cells in a volume of 50 μL to induce solid tumors. The tumors

were monitored daily and allowed to develop for 7-10 days yielding tumors approximately 4 mm to 6 mm in diameter. Once the tumors were established, the mice were treated.

Polystyrene microspheres (Polysciences, Inc., Warrington, PA) were suspended in 60μM SYTOX® green (S7020, Invitrogen, Carlsbad, CA) dye solution. SYTOX® green is a nucleic acid stain that will stain nuclei cells with a compromised cell membrane. Fuorescence is proportional to the fraction of permeabilized cells. SYTOX® green is positively charged with a net +3 charge

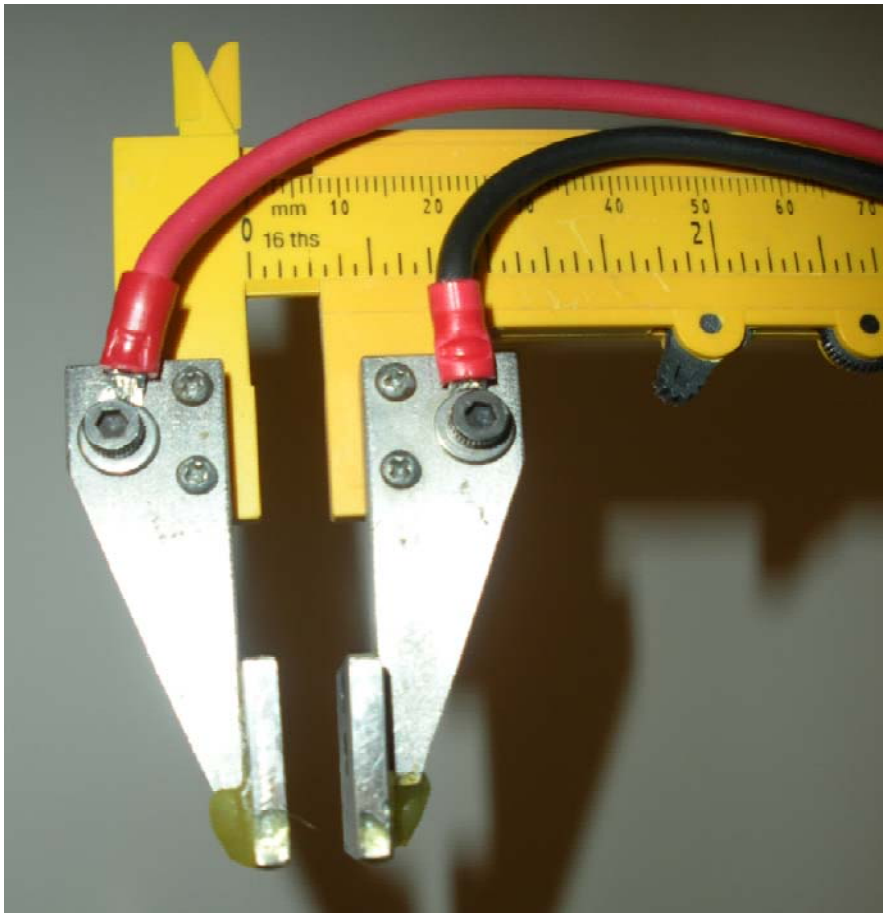

Figure 3.6. Parallel plate electrode used on tumors for electric field focusing *in vivo* experiments.

[54]. Microspheres used for the fluorescent study were 25 μm NIST traceable polystyrene microspheres (Polysciences). Melanoma tumors were extracted and stored in 20% sucrose in 0.01 M phosphate-buffered saline (PBS) at 4 °C for 2 days. Tumors were then rapidly frozen with dry ice and sectioned with a cryogenic microtome (Cryostat E110, Thermo Fisher, Kalamazoo, MI). Series of 50-μm-thick sections of the tumors were deposited in microscope slides and fixed for fluorescent microscopy.

Fluorescent imaging was accomplished using an Olympus FV1000 MPE Multiphoton Laser Scanning Probe (Olympus America, Center Valley, PA) in confocal mode and using a 4X and a 40X water submersible lens for larger and smaller field of view respectively. Fluorescent confocal (showing cell nuclei) and optical images (provided location of microspheres in xy plane) were recorded throughout the tumor sections. Using MATLAB, peak fluorescence (in arbitrary units) at cell nuclei was measured from 6 images representing different planes in sections of tumors. Fluorescence was measured radially from the location of microsphere edges. Peak fluorescence was then normalized to maximum fluorescence. This yielded normalized nuclei fluorescence as a function of distance from the edge of the microsphere. Maximum electric fields calculated from the microsphere edge were extracted from modeling results, then divided by applied nominal electric field as explained in the previous section. This maximum electric field was statistically correlated to the fluorescence using a logistic function.

3.2.3. Electric Field Focusing for Electrochemotherapy

The preparation of tumor bearing mice for the electrochemotherapy experiment was carried out using the same animal melanoma tumor model in the previous section. Additionally, mice were divided into eight groups consisting of 8 to 12 mice per group. The first group was the control group that received saline injection as treatment, the other seven groups received saline and electric pulses, bleomycin only, bleomycin and electric pulses, microsphere-saline suspension, microsphere-bleomycin suspension, and microsphere-saline suspension plus electric pulses, microsphere-bleomycin suspension plus electric pulses. Bleomycin stock solution (Sigma Aldrich, St. Louis, MO) was reconstituted in normal saline solution to a concentration of 4 units/mL so that each 50 μL injection volume contained 0.2 units of bleomycin to match a concentration used in a intratumor ECT protocol developed by Heller et al. [43] . Normal saline solution was used for groups using saline, and 20 μm Polybead® polystyrene microspheres (Polysciences) were used at $6 \cdot 10^3$ microspheres per mL of saline solution for the microsphere groups. Microspheres in solution were centrifugated and the microspheres resuspended in the appropriate solutions. Bleomycin is a positively charged chemotherapy molecule that destroys DNA and is endocytosed by the cell. The uptake of bleomycin is greatly increased by electroporation mechanisms [55].

Parallel plate electrodes consisting of 2x2cm flat stainless steel plates mounted on a vernier caliper were used. The calipers (shown in Figure 3.6) allow the measurement of the distance between the plates and therefore the

adjustment of the potentials so that pulse electric field intensity may be kept constant. These electrodes were placed to deliver a voltage potential across the shortest side of tumors. Conductive electrocardiography gel (Spectra 360 electrode gel, Parker Laboratories, Inc., Orange, NJ) was applied to each electrode to guarantee adequate electrical contact between the electrodes and the skin. Electrochemotherapy and control treatments consisted of a single treatment (Day 0) consisting of a single intratumor injection followed by 8 pulses, (four initial pulses followed by four with inverted polarity). Pulses applied were 1,300 V/cm electric field intensity (nominal field) with a duration of 100 μs and 1 s duty cycle following well established electrochemotherapy protocols used in the same animal model [42, 43]. Tumors were followed for 30 days every third day. Tumor volumes (V) were calculated using the following formula:

$$V=L\cdot W\cdot H\cdot\frac{\pi}{6} \tag{3.1}$$

where L (mm) was the longest dimension of the tumor, W (mm) was the shortest direction of the tumor, and H (mm) was the height of the tumor as measured using millimeter calipers. Per protocol, animals were humanely euthanatized and removed from the survivorship list if total tumor volume reached 1,500 mm^3.

Chapter 4. Modeling Electric Fields for Electroporation

4.1. Introduction

Model development for electric field mediated drug and gene delivery applications must explore the possible impact of protocols on target tissues. This chapter explains the most relevant considerations and principles for model development. It presents elements that demonstrate the adequacy of the modeling platform so that it may be applied to model *in vivo* and *in vitro* phenomena as it relates to applied electric field in tissues.

Electric field mediated *in vivo* agent delivery protocols use electroporation (EP) or electropermeabilization to facilitate the transport of molecules across the cell membrane and into the cell. *In vivo* EP occurs when short electric pulses are used to permeabilize cell membranes in tissues and thus improve uptake of therapeutic molecules into cells. These applied electric fields generate three populations of cells within treated tissues. First, cells which are reversibly electroporated, that receive the right amount of energy to permeabilize and considerably increase the uptake of therapeutic molecules, but regain cell function after membrane stabilization. Second, a population of cells that received a marginal quantity of energy and are not affected significantly. And last, a collection of dead cells that result from receiving an excess of energy. The excess of energy may result in irreversible permeabilization of cell membranes.

Cell death occurs for the most part close to the electrodes where electric field intensity is higher, and where undesired effects such as joule heating and electrochemical reactions are also most likely to occur.

The most investigated clinical application of *in vivo* EP is the treatment of solid tumors in cancer [35-37, 45]. As indicated in chapter 2, two modalities of electroporation are used in the treatment of cancer. In the first one, Electrochemotherapy (ECT), high field strength pulses are applied in combination with chemotherapeutic agents. The most common used chemotherapy agents for ECT are bleomycin or cisplatin. In the second cancer application, the membrane permeabilization provided by electric field pulses has been used to increase the uptake of anticancer genes such as interleukins. Both ECT, and *in vivo* electrogene therapy protocols, were developed in animal studies and then applied in clinical trials to treat solid tumors [34, 39, 41, 44, 56, 57].

In vivo electric field mediated delivery protocols require direct application of a potential differential across the targeted tissue. Different electrode systems (commonly called applicators), pulse duration and magnitude have been developed to match the specific target tissue and therapeutic molecule delivered. Depending on how deep into an organ the effect is desired, electric fields can be applied on the surface of organs, or into deeper tissue. Applicators designed for use on the surface of organs such as the skin use plate electrodes, skin pinching[58], or surface needle electrodes [59]. Surface electrodes can also be placed on catheters and used in hollow organs such as within the cardiovascular and digestive systems [60]. Applicators that use electrode arrays allow multiple

combinations of electrode pairs to deliver more uniform distributions of electric fields.

4.2. *In Silico* Design of Gene Electroporation Applicator

The generalized electrostatics module of the Comsol Multiphysics 3.3 modeling software was used to model and analyze the distribution and intensity of the electric fields. This module permits modeling of dielectric media and conductive materials in a single model. Thus, the animal tissue, and the evaluation of conductive materials such as the electrodes and other conductive objects can be assessed in a single model. The following are the subdomain COMSOL defined partial differential equations (PDE) and boundary equations [61]. Equation 4.1 describes the subdomain PDE generalized electrostatics COMSOL mode, and originates from the quasistatic approximation summarized later in this chapter.

$$-\nabla\left((\sigma+j\omega\varepsilon_0\varepsilon_r)\nabla V\right)=0 \tag{4.1}$$

where σ is the conductivity of the material (S/m), ε_0 is the permittivity of free space (8.8542.. F/m), ε_r is the relative permittivity of the material, ω is the angular frequency, and ∇V is the gradient of the potential differential equivalent to the electric field vector, **E**. The constitutive relationship defines the electric field flux vector, **D**:

$$\mathbf{D}=\varepsilon_0\varepsilon_r\mathbf{E} \tag{4.2}$$

The boundary conditions are defined as follows: Equation 4.3 indicates the continuity boundary condition, equation 4.4 defines the boundaries at the external limits of the model, and equation 4.5 indicates the electric potential boundary condition.

$$\mathbf{n}\cdot(\mathbf{J}_1-\mathbf{J}_2)=0 \tag{4.3}$$

$$\mathbf{n}\cdot\mathbf{J}=0 \tag{4.4}$$

$$V=V_0 \tag{4.5}$$

where **n** represents the normal vector, **J** represents the current density vector, the subscripts 1 and 2 refer to values of current in the boundary between adjacent elements, and V_0 refers to a potential value which if equal to zero represents a ground potential, and if different than 0, an applied potential.

Two *in silico* models were constructed using numerical methods to solve the equations described above. The first model uses a 3D geometry, and represents to scale, two surface electrodes on which the potential is applied. The model includes the cannula that is used to insert the implantable biosensor and is located in the rat subcutaneous tissue at the moment of the electroporation. The cannula is not electrically connected to any of the electrodes or ground. The second model also uses a 3D geometry, and represents to scale, a single surface electrode, and the cannula described above, with the difference that the cannula in this case is an electrode. The results from the modeling of these applicator design options are later discussed later in

chapter 8. The method is also used in chapter 9 to simulate electric fields for *in vitro* and *in vivo* applications of electroporation.

4.3. Electroporation Pulse Properties

Model development for electric field mediated drug and gene delivery must incorporate pulse properties. Electroporation pulse design is also specific to the application. Rectangular pulses are by far the most common pulses used for *in vivo* EP. In general, the duration of electric fields used have evolved into four different time scales[62]. Millisecond (1-200ms) duration pulses with magnitudes in the range of 10-500 V/cm have been typically used for large molecule delivery, as is the case of DNA vectors containing genes. Microsecond duration pulses (1-500μs) with magnitudes in the range of 100-2,000V/cm have been used to deliver smaller molecules such as chemotherapy agents and small tracers such as fluorescent dyes. More recently, nanosecond pulses (5-500ns) and electric fields with magnitude above 30,000 V/cm have been used to irreversibly electroporate cellular compartments of membranes causing apoptosis in tissues [63]. Finally, subnanosecond pulses (100-999ps) with electric field magnitude above 150,000 V/cm [64] which share many characteristics as nanosecond pulses. The magnitude of the electric fields necessary to generate the electroporation effects increase as pulse duration decreases.

Figure 4.1 provides a comparative representation of the electromagnetic spectrum with well known entities for comparison. The figure includes the electromagnetic spectrum in relation to frequency, equivalent wavelength,

equivalent frequency for electroporation pulse length, and the electromagnetic regimens as they pertain to numerical modeling, and imaging techniques used in the frequency ranges. The color transition from red through violet in the wave property bar represents the shift in frequencies in the visible range of the electromagnetic spectrum. The left end of the bar represents the lower frequencies that correspond to very long wavelengths. On the right side are radiations with higher frequencies that are associated with shorter wavelengths. For the entire spectrum, wavelength, λ (m), is inversely proportional to its frequency, f (1/s), and directly proportional to the speed of light, c ($3 \cdot 10^8$m/s in vacuum).

Fourier transform of electroporation rectangular pulses in the time domain

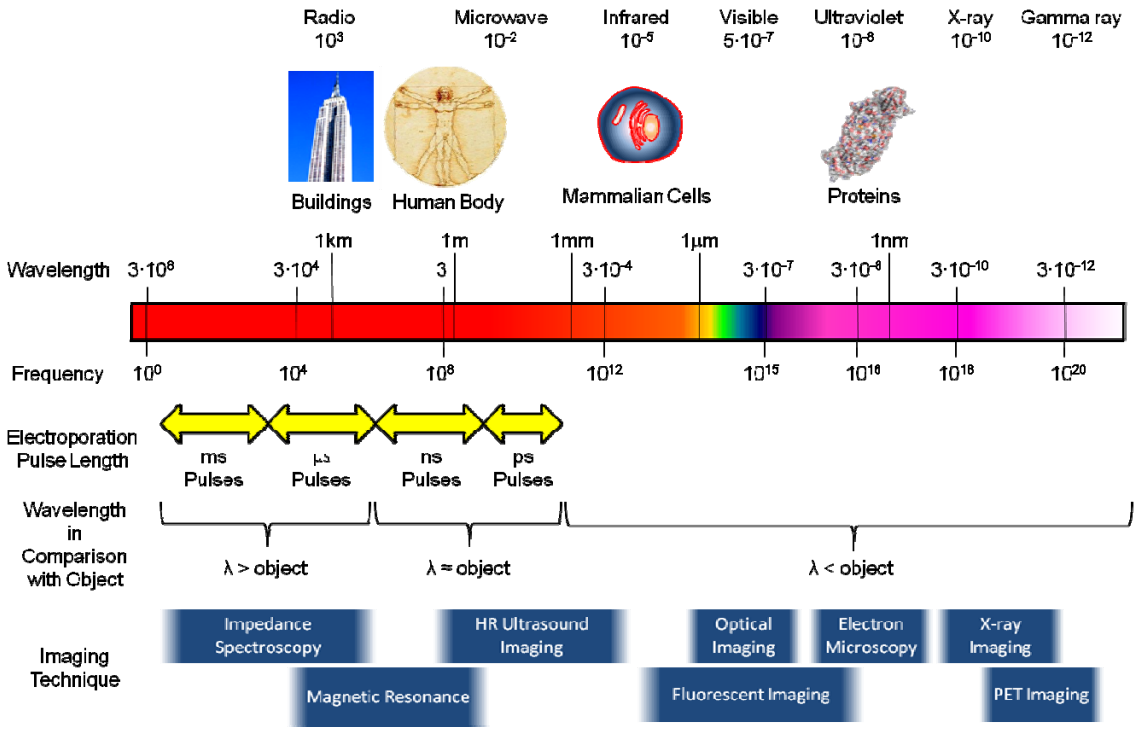

Figure 4.1. Electromagnetic spectrum and electroporation pulse length.

yield information about the electric field magnitude content in that corresponding frequency domain [65]. Figure 4.2 indicates the equivalent frequency domain magnitudes obtained by applying the Fourier transform to a rectangular pulse in the time domain. Since most of the magnitude of the pulse is restrained to a narrow frequency band, a convenient approximation is to use time-harmonic approximations in that frequency range to account for the magnitude of the electric field. Using such approximations, it is possible to represent regimens of electric field mediating pulses in comparison with the electromagnetic spectrum wave groups as highlighted by yellow arrows in Figure 4.1.

As suggested earlier, the wavelengths of the wave groups can be compared to various objects. By comparing the size of an object or affected tissue to the fundamental frequency of the applied electric pulse, it is possible to

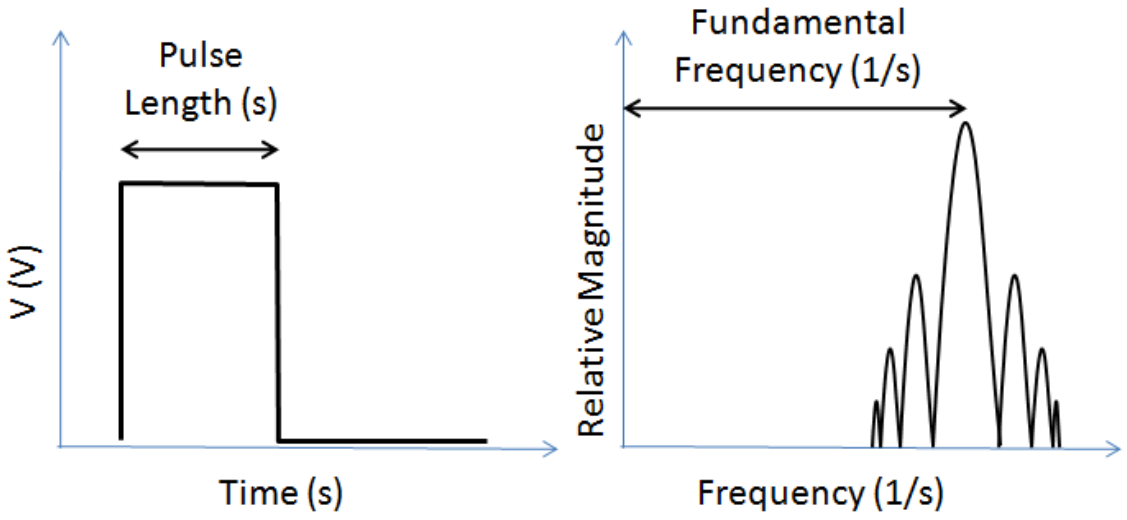

Figure 4.2. Fourier transform of electroporation rectangular pulse.

categorize the electromagnetic spectrum of the electric fields into three regions. The first region is when the equivalent fundamental wavelength of the electric pulse is much longer than the size of the affected tissue section. The second region is when the wavelength and the size are similar, and lastly, when the wavelength is much shorter than general volume dimensions of tissue affected by the pulse's electric field. In each case it is possible to use approximations to model the electric fields as they pertain to electroporation applications.

4.3.1. Wavelength Longer than the Size of Affected Tissue

Theoretical analysis and experimental evidence from impedance tomography investigations have led to approximations that can be employed when the wavelength of the applied electric pulse is much longer than the tissue section. In this case, the decoupling of the electric and magnetic fields can be used to modify Maxwell equations. Specifically, Ampere's Law (equation 4.6), can be represented in its time harmonic and vectorial form [66]:

$$\nabla \times \mathbf{H} = -(\sigma + j\omega\varepsilon_0\varepsilon_r)\mathbf{E} \qquad (4.6)$$

where ∇x denotes the curl operator, $\mathbf{H}$ is the magnetic field vector, $\mathbf{E}$ is the electric field vector, σ is the conductivity of the material (S/m), ε_0 is the permittivity of free space ($8.8542..\cdot 10^{-12}$ F/m), ε_r is the relative permittivity of the material, and ω is the angular frequency. The decoupling of the electric and magnetic fields makes the curl of the magnetic field 0 (equation 4.7):

$$\nabla \times \mathbf{H} = 0 \tag{4.7}$$

The approximation of the decoupled electric and magnetic fields is commonly known as the quasielectrostatic approximation. This approximation is represented here as equation 4.8:

$$-(\sigma + j\omega\varepsilon_0\varepsilon_r)\mathbf{E} = 0 \tag{4.8}$$

where the terms in parenthesis on the left hand side of the equation is also called the complex conductivity, or admittivity (κ) which is a descriptor for electric characteristics of biological materials for longer wavelengths than the object [67] (equation 4.9):

$$\kappa = \sigma + j\omega\varepsilon_0\varepsilon_r \tag{4.9}$$

The simulation quasielectrostatic module of COMSOL Multiphysics uses a form of equation 4.6 to solve problems involving electric fields in tissue systems [61]. This approximation has also been used for various impedance tomography applications [68-70]. Multi-frequency impedance tomography has validated such an approach in a frequency range usually from 10 Hz, and up to 1 MHz [71]. Furthermore, impedance tomography has been successfully utilized to image the changes in conductivity resulting in tissue affected by electroporation [72, 73].

4.3.2. Wavelengths Approximating the Size of Affected Tissue

The approximations used when wavelengths are longer than affected tissue do not apply because electric and magnetic fields are highly coupled. For

this case, it is more convenient to use wave theory because propagation effects dominate, and the wave behavior of electromagnetic energy is more relevant in this range. Phenomena such as resonance and oscillations are also relevant in this range of frequencies [74]. Diffraction, reflection and refraction must also be considered when modeling fields in this regimen.

4.3.3. Wavelength Shorter than Size of Affected Tissue

The case in which wavelength is much shorter than size of the affected tissue is not considered in this work. There is no background work for the use of such high frequency pulses in electric field mediated drug and gene delivery. This range of frequencies includes wavelengths in the visible spectrum, ultraviolet light, and x-ray and gamma rays. In this range of frequencies, ray behavior of electromagnetic energy is considerably more relevant [74]. The effects that occur at such frequencies cannot be considered within the domain of electroporative pulses.

4.4. Objects in Electric Fields

The understanding of the application of electric fields to objects in a isotropic media is an important initial step when developing models that study electroporation in tissues. A very convenient analytical analogy to interaction of electric fields and objects is that of irrotational fluid flow (Feynman, 1964) [75] or potential flow (Batchelor, 2000) [76]. Irrotational flow refers to flow which lacks vorticity. The photograph in Figure 4.3 shows the conduction of water molecules around a rock [77]. In this image, it is possible to appreciate the water

Figure 4.3. Flow of water around rocks [77]. Reproduced under the Creative Commons License Attribution 2.0 Generic (author: the_tahoe_guy).

streamlines as it surrounds the rock, and how the flow deviates around the rock. It is also possible to appreciate that far from the rock, the flow lines do not curve. At such distances, the rocks lack influence on the flow. The image allows one to visualize by analogy, how the electric field in a conductive medium behaves around a non-conductive object such as the rock in the figure. Feynman [78] describes such an analogy using irrotational flow which is much simpler than the incompressible Navier-Stokes representation. Feynman's develops the equations representing the electric fields analogy to irrotational flow for a sphere under an applied field (see Figure 4.4), starting with the continuity equation for a flow of constant density (equation 4.10), and Gauss' law in a charge free medium (equation 4.11) in the following way:

$$\nabla \cdot \mathbf{v} = 0 \tag{4.10}$$

$$\nabla \cdot \mathbf{E} = 0 \tag{4.11}$$

where **v** (m/s) and **E** (V/m) are the velocity and electric field vectors respectively. The irrotational-flow or “dry water” (equation 4.12) condition neglects the viscosity, compressibility, and surface tension of the fluid. The “dry water” term was coined by the mathematician John von Neumann and often used by Feynman [75] to describe an idealized fluid lacking viscosity and not subjected to vorticity effects. The electrical equivalent of equation 4.12 is shown in equation 4.13:

$$\nabla \times \mathbf{v} = 0 \tag{4.12}$$

$$\nabla \times \mathbf{E} = 0 \tag{4.13}$$

The gradient of the potential for flow ψ, (equation 4.14), and the electrical equivalent (equation 4.15) are as follows:

$$\mathbf{v} = -\nabla \psi \tag{4.14}$$

$$\mathbf{E} = -\nabla V \tag{4.15}$$

where ψ is the velocity potential (in m^2/s) and V is the electric potential (in volts or J/C) Feynman then develops the equations for a spherical object within a fluid potential or a electrical potential. The solutions for the potential at any given point in relation to the center of the sphere under a field are as follows for both the fluid (4.16), and the electrical equivalent (4.17):

$$\psi = -v_0 \cos\theta \left(r + \frac{a^3}{2r^2} \right) \tag{4.16}$$

$$V = -E_0 \cos\theta \left(r + \frac{a^3}{2r^2} \right) \tag{4.17}$$

where the coordinates are expressed in terms of the angle θ and the distance r from the center of the sphere, a is the radius of such sphere, and v_0 (m/s) and E_0 (volts/m) represent the nominal velocity and nominal applied electric field respectively. Nominal values for fields are those that are not influenced by the

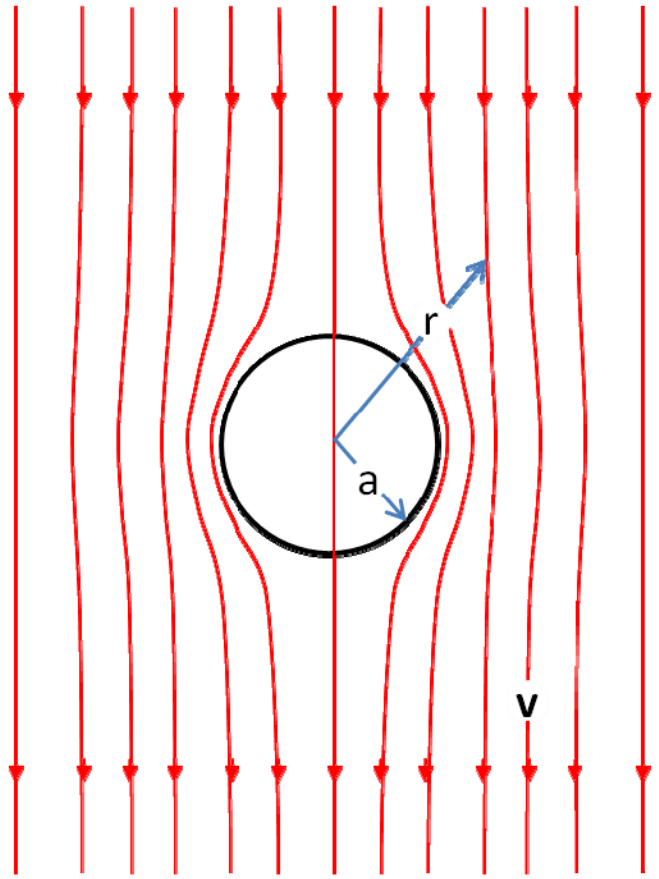

Figure 4.4. Flow of irrotational fluid around a sphere in a velocity field.

object. These values will be found at a distance greater than r which is several multiples of the radius of the sphere, a. The depiction in Figure 4.4 shows the sphere as positioned within a velocity field. The direction of the velocity field stream lines represents the direction of the velocity or electric field. A direct analytical analogy to electric fields is made from the velocity field analysis of such model.

The analytical solution of the potential ψ presented in equation 4.17 can be compared to the numerical solution approximation for ψ using the COMSOL

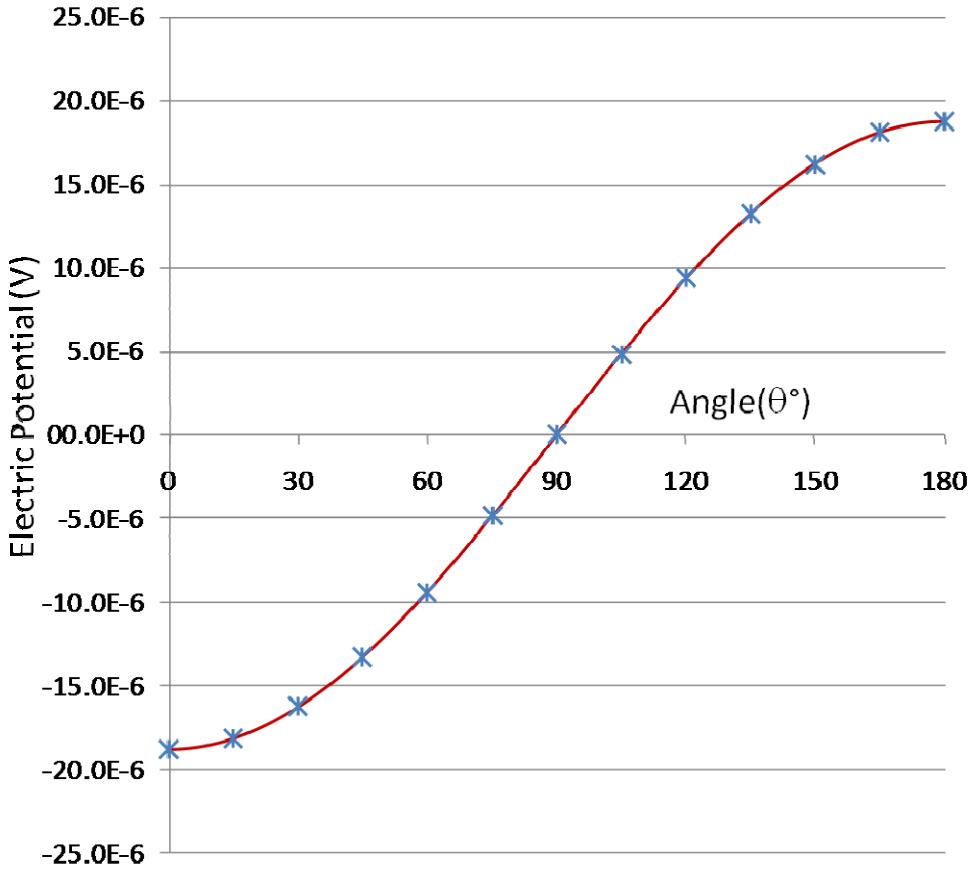

Figure 4.5. Comparison of the analytical and numerical solution for the electric potential (V) around a sphere.

Multiphysics based methods described earlier in this chapter (section 4.2). To show the agreement between the two solutions, the radial distance has been made to match that of the radius of the sphere r = a = $25 \cdot 10^{-6}$ m, and E_0 = 1 V/m. Figure 4.5 shows the numerical solution (red line) and the analytical solution (blue stars) provided by Feynman describing the potential around a spherical object. The horizontal axis represents the angle in degrees (°), and the vertical axis, the potential in volts (V). Numerical solutions built on the same COMSOL platform are used throughout this dissertation to represent electric fields in tissue.

Table 4.1. Models for electroporation that describe induced potential drop at cell membrane.

Description	Model	
Sharing of equipotential in core of cell, potential differential at maximum [18]	$\Delta V_M = 1.5 \cdot a \cdot E_0$	(4.18)
Introduces the radial position using the angle θ, and the cell shape factor, f_s, the shape factor, can vary, but becomes 1.5 for spherical cells [79, 80].	$\Delta V_M = f_s \cdot a \cdot E_0 \cdot \cos\theta$	(4.19)
Contains the conductivity factor, f_σ which takes into account conductivities of the membrane, media, and inside of the cell [81, 82].	$\Delta V_M = 1.5 \cdot f_\sigma \cdot a \cdot E_0 \cdot \cos\theta$	(4.20)
Introduction of the time dependence of cell permeabilization. Introduce time resolution by the relationship between pulse time t, and charging time of the cell membrane, τ [83, 84]	$\Delta V_M = 1.5 \cdot f_r \cdot a \cdot E_0 \cdot \cos\theta \cdot \left(1 - e^{-\frac{t}{\tau}}\right)$	(4.21)

4.5. Cells in Electric Fields

The events leading to electroporation of cells deal with the direct and indirect effects of electric fields on the cell membrane. The literature on electroporation that investigates direct effects of electrical impulses on cell membranes predict electrical breakdown of cell membranes at a threshold of induced transmembrane potential. The models describing the induced transmembrane potential have been compiled by Hickey in 2005 [85] and are shown in Table 4.1. In all instances, the common component of the formulations for electrically induced membrane breakdown of spherical cells by electroporation is the term $1.5 \cdot a \cdot E_0 \cdot \cos\theta$ describing the potential across the cell membrane. This factor coincides with the case for which equation 4.17 is simplified for a=r and which has been plotted using both analytical and numerical methods in Figure 4.5. It is important to note that most of these models were developed for cells in media, which usually was of higher conductivity than the cell cytosol.

Electric impulses also produce mechanical forces on the cell membrane due to the electrostrictive and electrodynamic nature of cells in tissues. These forces have been the subject of a substantial amount of research [86]. Evidence for such electromechanical force can be seen in extreme cases such as electrocution lesions, in which nuclei of cells in the affected tissue cluster and elongate in the direction of the applied field [87]. The electromechanical effect is not exclusive to the cellular scale, but also manifests itself at the tissue scale; even under applied electric fields similar to those used in electroporation [88].

Another electrophysical phenomena that is important in electric field mediated drug and gene delivery is the electrokinetic transport of particles. Such transport is dependent on local electric field intensity and direction, and can take the form of electrophoresis, dielectrophoresis, or electroosmotic flow, or a combination of these phenomena. Such phenomena have been the focus of study for small and large molecules in electroporation pulses. It is particularly important in the case of electroporation of large molecules such as DNA. This importance is evidenced by experiments in which labeled DNA was electroporated into cells in suspension and imaged using rapid time lapse photography. In these series of experiments, the labeled DNA was transported to the surface of the cell membrane during the electroporative pulse, but, uptake of the molecule to the nucleus was a separate process that had a much longer duration. This implies that the DNA transport to the nucleus is a biologically endogenous process to the cell [89, 90].

The interstitial transport of molecules resulting from applied electric fields is also the subject of theoretical, empirical, and numerical modeling. Hickey 2005 [85] built an analytical model of molecular transport of DNA in tissues based on data acquired from electrophoretic gel experiments. In support for the present dissertation, Rey et al (2010), modeled the electrokinetic facilitated transport of DNA during an electroporative pulse, and showed the interstitial flow and mass transport of DNA that resulted in increased concentrations of DNA at the cell membrane [91]. Figure 4.6 shows the mass transport results for this cell cluster model. The figure indicates increased available DNA at the cell

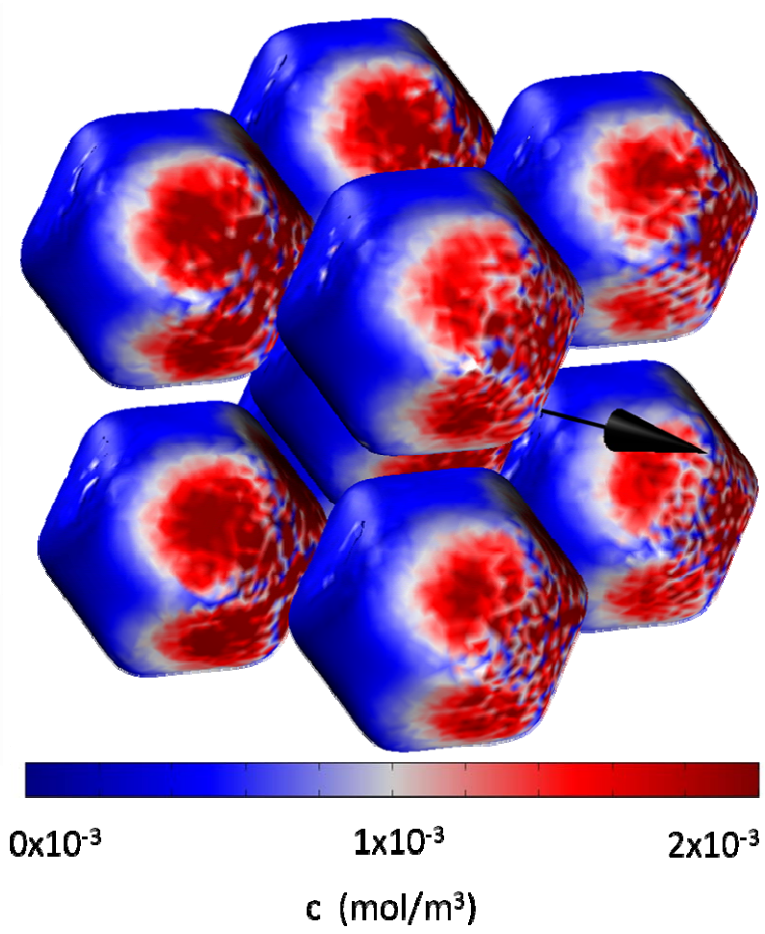

Figure 4.6. Available concentration of DNA at boundaries of cell membranes.

membranes on one side of the cells in the cluster. The availability of DNA in mol/m^3 is dramatically increased at the cell membrane portions that face in the opposite direction to the applied electric field. The concentration of DNA available at the cell membrane in the case of this model was 10 times larger than that of the initial concentration of DNA in the interstitial space. These numerical results, in addition to the analytical models and the experimental results mentioned above emphasize the significance of transport processes in electroporation.

4.6. Objects and Tissues in Electric Fields

The complexity of the phenomena occurring in tissue under the effects of electric fields is non-linear, and dynamic in nature. Such effects are not limited to occurring during the electroporation pulse duration, but can modify tissue for periods of time that exceed that of the pulse. Figure 4.7 shows a representation of a projection of a spherical object embedded in tissue. The hatched area represents a portion of the tissue that has been subjected to high electric fields.

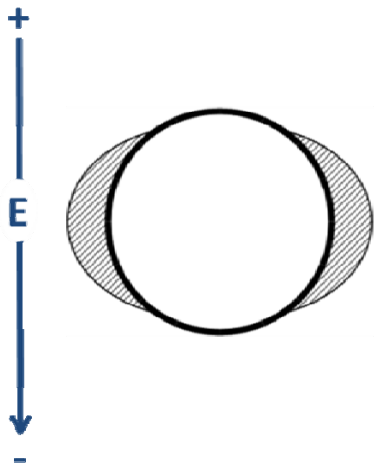

Figure 4.7. Conductivity changes due to electric fields.

The tissue response to electric fields is not linear in part because of the changes in dielectric characteristics due to tissue permeabilization [92]. These changes can be observed during and between applied pulses. The area subjected to the highest electric field intensity (shown in Figure 4.7) is likely to experience increased conductivity leading to modification of distribution of electric field vectors in consecutive pulses. This modification of tissues electrical characteristics during and in between pulses has been the subject of several studies [92-94].

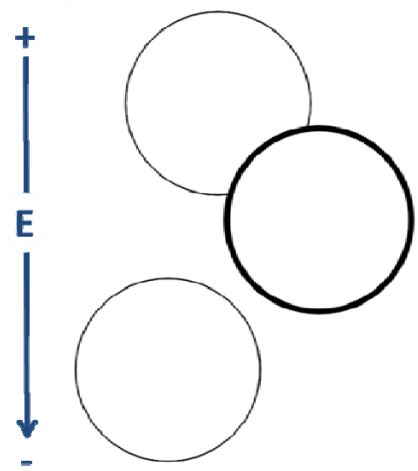

Figure 4.8. Modification of electric field path by nearby objects.

Furthermore, complexity also arises from the presence of adjacent objects within a tissue section (Figure 4.8). The path of electric fields, and how they are influenced by a particular object embedded in tissue will significantly vary due to other adjacent objects. Electric fields are not only modified by the presence of other foreign objects, but also by the composite electric characteristics of tissue, or other types of tissues. Model analysis of this effect involving a very simple case of two adjacent objects embedded in tissue is presented in Chapter 7.

The differences in dielectric characteristics, and compartmentalization provided by the cellular membranes modifies electric fields in a manner that is tissue and frequency dependent (Figure 4.9.a). Electric fields may also be modified for macroscopic aspects such as location of electrodes, asymmetry of contacts due to geometry and local differences in tissue conductivity (Figure 4.9.b). These alterations in an electric field are represented in Figure 4.10 as meandering red dashed streamlines.

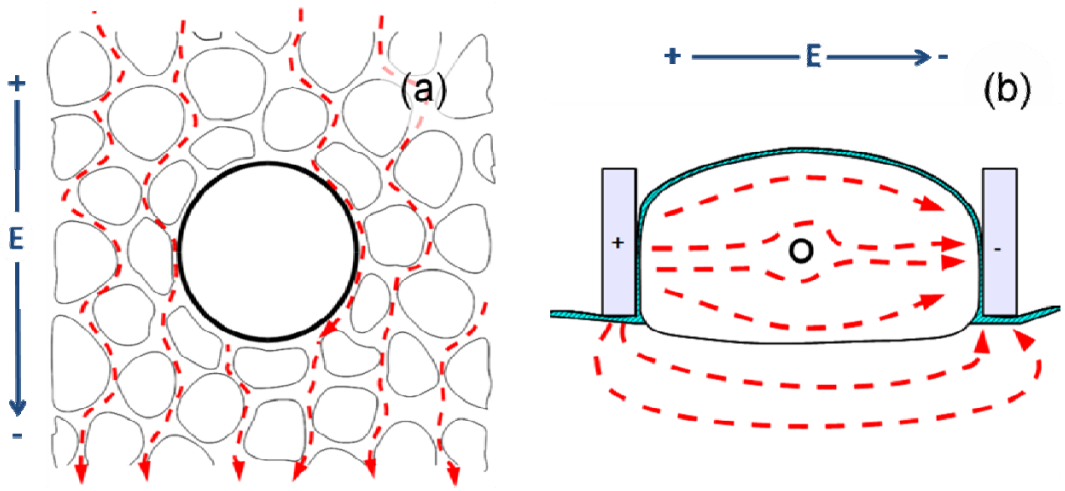

Figure 4.9. Modification of electric field path due to cells and macroscopic asymmetries.

The increased local electric field intensity in the proximity of the microspheres also gives rise to secondary events while the pulse is applied. electroosmotic flow (represented in Figure 4.10 by curved arrows) can both create local pressure gradients as well as drag forces in the proximity of embedded objects, such as a microsphere [95]. Such flow, pressure gradient, or force will depend on the characteristics of the surface of the material of the microspheres, the ionic nature of the surrounding fluid, and the geometry of interstitial space surrounding the microspheres. The electroosmotic flow can manifest itself in the form of flow, pressure gradients, and a force exerted by the microsphere on the matrix in which it resides [95]. Electroosmotic flow is generated when electric fields produce a drag force on fluid around a charged object. The flow velocities are proportional to the charge contained within the electrical double layer (Debye layer).

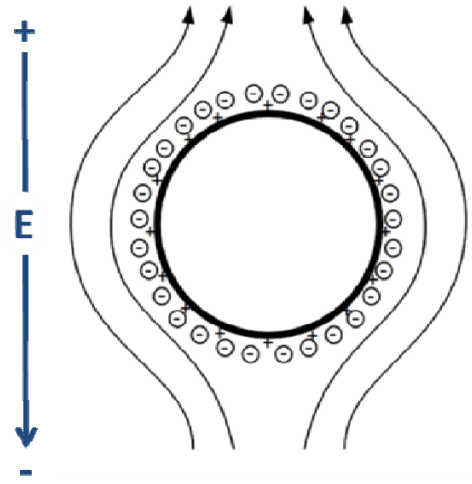

Figure 4.10. Electroosmotic flow due to electric fields and charged surfaces.

The pressure gradients generated by electroosmotic flow around particles in proximity turns the system into an electroosmotic pump [96]. Electroosmotic flow and electrophoretic facilitated transport might be responsible for accumulating higher concentration of charged drugs in certain regions such as near the surface of the object (see Figure 4.11). This concentration of material

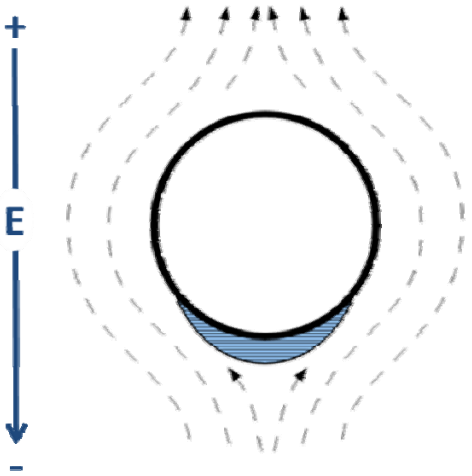

Figure 4.11. Concentration gradients due to electroosmotic flow.

around the embedded object is analogous to that of the concentration of DNA molecules at the cell membrane shown in Figure 4.6. Electrophoretic facilitated transport generates forces that act directly on charged molecules such as DNA, and is responsible for their transport in porous matrices such as gels and tissues [85]. Another source of pressure values on the surrounding cells may arise from polarization due to charge buildup in the surroundings of an embedded object. As shown in Figure 4.12, dipole forces (red vertical arrow) are a function of the electric field gradient and polarization, while dipole torque (curved dashed red arrow) originates from electric fields that are orthogonal to the polarization [97]. The resulting mechanical forces and torque can facilitate the permeabilization of cell membranes in the proximity of the embedded object.

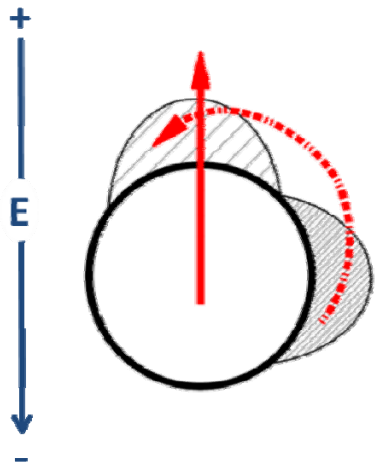

Figure 4.12. Polarization induced forces and torque.

Chapter 5. Summary Part I

The successful performance of the implantable glucose biosensor requires reliable long term function *in vivo*. As suggested in the Prelude to Part I, the dissertation research to address this challenge would be based on a strategy that merges two technologies and leads to two exploration pathways. The strategy is to modify the implant's tissue environment to enhance implant's performance. The two technologies, oxidation/reduction chemistry based biosensors and electric field mediated agent delivery, actually dictate two tissue engineering pathways for this strategy:

(a) Modify the surgical implantation procedure to include the corrective agent that alters the tissue in the proximity to the implantation site. This pathway will be referred as the preemptive approach.

(b) Modify the tissue in the proximity of the sensor sometime after the sensor enters its operational phase. Hereafter referred as the reactive approach.

Both preemptive and reactive pathways are visualized in Figure 5.1. The figure is an enhanced version of the injury impact after implant illustration in originally shown in Figure 2.3. Figure 5.1 indicates the timing for the two tissue intervention options. For the surgical implantation procedure option, the tissue modification at the implant site would begin at the blue arrow, and would have an

influence (expression) profile similar to the blue curve in Figure 5.1, as the implant begins its operation. For the second option, the tissue would be modified after the impact of the fibrous encapsulation process, the green curve in the figure represents the influence profile that is synchronized with the encapsulation process.

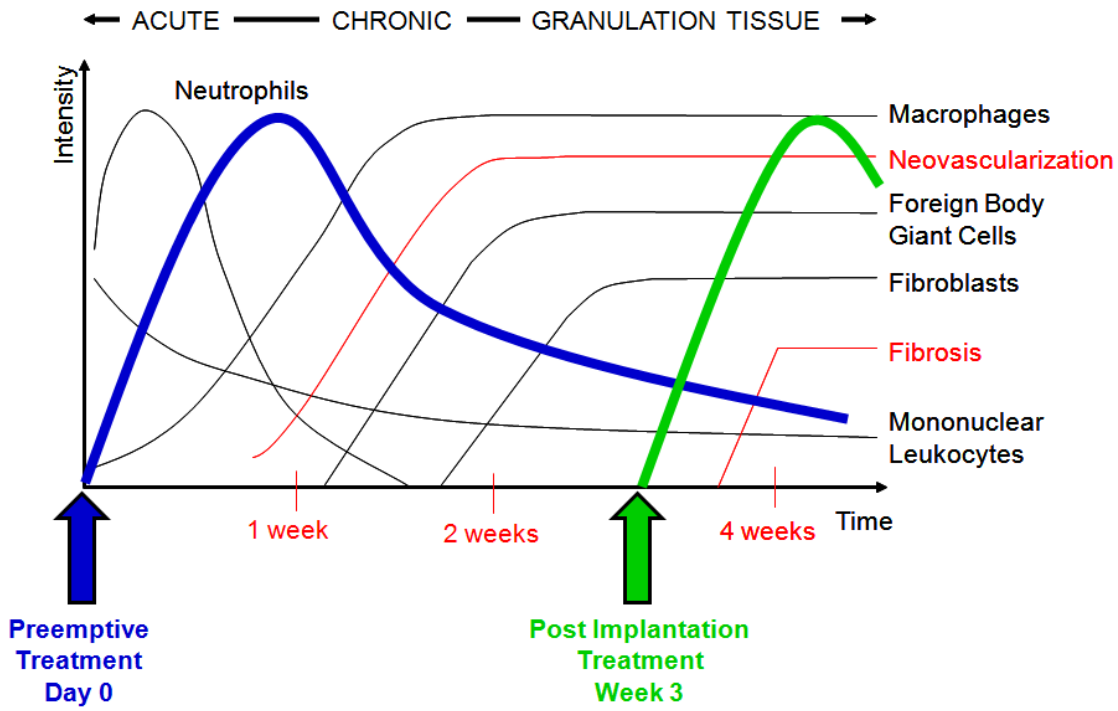

Figure 5.1. Tissue reaction to implanted biosensor, and two potential tissue modification strategies.

Although the strategic options are clear, their potential to really address the performance challenge of a biosensor requires verification of fundamental assumptions. These assumptions support the premise that the challenge to an implant biosensor's performance may be overcome. The literature and modeling review presented in Part I combined with the wealth of information provided from the corresponding references provide that assurance. The application of electric

field for delivery of drugs and genes is a proven technology with protocols and documented applications available as resources for this research. The redox reactions, implant design, operational expectations for glucose implantable biosensors are also well established. In addition, the literature provides evidence that tissue engineering DNA based strategies can impact the sensor's life expectancy and signal performance *in vivo*.

The final component needed for a successful research effort is the resident expertise to support the effort. Again, the literature and modeling review provided indicates the excellent juxtaposition of expertise in both technologies resident at USF and represented in this research dissertation committee. Besides the continuous injection of state-of-the-art ideas and best practices, the practical execution of the experimental protocols summarized in chapter 3 were effectively modified when needed to assure optimal use of research time and resources.

Part II

Chapter 6. Research Plan

The confidence that there is a basis for the research to be conducted generates the need for a research plan to be developed and executed. This research plan depends on a modeling exploratory approach prior to an experimental heuristic attack. The plan is presented below as a series of asynchronous steps. However, the steps are executed in a sequence that highlights the milestones required to denote the overall progress of the work.

6.1. Development of Experimental Protocols

As suggested in the Summary of Part I, the development of experimental protocols was facilitated by the *in vivo* animal protocol expertise resident within the two research groups at USF. All of the experimental methods with their specific details summarized in Chapter 3 were built on demonstrated techniques used in electroporation and biosensor based investigations conducted at USF. This literally represents experiments that involved hundreds of animals and includes competent use of and analysis from appropriate instrumentation and assay procedures. Modification of either protocol implementations or analysis methods specific to this research will be noted when appropriate.

6.2. Verification of Model Tools and Developed Mathematical Models

The essence of this dissertation effort is mathematical model driven. The *in vitro* and *in vivo* experimentation was instigated to explore and/or confirm a model expectation. Thus, a precursor model verification exercise involving the software platform was essential. The COMSOL Multiphysics platform selected for this research was tested with respect to the expected use of Maxwell type formulations of partial differential equations. That verification exercise was reviewed in Chapter 4 and the software's ability to support a partial differential equation model with form and boundary conditions similar to specific models to be developed in this research summarized in Figure 4.5. Experimental and analytical verification for specific models developed for this dissertation will also be performed and discussed relative to their respective research milestone. These milestones are posted below as research questions which, when answered, will define the totality of this dissertation.

6.3. Dissertation Milestone Requirements

The intended purpose of this work relies on the ability to answer the four milestone questions presented below. This section indicates the chapter that addresses the answers to each milestone question. These questions guide the model development and experiments presented in this work.

6.3.1. Is The Modeling Platform Adequate To Provide Results That Comply With The Engineering Science Principle Under Investigation?

The answer to this question was partially provided in Chapter 4 with the demonstration of each

modeling element. Chapter 7 presents further evidence to support this milestone.

6.3.2. Can The Modeling Platform Support Further Complexity That Indicates Physical Processes Related To Compartmentalization In The Tissue? This milestone is addressed in Chapter 7 for a compartmentalized system. Section 4.5 provides an application to electrokinetic phenomena for a compartmentalized cluster of cells.

6.3.3. How Do Conductivity And Permittivity Values Of A Target Tissue Impact The Influence That Electric Fields Have On That Tissue? This question is addressed in Chapter 7. This chapter demonstrates electrostrictive phenomena occurring as a consequence of conductivity and permittivity values for an applied electric field of varying frequency.

6.3.4. Is It Possible To Use Model Representations To Determine *In Vivo* Applications Of Electric Field Mediated Drug And Gene Delivery That Can Be Adapted To Improve Implantable Biosensor Function As Per Summarized In Chapter 5? This question is addressed in Chapter 8 with the application of electric field mediated gene delivery to modify the implantation surgical protocol in a preemptive approach. Chapter 9 provides a novel electric field mediated drug delivery application supporting a reactive approach.

Chapter 7. Conductivity and Permittivity Impact on Electrostrictive Force Fields

With the confirmation of the COMSOL Multiphysics software platform as a model construction tool for this research, milestone question 6.3.1, in addition to the ability to model complex processes, milestone question 6.3.2., as provided in Chapter 4, attention quickly shifts to modeling application to study and understand the impact of conductivity and permittivity values on target tissue exposed to an electric field, milestone question 6.3.3. The combined modeling work by Lewis [98] on bilayer membrane electroporation and experimental investigations by Dimova et al. [99-101] on the impact of electric fields on giant vesicles indicate that electric fields generate a Maxwell stress resultant force that mimics compression force normal to the target membrane. The creation of a model with the resolution to delineate the roles of conductivity and permittivity with respect to the impact of this stress force on tissues represents a first step to understanding the effect of electric fields on tissues near a biosensor implant. In addition, the ability to compare this new model's predictions to the existing giant vesicle experimental information contributes to the validity of a comport using the model information relative to research milestone 6.3.3.

The basis for this model approach is the recognition that Maxwell stress tensors can be used to render mechanical forces from the interaction of differentially charged bodies to electric fields. The force acting on the cell

membrane can be expressed as the resultant of the stress tensors acting on the cell membrane. Several models attempt to explain how the stresses influence the cell membrane. By idealizing cell membrane as a compartamentalization entity, the resulting stress on cell membranes can be generated from the resultant of the internal ($\mathbf{T}^{in}$) and external ($\mathbf{T}^{out}$) Maxwell stress tensor $\mathbf{T}^{R}$ (equation 7.1) acting on the membrane [102]. $\mathbf{T}^{in}$ and $\mathbf{T}^{out}$ are calculated following equation 7.2.

$$\mathbf{T}^{R}=\mathbf{T}^{in}+\mathbf{T}^{out} \tag{7.1}$$

$$\mathbf{T}^{j}=-\frac{\mathbf{E}\cdot\mathbf{D}}{2}\mathbf{I}+\mathbf{E}\cdot\mathbf{D}^{T} \tag{7.2}$$

where **E** (V/m) is the electric field vector, and **D** (C/m^2) electric flux density or displacement vector as defined earlier in this chapter using equation 4.2; ε_0 is the permittivity of free space, and ε_r is the relative permittivity of the polarizable material in the electric field.

Figure 7.1 shows a diagram of a differential area and an axial section of a cell under such stresses. Figure 7.1(a) is a representation of the differential area of cell membrane submitted to inside $\mathbf{T}^{in}$ and outside $\mathbf{T}^{out}$ tensor and representative forces $\mathbf{F}_{in}$ and $\mathbf{F}_{out}$. Figure 7.2 (b) is an axial representation of cell membrane with tensor $\mathbf{T}^{in}$ and $\mathbf{T}^{out}$ resulting in $\mathbf{T}^{R}$. A more complex model by Lewis 2003 that uses similar methodology but that takes into account the internal stresses and deformations generated within the lipid bilayer of the cell membrane predicts a collapse at local electric fields between $7.1\cdot10^7$ and $2.3\cdot10^7$ V/m [98].

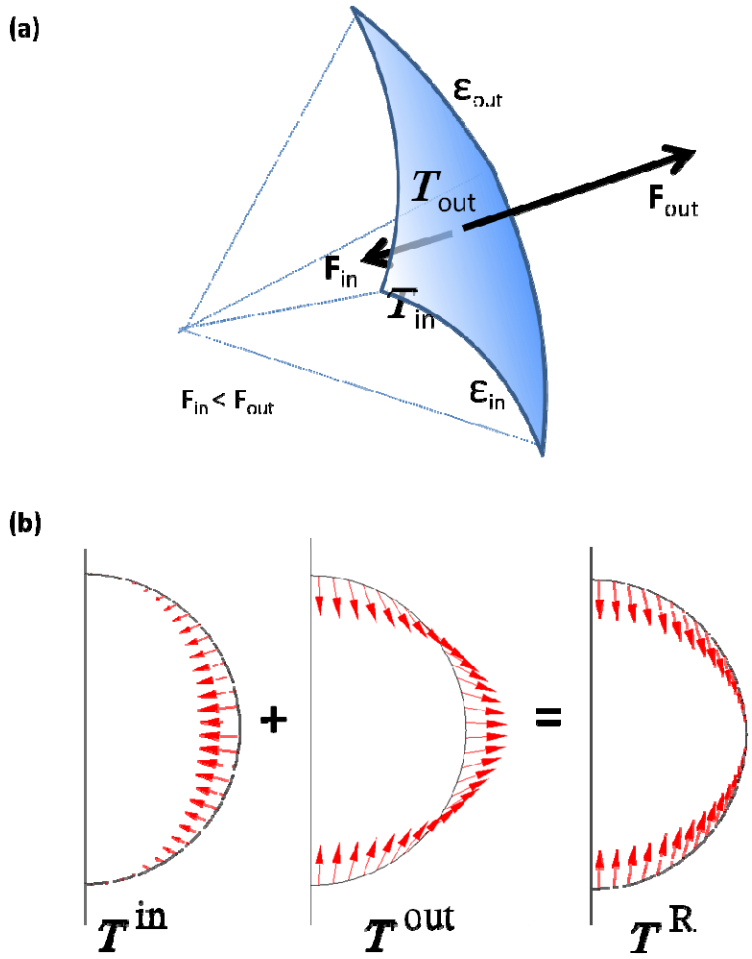

Figure 7.1. Resultant Maxwell stress tensor on the cell membrane. From Rey 2009 [102]. Reproduction permission granted by IEEE.

Complete details and the results of this intensive modeling effort have been published [102]. The model provided additional insight into membrane deformations in terms of the compartmentalized dielectric properties, conductivity and permittivity, values. A summary of these results is shown in Figure 7.2. Of particular importance to this dissertation research was the confirmation that the COMOLS Multiphysics model platform does support complex models for predicting the cumulative effect that electrical properties of cells in tissue have on a target tissue region that is affected by an electric field.

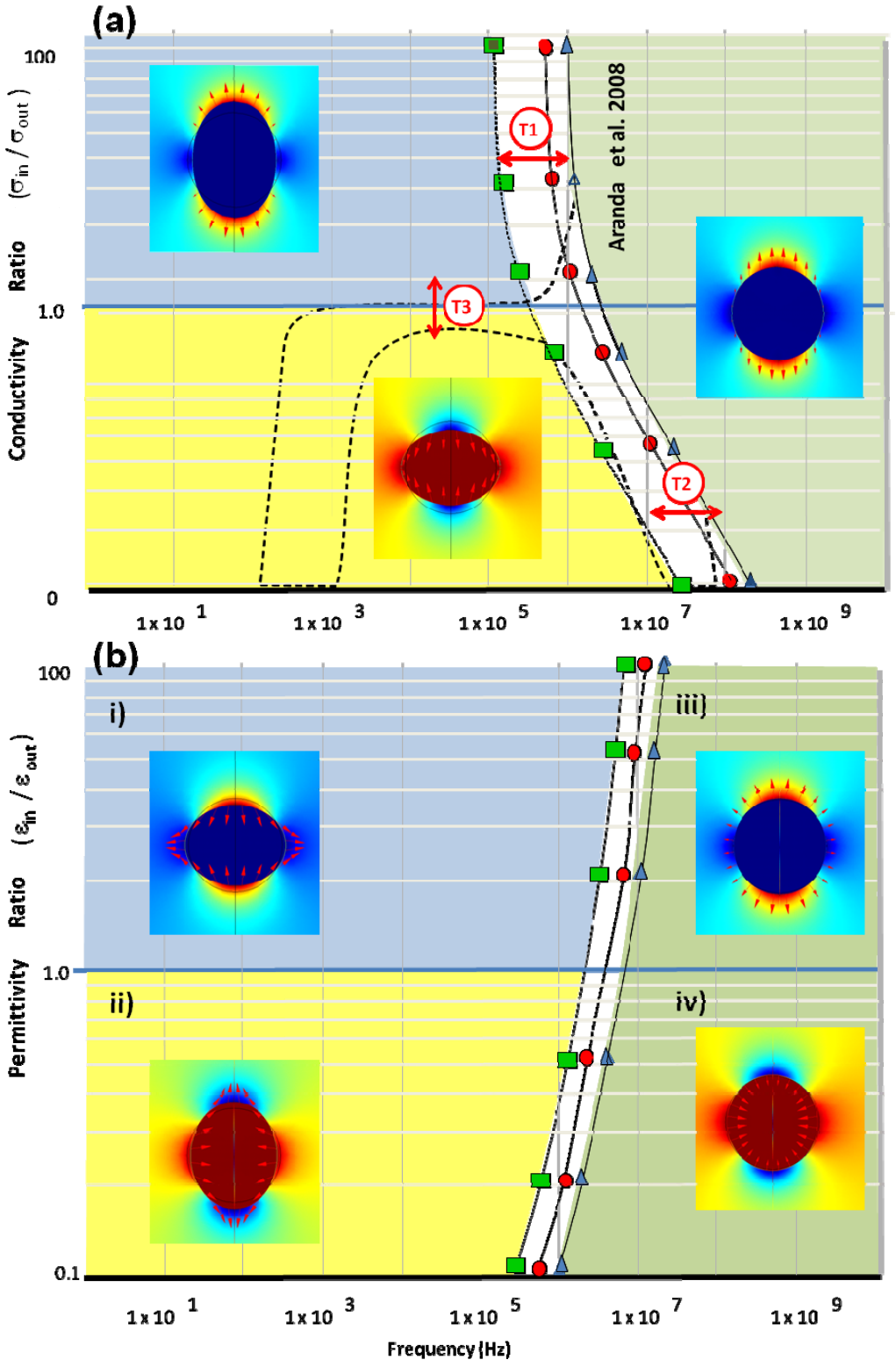

Figure 7.2. Conductivity and permittivity influence in electrostriction forces. From Rey 2009 [102]. Reproduction permission granted by IEEE.

Figure 7.2a shows a superposition of modeling results for conductivity to experimental results by Dimova el al. [99]. The model predicted results in the graph contrast conductivity ratios (in the vertical axis) with frequencies; in specific, the transition frequencies shown as dashed lines. The model predicted this relationship for frequency values between 1Hz and 1GHz. For this specific model, the predictions matched the experimental results that indicated that the giant vesicle shape change in terms of the transition frequency (T1, and T2, in Figure 7.2a) in which the vesicle changes shape. A particular transition range of frequencies (T3 in Figure 7.2.a) was not predicted by the model. Yamamoto et al. 2010 later indicated that the reason for this discrepancy might be in the modeling of the boundary conditions for the cell membrane [103]. The model included a prediction of the changes in permittivity values between the interior and exterior of the giant vesicle. These results in the form of transition frequencies and predicted acting forces on vesicles are shown in Figure 7.2b. The effort necessary to isolate permittivity values while keeping the conductivities constant as provided in these results is a difficult task to achieve using the experimental platform used by the Dimova and Yamamoto's groups.

The model predictions represented in Figure 7.2 however are of particular importance in electric field focusing. This figure introduces the concept that biological entities with an electric field applied are subject to have forces that change considerably at transition frequencies. The material properties of objects embedded in tissue can be selected depending on the available materials and their dielectric properties. Figure 7.2a presents the case for conductivity while

7.2b presents the case for relative permittivity. In conclusion, the modeling results provided in this chapter indicate a platform to analyze the effect of compartmentalized dielectric characteristics in biological systems, and strengthen the dissertation's modeling platform as presented in milestone questions 6.3.2, and 6.3.3. This paves the path to the realization of milestone question 6.3.4 by validating the behavior of the electric field in complex biological systems.

Chapter 8. *In Vivo* Gene Electroporation for Implantable Glucose Biosensor

8.1. Introduction

The driving force for this research, milestone 6.3.4, is to investigate the implementation of electroporation as a transport mechanism to improve the long-term function of an implantable glucose biosensor. It is addressed with an increased understanding of the dependence on dielectric properties of tissues in frequency and the impact of electric fields on target cell membranes. This chapter presents electric field modeling and simulation work that supports the design of an applicator and protocol, and their combined implementation to effectively target the tissue of interest at the moment of implantation, as a preemptive approach. Specifically, pulses of high electric field magnitude in the proximity of the biosensor implantation site will allow localized transfection of genes in surrounding cells. A model that addresses the magnitude and distribution of these electric fields is needed for this purpose. This study began with the model assisted examination of applicator design options and culminated with the *in vivo* testing of a selected design.

8.2. Applicator Design

Models were developed to generate juxtaposition of applicator and target tissues. Three dimensional geometries were generated for these models. These

Table 8.1. Electrical parameters used in numerical modeling.

Subdomain Group	Conductivity (σ, S/m)	Relative Permittivity (ε)
Electrodes	1.12e7	1
Tissue	0.5	80

3D models were used to select the best electrode configuration, and then to assess the magnitudes of the electric fields at the target tissues. The selection process was intended to maximize the electric field exposure of the target tissues while minimizing its impact on non-interest tissues. The 3D models were developed using the Generalized Electric Fields application mode in COMSOL Multyphysics; as it allows utilization of both permittivity, and conductivity properties of materials. The materials represented in the model were collected into two groups that define the subdomains. The first, represented conductive materials, and the second, represented the tissue of the animal where the electric fields are to be applied. The electrodes were modeled as inactive domains and had boundaries that represented either a potential, or ground. The COMSOL multiphysics subdomain assignments are shown in Table 8.1.

Table 8.2. Boundary conditions in 3D electrode system 3D models.

Boundary	Two surface electrodes	Cannula as electrode
Tissue – Surface Electrode	Ground	Surface electrode broken in two: One is ground, the other is at a Potential
Tissue – Cannula	Applied Potential	Continuity
Tissue – Air	Insulation	Insulation

Boundary conditions were required to represent physical conditions at the interface between subdomains. At the interface between electrodes and tissue, the boundary conditions selected either describe an applied voltage, a ground condition (V=0), or a continuity in the case of the cannula when it has no applied field. Any outer boundary is represented as an inhibition to normal current flow. Table 8.2 summarizes the boundary conditions for the applicator design models.

The finite element meshing for the models used 140,766 and 138,530 tetrahedral elements for the cannula electrode model and the two surface electrode model, respectively. The number of elements represents a balance between the minimal number of elements required to solve the equations and limited computing power. Both models were solved using the generalized minimum residuals (GMRES) linear system solver and algebraic multigrid conditioner [104]. Post-processing of data was used to calculate and analyze electric field maps that generated estimations of the distribution of electric fields at the electroporation region within the rat tissue.

Two electrode configurations (illustrated in Figure 8.1 and 8.2) were the subject of model calculations. In the first model, depicted in Figure 8.1, two surface electrodes (shown in blue) are used to apply electric fields at the site of implantation. In this design, the cannula (in green) only serves to insert the implantable biosensor in the subcutaneous tissue while insulating the implantable biosensor from the applied electroporation pulses. The cannula in this case is not an active electrical component. The simplified 3D shape of the targeted tissue is shown in gray.

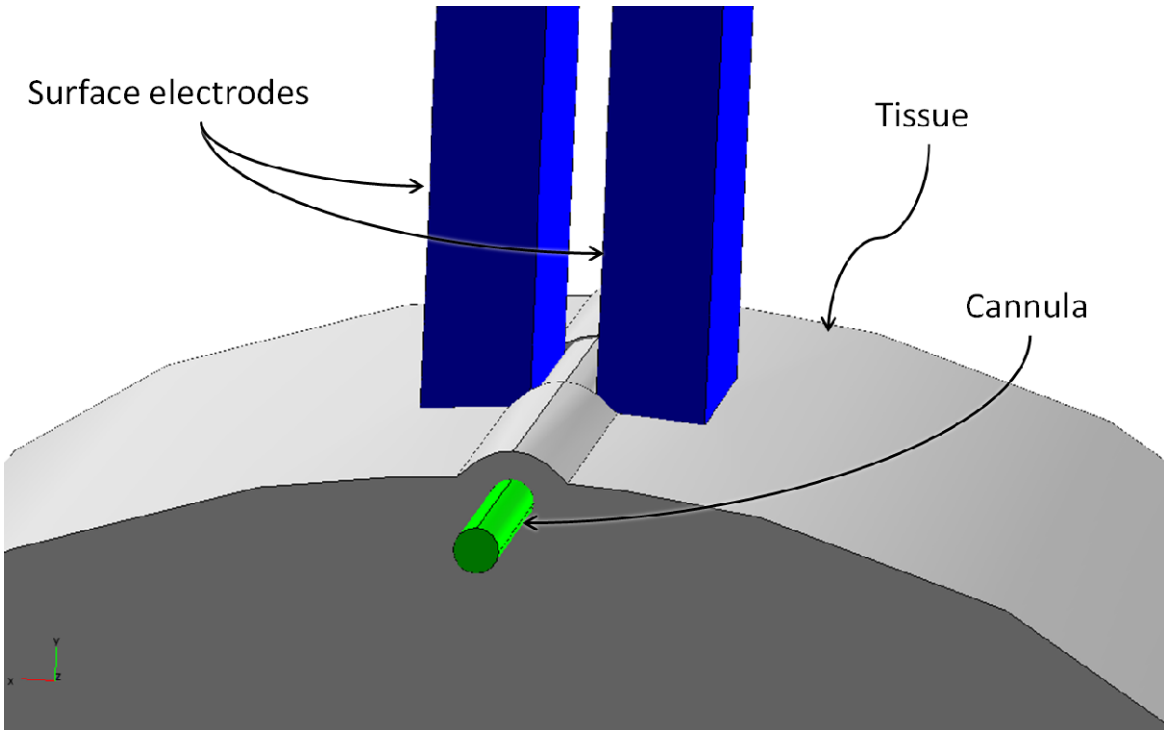

Figure 8.1. Two surface electrode model.

In the second electrode configuration, shown in Figure 8.2, the cannula (in green) used to insert the biosensor serves as an electrode used in the electroporation process. The counter electrode is a surface electrode on the skin of the animal (in blue), covering the area on the surface of the implantation site. Again, the simplified 3D shape of the targeted tissue is shown in gray. The implantable biosensor can be inserted after or before the pulses are applied, as long as the sensing element is positioned at the required electroporation site.

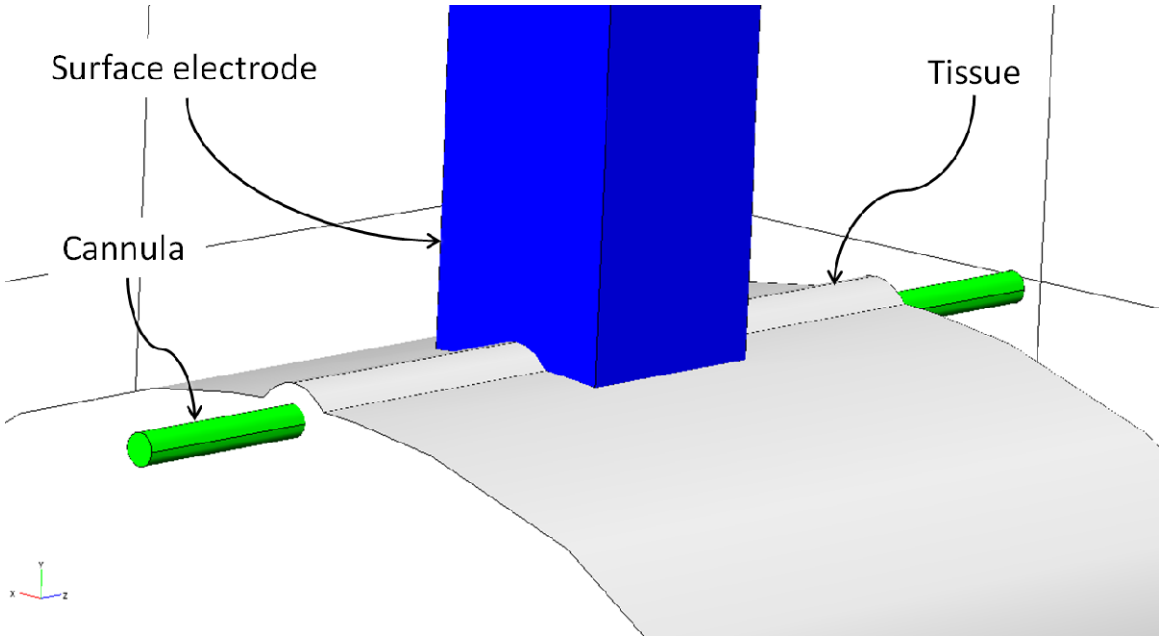

Figure 8.2. Cannula and single surface electrode model.

The two electrode configurations were evaluated using a nominal applied electric field of 1,250 V/cm. The model predictions of electric field distribution for both electrode configurations are shown in Figure 8.3. This information provides insight as to which electrode configuration option best matches the biosensor surgical implantation protocols and provides the most favorable electric field distribution in the volume surrounding the implantation site. The configuration with the two surface electrodes (Figure 8.3a) had field intensity in excess of 5,600 V/cm at the electrode-skin interface and an average electric field intensity of 1,400 V/cm within 0.5mm of the cannula. The electrode configuration that uses the cannula as an electrode had maximum electric field intensity of 2,500 V/cm at the electrode-surface interface and an average electric field intensity of 2,000 V/cm within 0.5mm of the cannula. By this measure, the electrode configuration using the cannula as an electrode provided a reduction of electric

field intensity of 56% at the skin-electrode interface, while provided an average electric field intensity in the immediacy of the implantation site that is 43% higher than that of the two surface electrodes.

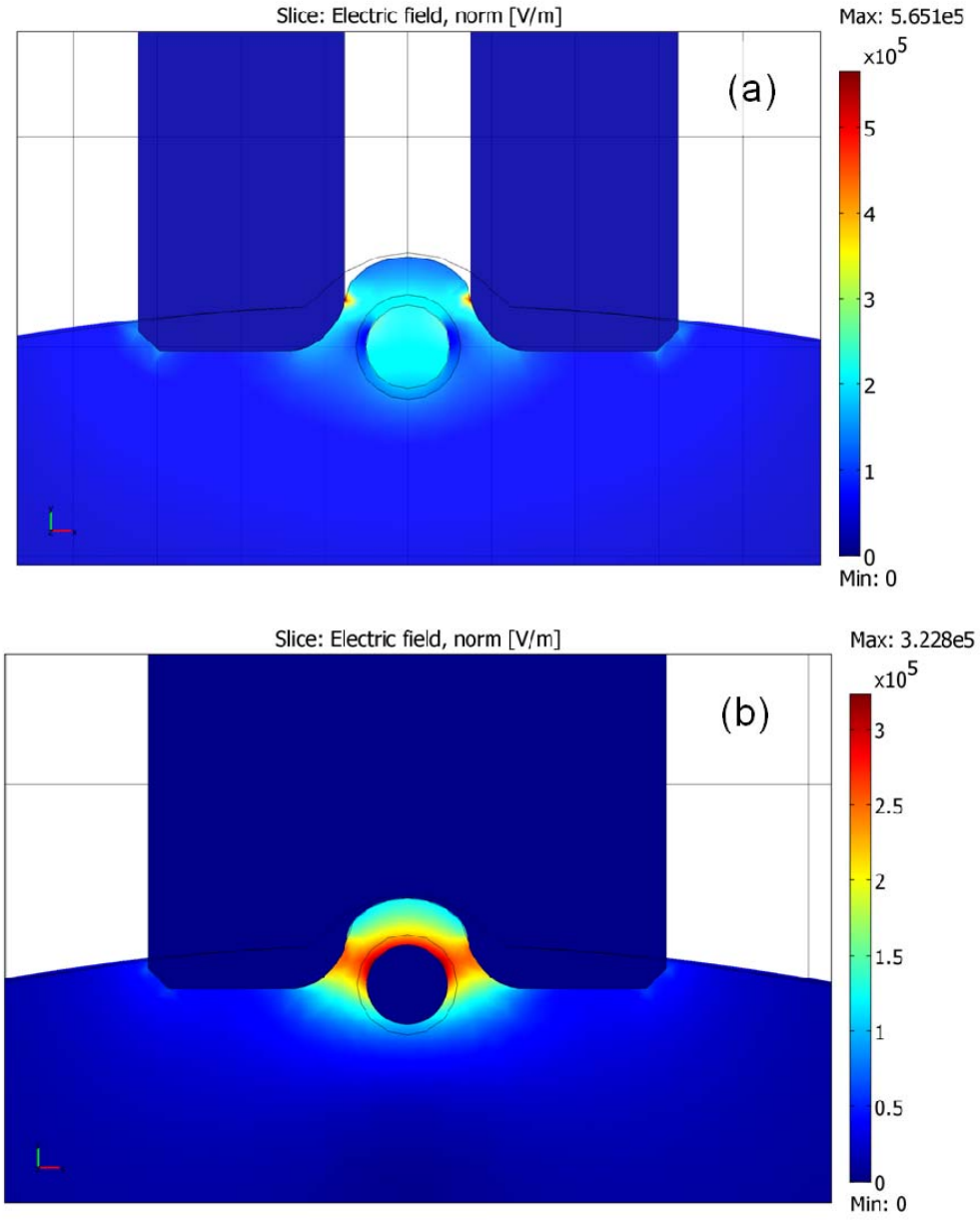

Figure 8.3. Cut plane of the electric field map from a 3D simulation of the electroporation applicator for both cases.

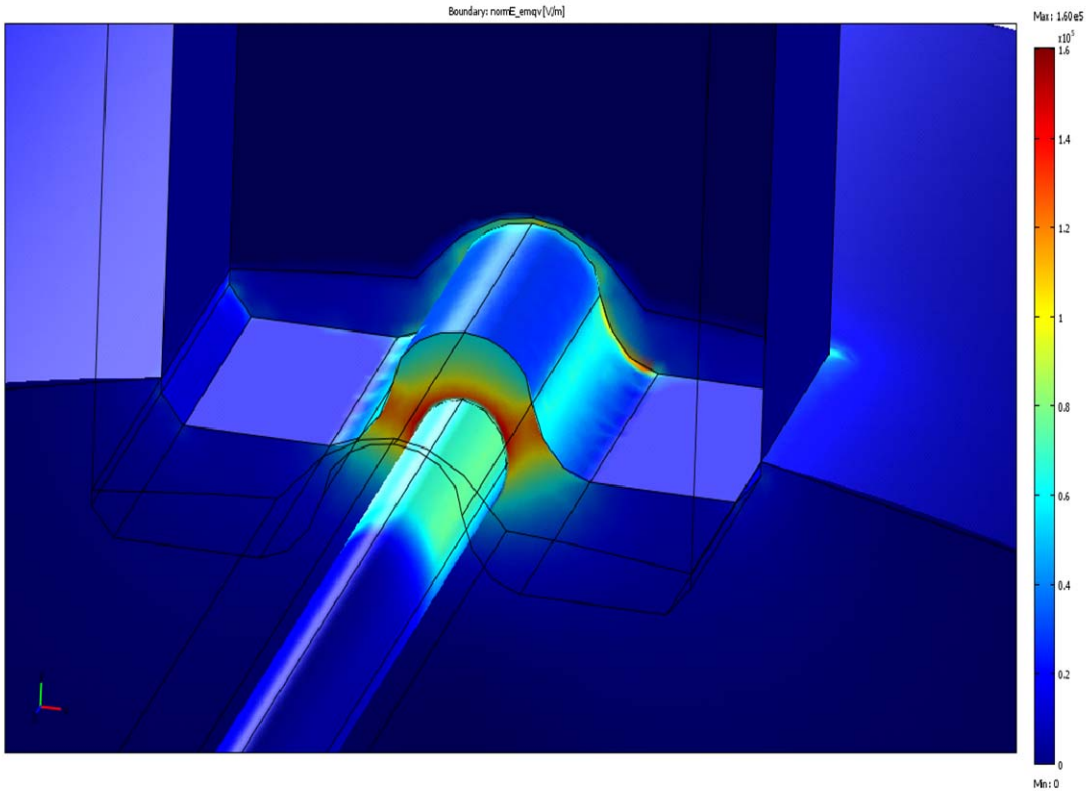

Figure 8.4. Electric field intensities from post-processing output of finite element analysis model.

Figure 8.4 indicates the cannula applicator model from a 3D perspective. The results also provided information about field distributions along the cannula and was used to ensure that such field intensities were kept within the confines of the implantation site. The 2D representations in 8.3 are a cut through the mid section of the surface electrode.

8.3. Protocol Development

The delivery protocol developed is summarized in section 3.1.1. The *in vivo* imaging analysis provided useful information in the determination of effective

electroporation parameters, and time (in days) for maximum expression. The totality of the expression results from the IVIS imaging system on control and experiment animals are presented in Figure 8.5. From this data, the effective magnitude of the electric field can be estimated between 1,250 and 1,750 V/cm (Figure 8.5) with a maximum expression between 8 and 15 days (Figure 8.6).

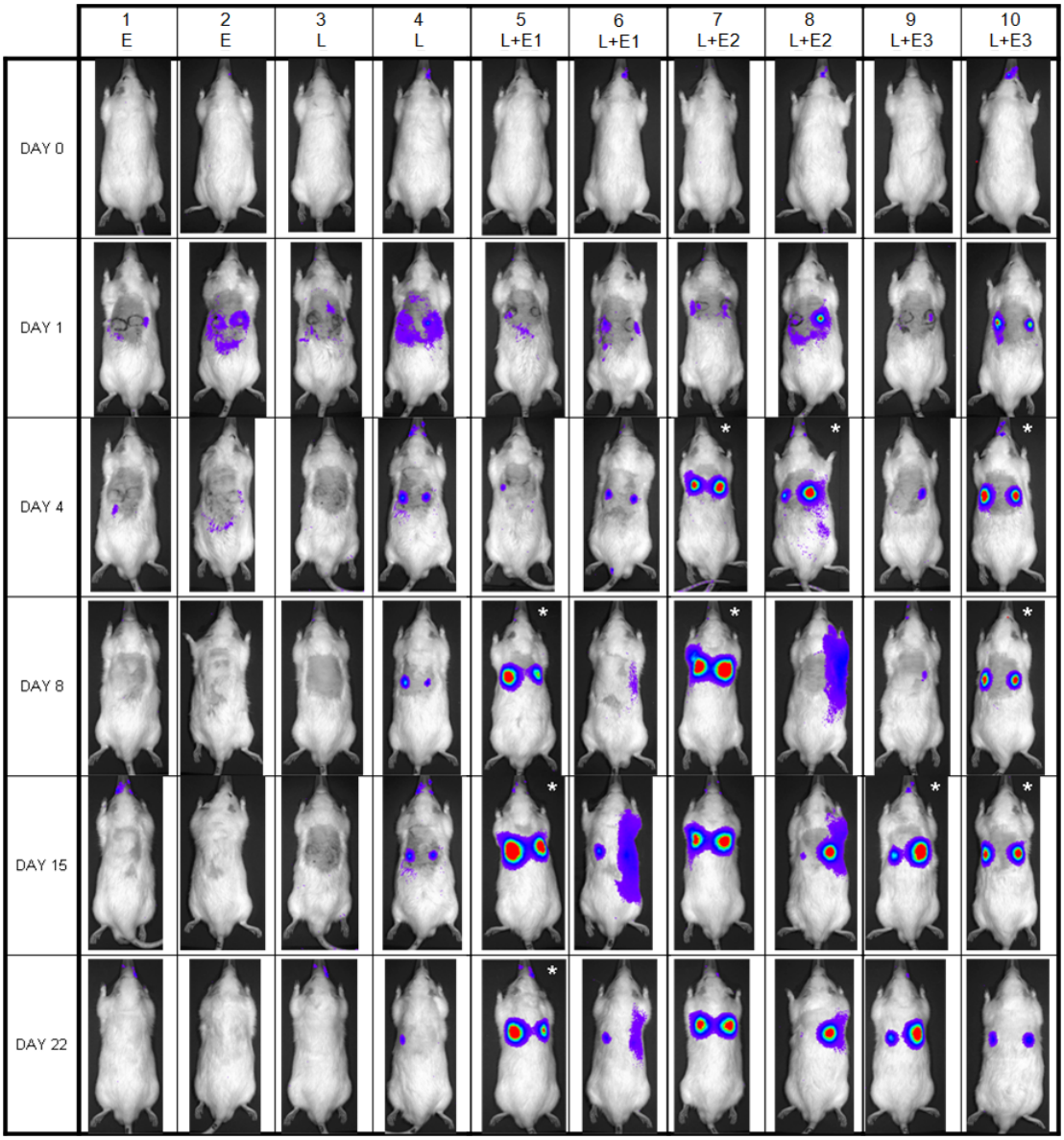

Figure 8.5. Bioluminescent results for rats in groups for days 0, 1, 4, 8, 15, and 22.

The results from bioluminescence expression are provided graphically in Figure 8.6. The graph's vertical axis is photon flux (photons/sec/cm^2), the horizontal axis is in days (0, 1, 5, 8, 15, 22). The plotted lines represent selected experiments electric fields in axis (E = electroporation only control, L = Luciferase only, L+E1 = 750 V/cm electroporation, L+E2 = 1,250 V/cm, L+E3 = 1,750 V/cm. Points with a star (*) represent results which are statistically significant ($p<0.05$) from the control.

The *in vivo* delivery of reporter genes provided the necessary information to select a single electroporation parameter and improve the technique to effectively deliver genes in the subcutaneous tissue. For the *in vivo* delivery of future neovascularization factors coding plasmids, a single electroporation parameter was chosen as 1,250 V/cm, 150μs, and 4 pulses separated by 1 a second delay. The same concentration of 2 mg/ml of plasmid in saline solution was used and two different volumes were tested, 50 μL and 100 μL. Using the information gathered from the previous study the plasmid injection technique, a very critical step of the protocol, was improved in order to ensure that the plasmid solution is at the targeted subcutaneous site before the electric field that supports electroporation was applied.

Regarding other studies that use electroporation protocols in cutaneous tissue, Colman et al. 2004, reports maximum Luciferase activity at 14 days post electroporation in cutaneous wound border (intradermal). In this study, 50μL of 2 mg/ml (100 μg) gWiz plasmid was used and different parameters were tested to find the most effective protocol [105]. A later study (Lin et al., 2006) found that

luciferace expression resulting from intradermal injection was 63-fold higher than that for subcutaneous injections. However, the pin electrode used in both of these studies was designed for intradermal and not subcutaneous delivery of plasmids [106]. In the case of the cannula and surface electrode configuration used in this chapter, the electrode was used for subcutaneous electroporation.

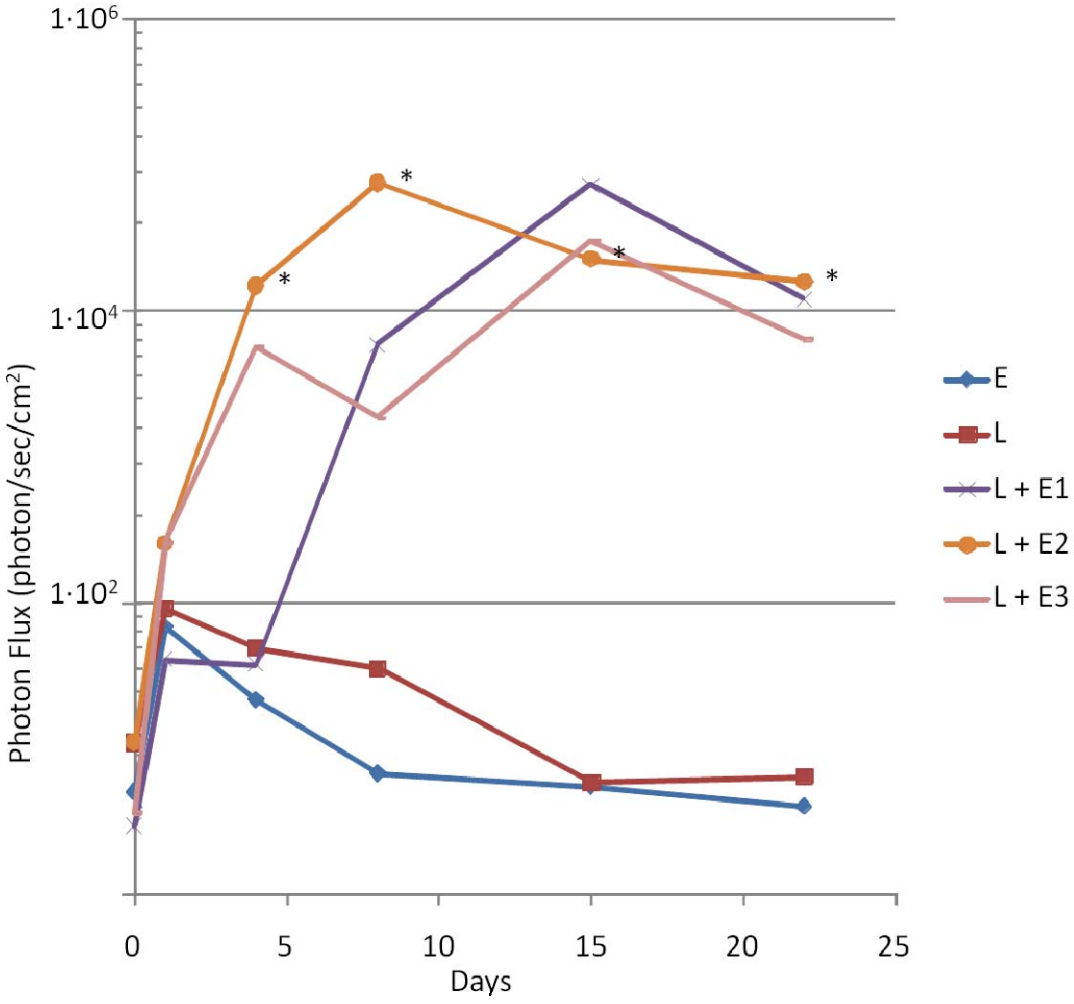

Figure 8.6. Selected electroporation parameters and progression in time of gene expression.

The modeling and experimental results from this chapter provide information needed to improve the electroporation protocol, select electroporation parameters, and estimate the expression chronological profile for plasmid DNA for subcutaneous tissue in rats. This information allows the estimation of the timing at which neovascularization factor expression occurs, as long as its expression profile is similar to that of the Luciferase plasmid used here. This chapter provides a protocol to deliver plasmid DNA to the site of an implantable biosensor at the time of implantation, in fulfillment of the preemptive approach as presented in Chapter 5 and milestone 6.3.4.

Chapter 9. Focusing of Electric Fields for Electroporation

9.1. Introduction

The distribution of the electric field intensity generated for electric field mediated therapeutic agent delivery is dependent upon many factors including electrode geometries, electrical characteristics of tissue, and electric pulse parameters. A typical electrode configuration used for electroporation purposes has higher electric field intensity closer to the electrodes; this creates electric field gradients that produce regions with different cell permeability [4]. As the models presented in Chapter 8 suggest, electrode configuration greatly impacts the location and distribution of such regions.

The impact the electric field has on cells inevitably depends on the magnitude of the applied potential between the electrodes. As discussed in section 4.1, the application of pulses might result in areas with higher electric field intensity where some cells die due to irreversible permeability, increased Joule heating, or local electrochemical effects. In electric field mediated drug and gene delivery, the objective is to maximize the regions with appropriate electric field intensity defined between regions with irreversible electroporation and no resulting cell permeability.

The ability to focus electric field intensities at target regions should provide a means to deliver the appropriate electric field intensity to a target site while

reducing the required applied nominal electric field. A lower applied nominal field should result in reduced localized adverse effects at the electrode-tissue interface. Electric field focusing is a phenomenon that results from the insertion of an object in the path of an electric field in an otherwise isotropic media. As suggested in section 4.4, an object with electrical characteristics sufficiently different than those of the media will induce localized zones of high and low electric field magnitudes in its vicinity. Figure 9.1 demonstrates this phenomenon as part of an *in vitro* feasibility study that has been published with the experimental details provided in section 3.2.1 [107].

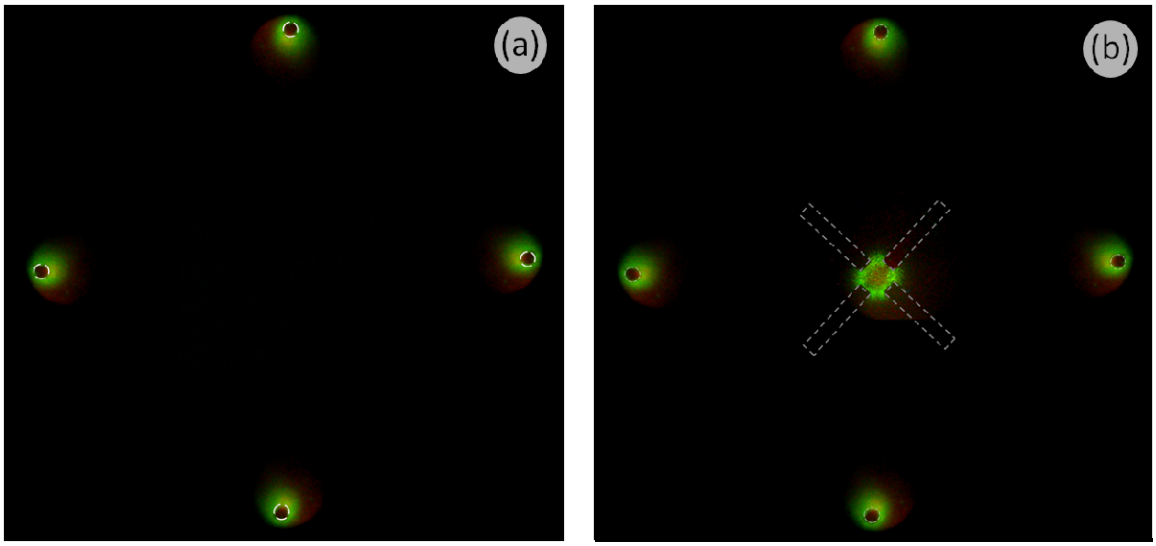

Figure 9.1. Image compositions from an electric field focusing feasibility study.

The figure shows electric field focusing in a 2-dimensional dish. The nominal field strength did not produce significant calcein uptake (Figure 9.1a). However, as is visibly evident in Figure 9.1b, the case with the field focusing element (four rectangles arranged in an “X” shape) caused amplification above a threshold that allowed increased uptake of the fluorescent dye. This

phenomenon has also been used *in vitro* by Golan et al. in a microfluidics application to transport cells using dielectrophoretic forces resulting from electric fields focused by floating electrodes. In this dielectrophoresis application, erythrocytes accumulated on the surface of the floating electrodes by following the gradient towards higher electric field intensity [108, 109].

9.2. Electric Field Focusing Model Predictions

The clear evidence of field focusing presented in Figure 9.1 generates the rational to develop a model to study the phenomena, as well as two additional concepts developed in the course of this dissertation which indicate the complexity of the assignment. The first consideration, as discussed in Section 4.3 is the fact that the energy associated with an electroporation pulse can be analyzed based on its frequency components. The second consideration materializes from the exploration of milestone question 6.3.3. As indicated in Chapter 7, the model prediction confirmed independent experimental evidence that conductivity and permittivity also influence the effect of an applied field as the frequency components of such field are swept across the frequency spectrum. Thus, a viable model that will predict the local electric field intensity due to the field focusing effect of an object in the field must include pulse frequency in conjunction with exposed media conductivity and permittivity.

Because of the predominantly low frequency content of the pulsed electric fields used for *in vivo* electroporation applications, and the dielectric nature of tissues, the assumptions in section 4.3.1 apply. Under such conditions,

conductivity and permittivity are the parameters of biological materials commonly used to describe applied electromagnetic phenomena [110]. To represent the effects of electric field focusing at the scale of the implant, COMSOL Multiphysics' axial symmetry and three-dimensional geometric descriptions of features were utilized.

With the purpose of comparatively representing how electric fields are focused by microspheres used in the experimental section of this chapter, electric field intensity (E) in the model was divided by the applied nominal electric field (V_0/d). V_0 corresponds to the applied voltage, and d to the distance between the parallel plates used to apply the potential across the tissue section in the model. The resulting ratio (E*) is the non-dimensional electric field intensity which is presented in equation 9.1. In the absence of microspheres, the non-dimensional field intensity values are evenly distributed in the geometric volume. In the presence of microspheres, these intensity values vary as they are focused in specific regions of the geometry.

$$E^* = \frac{E}{V_0/d} \tag{9.1}$$

Modeling results show that polystyrene microspheres embedded in tissue exposed to an electric field generate focusing of the field that is related to geometric variables and material characteristics of the microspheres and tissue. The two principal material characteristics used in the models are conductivity and relative permittivity. They are both significant in focusing electric fields, however, their significance is dependent on the frequency of the applied electric field; this frequency dependence will be discussed later in this chapter.

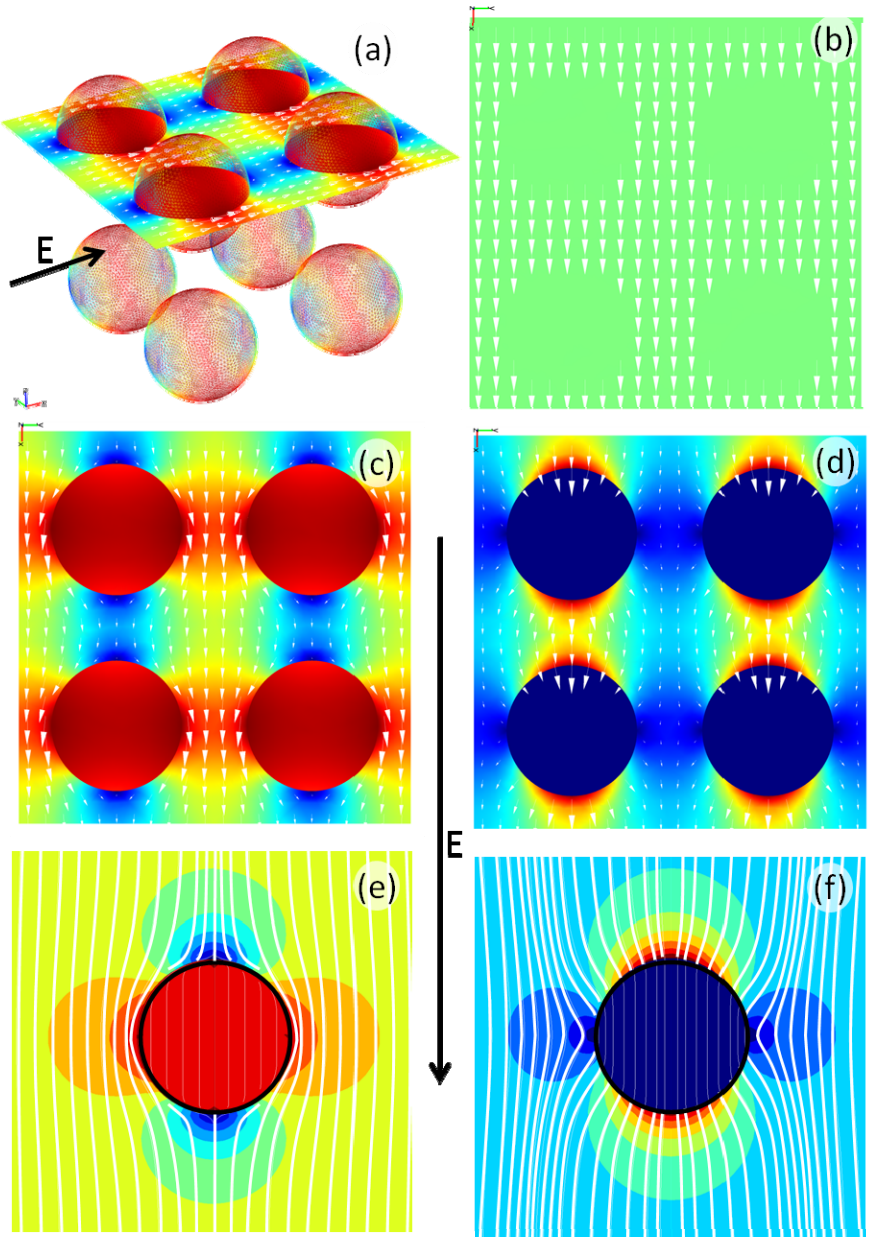

Figure 9.2. Representation of electric fields as they are modified by spheres in the media.

Figure 9.2 is a collection of visual depictions of the electric field focusing phenomena and how the contrast in dielectric characteristics (conductivity and permittivity) of the microspheres and the surrounding media creates gradients of the electric field in the media. Figure 9.2a is a 3D representation of tissue with

multiple microspheres. Figures 9.2b, 9.2c, and 9.2d show three different cases in a simplified view of a slice of electric field intensities in a plane on the upper spheres in 3D representation in 9.2a. Figure 9.2b. represents the case in which microspheres have the same dielectric properties as tissue; in this case, the field is not focused, thus the non-dimensional electric field intensity value is 1 throughout the volume. In the case where either the conductivity or the permittivity are lower than the tissue (Figure 9.2c), the focusing effect generates higher electric field intensities in the vicinity of the microspheres that arranged transversally to the direction of the applied field. The direction of the electric field vectors on the plane (white arrows) are approximately tangential to the surface of the microspheres. This case is similar to that of analogous flow of fluid around an obstacle presented in Figure 4.3. Alternatively, the case in which microspheres have either higher conductivity, or higher relative permittivity than the media (Figure 9.2d), the higher intensities of the electric field focus parallel to the direction of the applied field. In this case, the direction of the electric field vectors (white arrows) on the plane steer normal to the surface of the microspheres.

Figures 9.2e and 9.2f show pseudocoloring depicting electric field focusing around single spheres which have an electric field applied in the direction of the large arrow pointing down. Figure 9.2e shows the case in which either conductivity or relative permittivity are lower than that of the surrounding media; white streamlines represent electric field lines around the spheres. The analytical solution to the case presented in Figure 9.2e is presented by Cole et

al. 1964 and is presented section 4.4 of this work as well [111]. Figure 9.2f presents the case in which the conductivity or relative permittivity of that sphere is considerably higher than the surrounding media. The way in which electric field intensity is focused depends on how marked the contrast of dielectric characteristics are from the microsphere to the media. In the case of this example, the microsphere being a perfect conductor, and the media a material of very low conductivity, the electric field streamlines become close to normal to the surface of the microsphere.

Although the experimental portion of this work is limited to using polystyrene microspheres, it is possible to estimate by way of numerical modeling the potential electric field focusing effect that different materials may have if they are embedded in tissue. Figure 9.3 shows analysis of non-dimensional electric field maxima for several material cases in Table 9.1. Figure 9.3a uses pseudocoloring to present higher magnitude electric fields focused in the longitudinal direction (represented in red and the letter 'L') with respect to the microsphere, and focused in the transversal direction (represented in red and the letter 'T') with respect to the microsphere. Non dimensional electric field intensities for polystyrene microspheres which are used in the experimental section of this chapter are presented in Figure 9.3b. Polystyrene has lower conductivity ($1.0 \cdot 10^{-16}$ vs. 1 S/m for tissue) and lower permittivity (4 vs. 65 for tissue) when compared to tissue. The blue line in Figure 9.3b represents the

field focused in the transversal direction to the direction of the applied electric field. In the low and high frequency regions (horizontal axis), the non-

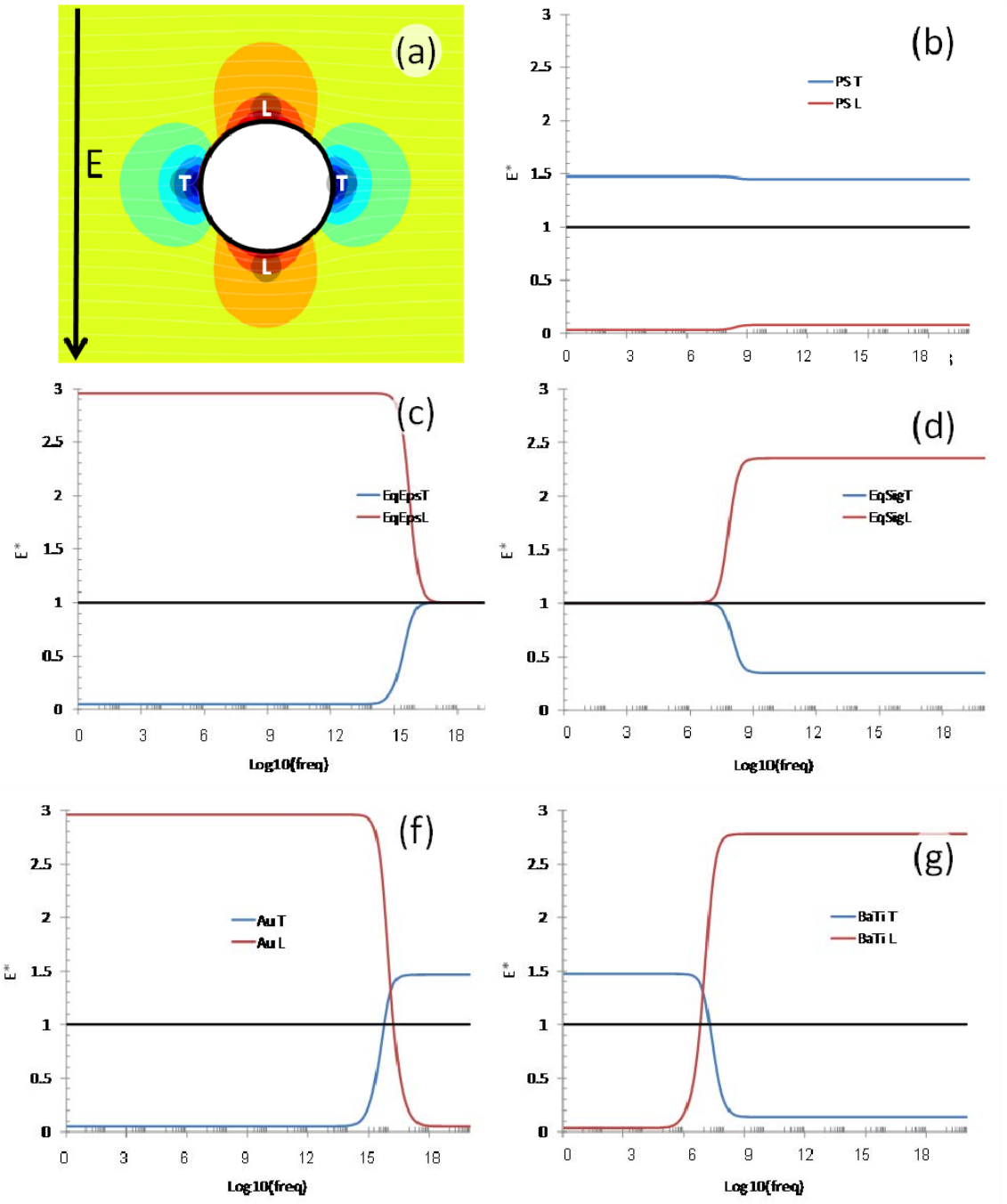

Figure 9.3. Microsphere subjected to electric field 1 V/cm, and electric field intensity behavior depending on material and frequency.

dimensional electric field in the tissue is increased by a factor of about 1.5X (vertical axis).

Figure 9.3c presents the case of an idealized material that has higher conductivity ($4.5 \cdot 10^7$ vs. 1 S/m), but the same permittivity as tissue. In this case, the electric fields are focused in the longitudinal direction by a factor of about 3X, represented by the red line. This idealized higher conductivity material has a focusing factor that is restricted to the lower portion of frequencies; the frequency about which the transition occurs is here defined as the transition frequency, and represented in Table 9.1 as f_T. The transition frequency for this idealized high conductivity and same permittivity material is about $1 \cdot 10^{16}$ Hz. The focusing effect of the difference in conductivity is only in effect under this transition frequency. Thus, the difference in conductivity between the microsphere and the tissue has a focusing effect only under this transition frequency.

Figure 9.3d presents the case of an idealized material that has higher relative permittivity ($2.0 \cdot 10^3$ vs. 65), but the same conductivity as tissue. In this case, the electric field intensities are focused in the longitudinal direction by a factor of about 2.4X, represented by the red line. This idealized higher permittivity material has a focusing effect that is restricted to the higher portion of frequencies above the transition frequency of $2 \cdot 10^7$. The transition frequency for the idealized high conductivity material (in Figure 9.3c) is considerably high, well above frequency components of electroporation pulses and the approximations used for this model. In contrast, the transition frequency for the idealized high

permittivity material (in Figure 9.3d) of $2 \cdot 10^7$ Hz is well within the range of frequencies considered in the approximations presented in section 4.3.1.

Table 9.1. Microspheres of different materials and their potential electric field focusing effect.

Material	σ (S/m)	ε_r	E* max. (l.f)	E* max. (h.f.)	f_T (Hz)
Polystyrene [112]	$1.0 \cdot 10^{-16}$	2.6	1.49	1.47	~ $2 \cdot 10^8$
Conductivity and Permittivity are same as tumor tissue [113]	1.0	65.0	1.00	1.00	-
Conductivity different than tissue	$4.5 \cdot 10^7$	65.0	3.00	1.00	~ $1 \cdot 10^{16}$
Permittivity different than tissue	1.0	$2.0 \cdot 10^3$	1.00	2.57	~ $2 \cdot 10^7$
Gold [112]	$4.5 \cdot 10^7$	1.0	3.00	1.44	~ $1 \cdot 10^{16}$
Barium Titanate ($BaTiO_3$) [114]	$1.0 \cdot 10^{-10}$	$2.0 \cdot 10^3$	1.49	2.57	~ $2 \cdot 10^7$

Figures 9.3f and 9.3g represent the case of gold (Au) and barium titanate ($BaTiO_3$) respectively. In both cases, there is electric field focusing arranged in one direction, which reverses at the transition frequency. The case of the gold presented in Figure 9.3f is similar to the idealized high conductivity material model, with the addition of the reversal in focusing effect. In the case of gold, electric field intensities are focused by a factor 3X at lower frequencies in the longitudinal direction (red line), and are focused at 1.5X at higher frequencies, but in the transversal direction (blue line). Barium titanate, a ceramic with high relative permittivity, presents a case in which the electric field focusing is higher at high frequencies (~2.6X) than at low frequencies (~1.5X); the longitudinal and transversal focusing of fields is inverse to that of gold.

The cases presented in figures 9.3f and 9.3g are of particular interest because of the reversal of the direction of the focusing effect (from longitudinal to transversal, or transversal to longitudinal directions) as frequency changes from low to high. Figure 9.4 presents a three dimensional representation of electric field focusing for a microsphere of a material similar to barium titanate, which has lower conductivity, but higher relative permittivity than tissue. Figures 9.4a and 9.4b correspond to the frequency range below the transition frequency, and figures 9.4c, and 9.4d represent frequencies above this value. The focusing effect is represented by a volume enclosing the non-dimensional electric field intensity higher than 1.1 with a red surface (figures 9.4b, and 9.4d). Focusing in the transversal direction has a “toroid” like shape (Figure 9.4b), while the focusing in the longitudinal direction has an hourglass or dual spheroid shape (Figure 9.4d). This is for the case of a spherical object in the electric field; other geometries will focus the electric field in different ways. Note that the streamlines at lower frequencies are almost tangential to the surface of the microsphere (Figure 9.4a), streamlines at higher frequencies tend to become normal to the surface of the microsphere (Figure 9.4c). This frequency dependant transition effect in electric field focusing brings an opportunity of focusing electric fields that will be briefly discussed in Chapter 9.

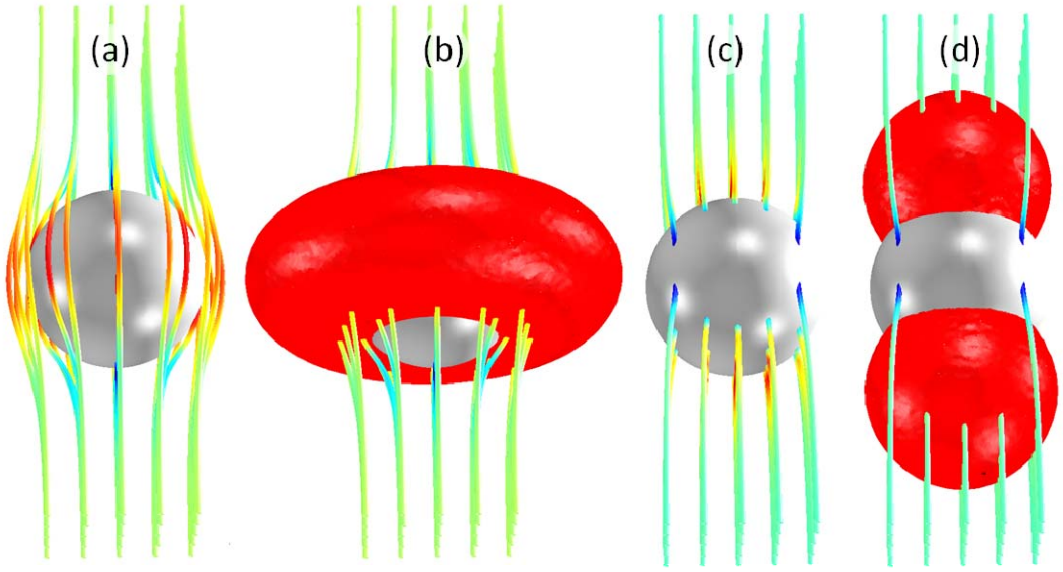

Figure 9.4. 3D rendering of electric field focusing on a single microsphere.

As briefly presented in section 4.6, the focusing effect of a single microsphere is modified when more microspheres are in close range. The simplest example of the effect of multiple spheres is that of two spheres within an electric field. The results from such a numerical model are depicted in Figure 9.5. As two microspheres are brought closer together, the focusing of the electric field intensity between them is amplified. Figure 9.5a shows a graph of the numerical results of two microspheres approaching. The horizontal axis represents the cross section distance to the edge of each sphere. Figure 9.5b shows two spheres separated, and pseudocoloring of the non-dimensional electric field. In Figure 9.4a, the vertical axis represents the non-dimensional electric field between the two spheres. The dark green U shaped curve at the bottom of the 9.4a is that of two spheres separated by a distance equivalent to 2 diameters (2φ); in this case, the focusing factor has a high value of 1.5X at the

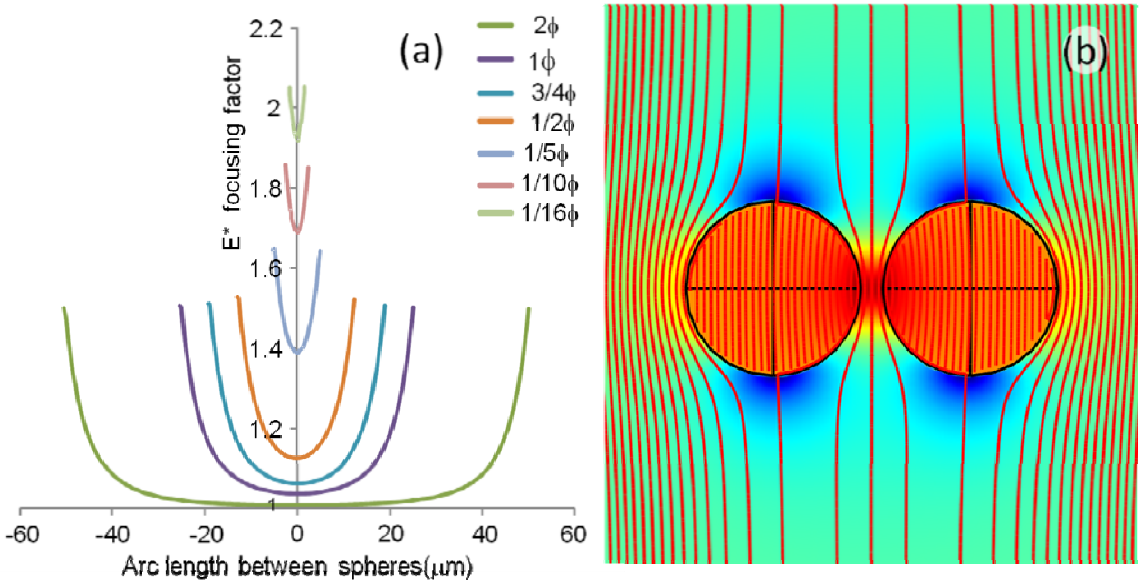

Figure 9.5. Numerical results of electric field focusing due to two microspheres.

surface of the microsphere that drops to 1X (no focusing) at the center point in between the two spheres. The other case in which the separation between microspheres is 1/16 diameters (light green line shaped as a small v) at the top of the graph has a high value of 2.05X and a low value of 1.95X. These results show that as spheres are closer together, there is a magnification of the focusing effect. The presence of more than two spheres, or groups of spheres has the potential to further increases the magnification shown in Figure 9.5.

9.3. Electric Field Focusing Model Experimental Verification

9.3.1. *In Vitro* Electric Field Focusing Model Verification

As an initial test for the electric field focusing model, the first assignment was to produce a modelled electric field intensity view of the experimental results shown in Figure 9.1b. For visual comparison convenience, these results are

shown in Figure 9.6b. Various model verification perspectives are also provided in the figure.

The control experiments equivalent to the geometries in the control simulation (Figure 9.6b) did not exhibit calcein fluorescence in the center of the cell culture dish. The actual control experiments shown in Figure 9.1a did not use the rectangular elements, described in Figure 3.5, at the center of the dish. Results from control experiments only showed fluorescence due to electroporation only at the electrodes. This is another indication that the electric

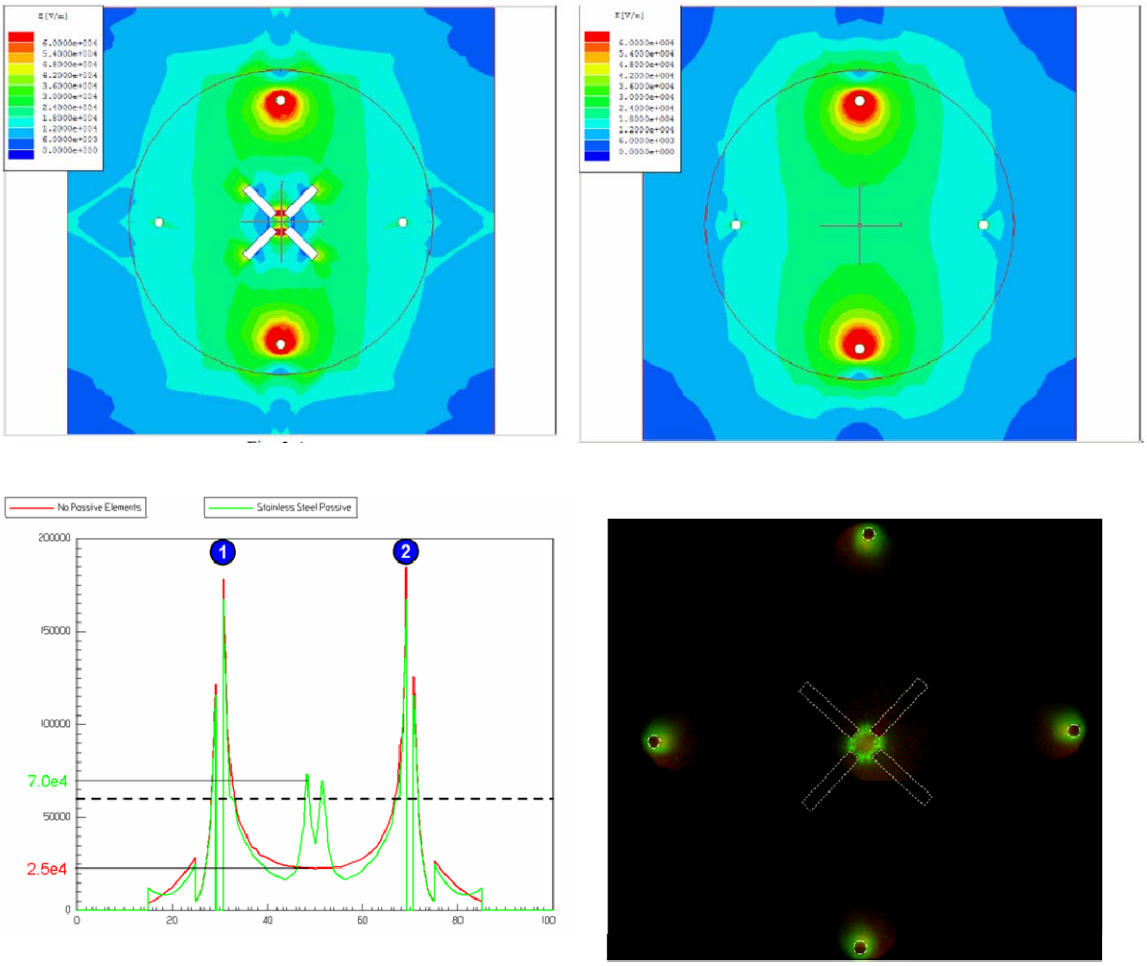

Figure 9.6. Results from *in Silico* models and *in Vitro* experiment. Reproduced with permission from IEEE.

field mediation effect that promotes electroporation was present concentrated at the electrode. However, the inserted rectangular objects altered the electric field intensity in proximity of such objects and promoted electroporation at the center of the dish.

The experiments that included the rectangular focusing elements in the center of the dish (Figure 9.6d) produced a picture similar to those projected by computer simulation that included these elements (Figure 9.6a); that is, the presence of the non-grounded rectangular stainless steel geometries in the center of the dish redistributed the electric fields and created a focusing effect that raised the electric field above the threshold for electroporation and resulting transport of calcein inside the cells in the dish. The threshold was defined as 600 V/cm for the system in the simulation, and is shown in Figure 9.6c as a horizontal dashed line. Figure 9.6c is cross section graph that depicts the values (vertical axis) of electric field intensities across the dish. The green line in Figure 9.6c represents the electric field intensities for the case of Figure 9.6a (focusing experiment), and the red line represents those of Figure 9.6b (control). The mentioned field focusing effect produced adequate electric field mediated calcein delivery to demonstrate effective EP at the center of the cell culture dish in the *in vitro* experiments (Figure 9.6d). Furthermore, for the rectangular elements when compared to the control (Figure 9.5b), the simulations show that the redistribution of electric fields lowered the electric field magnitude peaks near the electrodes. This will provide the additional benefit of reducing possible field related cell and tissue damage generated by the activated electrodes.

9.3.2. *In Vivo* Electric Field Focusing Model Confirmation

Fluorescent imaging analysis of dye electroporation experiments provided qualitative and quantitative information on microsphere distribution and dye uptake that coincides with electric field focusing expectation. SYTOX® green is a nucleic acid stain that will stain cell nuclei of both reversibly electroporated and irreversibly electroporated cells. Figure 9.7 shows an image at two different scales of such results. Figure 9.7a shows about a fourth section of a tumor with the periphery of the tumor delineated by a darker region on the left, and bottom of Figure 9.7a. Figure 9.7b shows a magnified section (red square) of Figure 9.7a. The green pseudocoloring superimposed on the optical image (in gray) shows nuclei that have higher fluorescence due to Sytox® Green dye that penetrated the cell nucleus and stained the DNA.

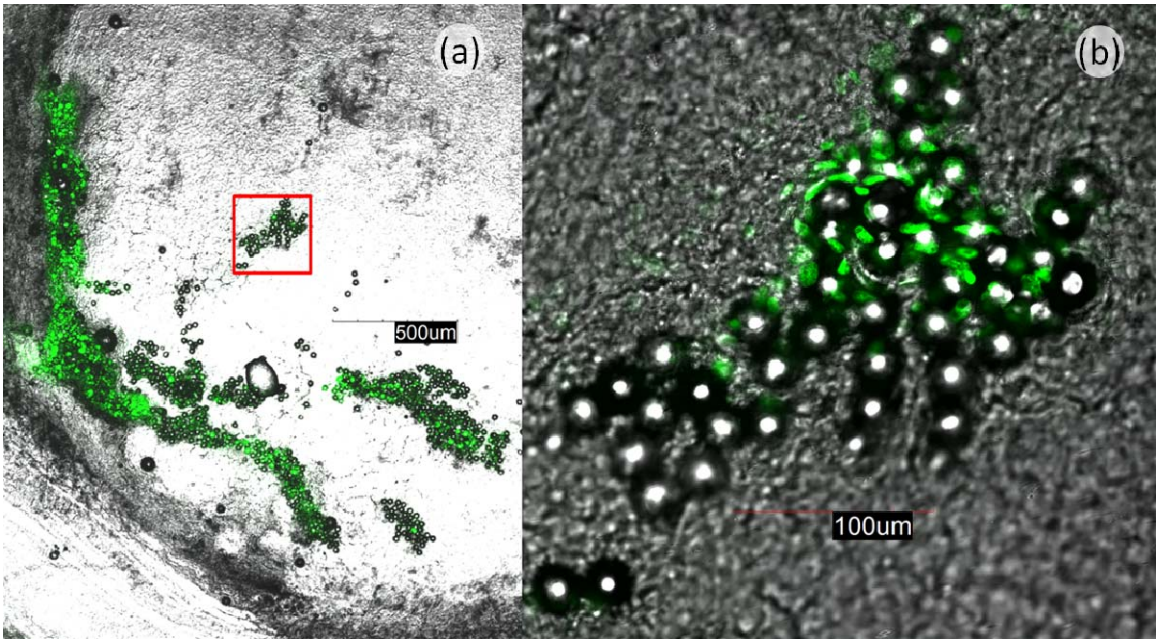

Figure 9.7. Microscopic view of Sytox Green uptake in melanoma tumor cells. Bars with length in μm show scale.

Visual analysis of lower resolution (3 mm field of view) fluorescent and optical composite images of tumors such as shown in Figure 9.7a provided a qualitative distribution of microspheres. In most images analyzed, it was observed that microspheres tended to concentrate in the periphery of the melanoma tumor. Analysis of higher resolution fluorescent images such as that shown in Figure 9.7b provided visual information about distribution of fluorescence intensity.

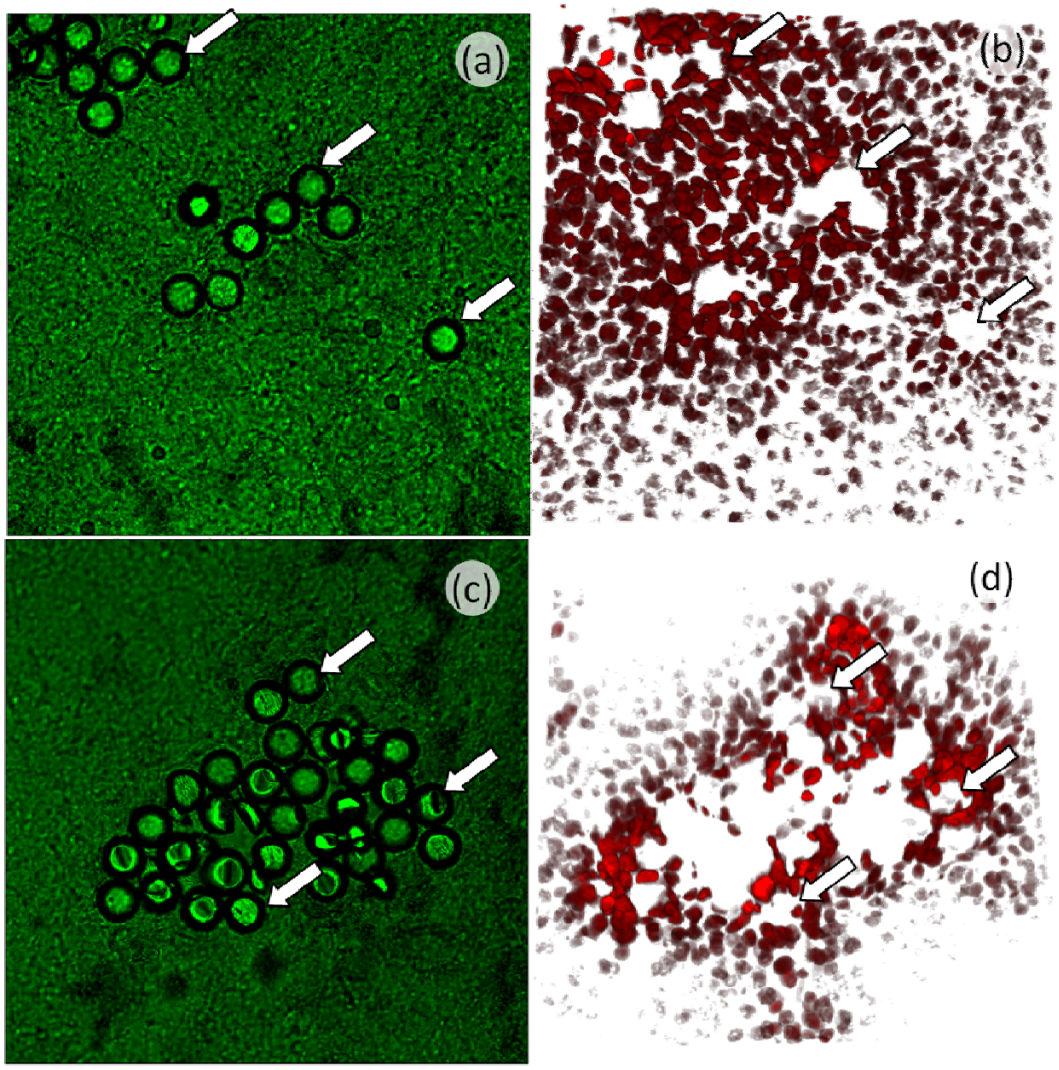

Figure 9.8. Optical and fluorescent images of microspheres in tissue section.

Figure 9.8 provides additional images from the fluorescent dye experiment. Figures 9.8a and 9.8c show optical images of the microspheres. Figures 9.8b and 9.8d are fluorescent images of stained nuclei corresponding to 9.8a and 9.8c. The white arrows are provided as a visual queue for aligning these images.

The intensity of florescence in cell nuclei had an apparent decay with respect to the distance from the surface of the microsphere. This decay in fluorescence in relationship to distance was recorded and presented in Figure 9.9. The relationship between peak fluorescence in cell nuclei and maximum electric field calculated radially from the edge of a 25 μm microsphere in tissue is shown in Figure 9.9. The near exponential decay of the fluorescence and the electric field can be related by a logistic function to the decay in maximum electric field intensity calculated numerically and starting from the edge of the microsphere. This relationship takes the form presented in equation 9.2:

$$f_N = 1 - \frac{1}{1 + \left(\frac{E^*}{E_0}\right)^p} \tag{9.2}$$

where f_N is the measured fluorescence which is a function of the membrane permeability P_m. This relates to the normalized electric field E* with the logistic function with constants E_0 taking a value of 1.03528, and p with a value of 31.87197. The R^2 statistic value for this correlation is 0.68. Logistic functions such as the one used to relate the fluorescence to the normalized electric field are commonly used in the field of electroporation to relate conductivity changes to applied electric field intensities in pulses [92-94]. Changes in conductivity and

total impedance have also been used in the field to describe cell membrane permeability and thus likelihood of intracellular drug delivery. Figure 9.9 is a graphic showing the relationship between peak fluorescence in nuclei, and electric field focusing factor in relationship to distance from edge of microspheres. The red 'x' in the graph pertain to normalized measured values at nuclei, the blue line is the maximum electric field in relation to the non dimensional electric field, and the red dashed line represents the correlated fluorescence as a function of electric field intensity.

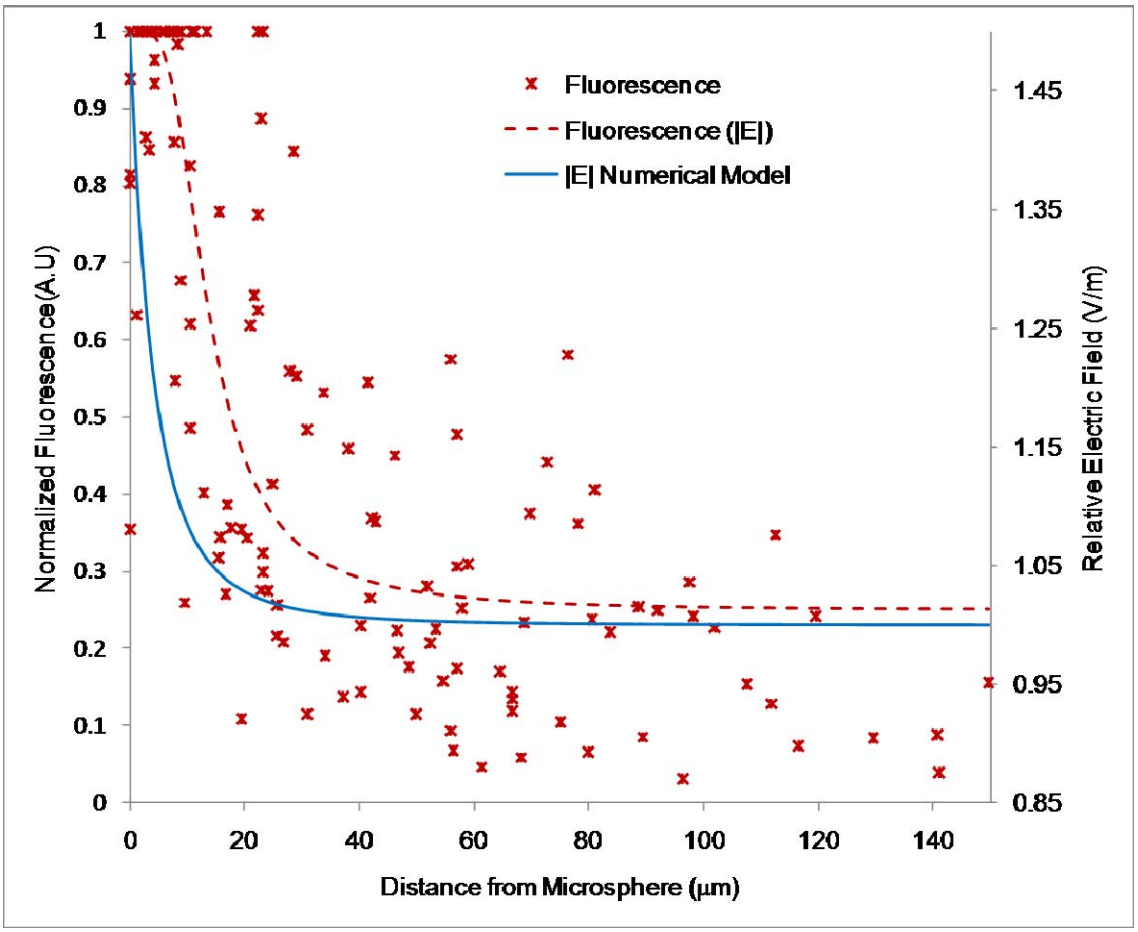

Figure 9.9. Relationship between peak fluorescence in nuclei, and electric field focusing factor in relationship to distance from edge of microspheres.

9.3.3 Electric Field Focusing *In Vivo* Application

This experimental protocol was conducted as a demonstration of electric field focusing in an electrochemotherapy application. An electroporation protocol was modified to include polystyrene microspheres. Both survival analysis and tumor volume data provided complementary information to the results presented in Section 9.3.2.

In both cases, the group utilizing the microspheres, bleomycin, and applied electroporation pulses showed significant improvement over classical experimental conditions. Survival analysis using a Logrank test [115] determined that only bleomycin plus electroporation increased survival significantly from control, also, bleomycin plus electroporation group had a

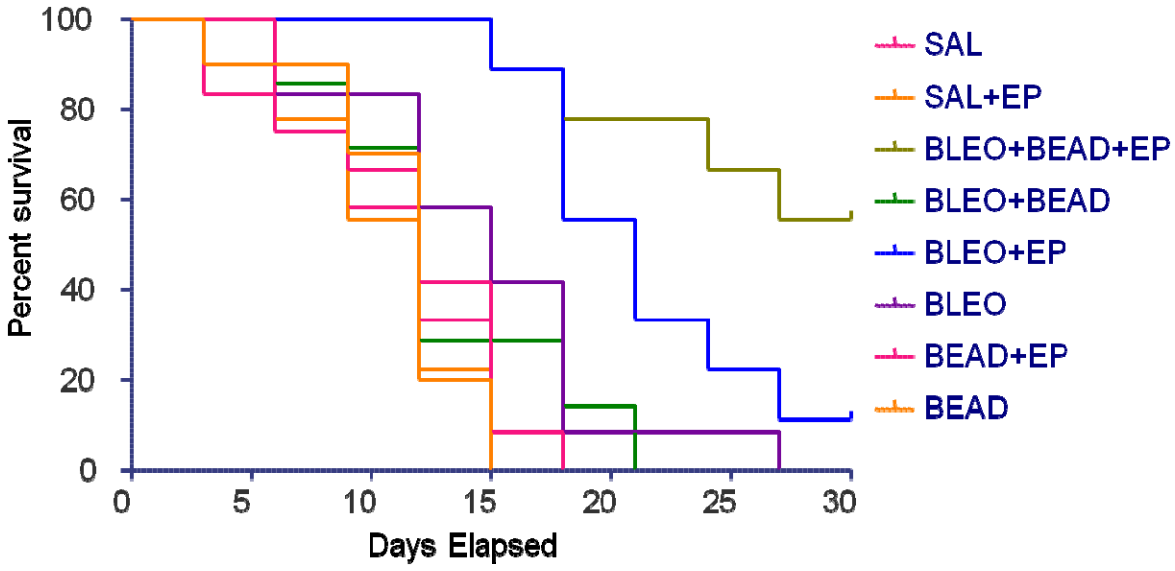

Figure 9.10. Survival per groups as a percentage of initial group size.

significantly higher survival ($p<0.05$) than control and bleomcyin, and the group that received microspheres in addition to bleomycin and electroporation had also significantly higher survival than control, bleomycin, and bleomycin plus electroporation. Survival for all experimental groups is shown in Figure 9.10.

Tumor volume presented in Figure 9.11 is the average volume per group with the condition that $n \geq 2$. The control was a simple injection of saline (solid line with circles). The bleomycin injection and electroporation (solid line with triangles) group had significantly slower tumor growth ($p<0.05$) than control. The group that included the microspheres in the chemotherapeutic solution had a significantly slower tumor growth than the control, and than that of the bleomycin plus electroporation group until day 21. The apparent decay of tumor growth in advanced dates is due to mice with larger tumors dying or being euthanatized

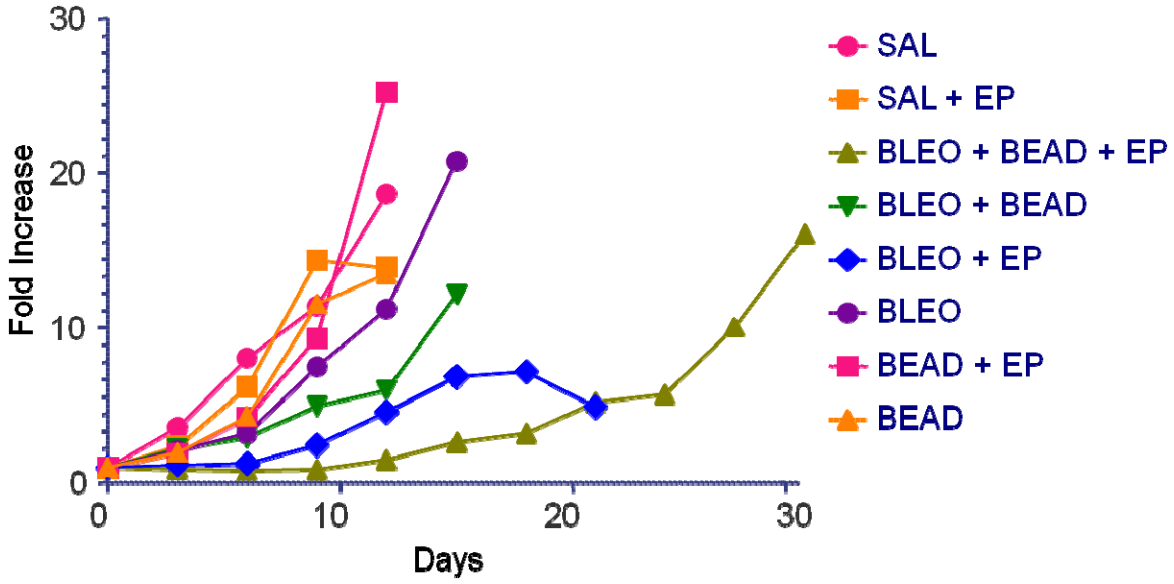

Figure 9.11. Tumor volume as a percentage of initial volume.

due to protocol maximum tumor volume. The reduction in tumor growth and the survival improvement for the group that received the chemotherapy agent containing the microspheres represents a significant improvement to all other groups. The control group that contained microspheres in addition to bleomycin did not show a significant improvement with respect to the group that received bleomycin alone. This shows that for this case, the introduction of the microspheres did not improve the delivery of chemotherapy agent in the absence of applied electric fields.

9.4. Discussion

The use of the focused electric fields for therapeutic molecule delivery applications is advantageous as a desired effect can be accomplished remotely from the electrodes. The application of the underlying phenomena to electric field mediated molecular delivery can allow the application of lower intensity electric pulses to achieve a similar result at the desired location. The protocol used not only enhanced molecular delivery, but also survival in the case melanoma tumor bearing mice.

The mechanisms for this increased uptake of drugs in the proximity of the microspheres can be correlated to the local electric field intensity generated by field focusing. However, the same local electric field intensity values can generate secondary mechanisms that produce a cumulative effect in the permeabilization of cell membranes and enhancement of delivery. Such secondary mechanisms have the potential to increase or decrease the

effectiveness of the electroporation pulse. The field intensity may be modified in at least three different ways as explained in Section 4.6. First, the change in dielectric properties of tissue during the application of the electroporation pulse as presented in Figure 4.7, modifies the distribution of electric field intensities. Second, as depicted in Figure 4.7 and summarized in Figure 9.5, the cumulative effect of other microspheres modifies that of a single microsphere. Third, the compartmentalized nature of tissues and macroscopic aspects as depicted in Figure 4.9 modify electric field intensities in addition to the focusing effect.

Other secondary phenomena result in mechanical forces and flows that can increase the electroporative effect of the local electric field. These include electroosmotic flow that creates pressure gradients as represented in Figure 4.10. A result of the electroosmotic flow is varying concentration gradients as shown for a spherical object in Figure 4.11 and a cluster of cells in Figure 4.6. Finally, the charged nature of the polystyrene microspheres subjects them to torque and forces (Figure 4.12) that translates as reaction pressures on the adjacent tissue.

The application of this technology could be extended to use of smaller particles such as nanoparticles, or can be scaled to larger objects such as implants. In the case of nanoparticles, these could be targeted to specific tissue regions by means of antibodies or other tagging mechanisms, and then used to focus the applied electric field once they have accumulated at the desired biological target. Nanoparticles of different dielectric characteristics can be combined to enhance the electrical contrast needed to focus the applied electric

field. There is the possibility that in the process of the injection of the microspheres, the accompanying pressure on surrounding cells can lead to more permeable cell membranes. Although the increase in pressure in absence of the application of electric fields is a possibility, the results of the ECT experiment indicate that improvement in delivery necessitates the presence of the electric field focusing phenomena.

Applications to implants present an opportunity to combine materials with contrasting dielectric characteristics and composite geometries. The effect on local electric field intensities by composite materials such as Janus particles could be of particular interest for electric field focusing [116, 117]. The focused electric field intensities near an implantable biosensor can be used for therapeutic molecule delivery, or used for strategies using secondary effects such as electroosmosis and electrophoresis. The application of this work is also suitable to other electric field mediated technologies such as ultra short pulse (nanosecond) electroporation, which has been developed with remote delivery in mind. The results presented in this chapter also provide an elegant solution to the execution of the reactive approach as summarized in Chapter 5, and milestone 6.4.4. If the targeted tissue site in the proximity of the implanted biosensor is to be instigated after the sensor performance decays, the approach would be to apply a nominal electric field that produces the electroporation conditions necessary to mediate the delivery of the required plasmid. Electric field focusing provides the basis to attain these intended results.

Chapter 10. Conclusions

This dissertation explored two basic approaches to blending electric field mediated drug and gene delivery with the improvement operation of implantable biosensors. An exploratory approach was adopted to ensure that the new modeling tools have a bioengineering basis to assure the merit of the researched, pursued, and presented results. The dissertation built on the basic demonstrated premise of electric field mediated drug and gene delivery, electroporation, to create mathematical constructs that model the impact that electric fields have on target tissue. These models were validated with analytical and experimental tests and the execution of the task lead to new knowledge pertaining to electromechanical forces present in tissues under the influence of an electric field, and applications of electric fields to optimize agent delivery to a target tissue as well as the modeling of DNA transport in the interstitial space.

The electromechanical forces model represents a modeling tool that successfully uses material parameters, conductivity, and permittivity, combined with electric field frequency components to accurately predict what would happen to the shape of the biological target exposed to the electric field. This new tool has immediate value in the exploration of electric field effects on complex biological systems that have inherently compartmentalized values of conductivity and permittivity. The cell cluster modeling tool used in DNA transport and the

vesicle electromechanical model representative tools that researchers may employ to analyze effects of an applied electric field on compartmentalized systems.

The electroporation applicator design model set is a flexible implementation that guides researchers to effectively develop applicator geometries with expected electric field intensity gradient predictions prior to prototype construction. A design approach that provides a rational for using electric field intensity values minimizes *in vivo* prototype applicator performance studies and optimizes the impact of the expected electroporation within the target tissue. A fundamental contribution that meets the goals of the project, effectively modifies current subcutaneous implantation procedure to accommodate the use of electric field mediated gene delivery. It provides important information regarding the expression profile of genetic material delivered by *in vivo* electroporation. This approach provides a palpable path to a preemptive approach to improving the long term function of the glucose implantable biosensor.

The development of electric field focusing meets project goals and opens a new set of possibilities regarding its development as a viable method to improve electric field mediated delivery of drug and genes. The use of this method provides an alternative to delivering necessary electric field intensity to tissues in the proximity of the subcutaneous biosensor post implantation. This approach, if used with proper neovascularization factors constitutes a responsive approach to solving the fibrous encapsulation problem. The new electric field

focusing platform was presented from a theoretical perspective, and was confirmed both *in vitro* and *in vivo*. The use of electric field focusing was extended to an electrochemotherapy application that proved in a very elegant manner the feasibility to apply the concepts of electric field focusing. The "Recommended Applications" chapter (Chapter 11) provides a brief explanation of the possible applications that project the use of electric field focusing to solve problems where electroporation may play an important role.

Chapter 11. Recommended Applications

The theoretical development and experimental verification of electric field focusing opened a myriad of potential applications of the technology, as well as new strategies for improving the state of the art. The application of the principles outlined in Chapter 9 can be directly translated into tangible applications. Applications include improvements to current technology such as needle electrodes, and modifications to implantable device protocols to include the technology. Electric field focusing creates the rationale to allow the use of electroporation in combination with biomedical applications that have never been used with this technology, but with the light on electric field focusing become relevant. Additionally, it allows the improvement of electric field distribution by modification of electroporation protocol basic parameters, such as the electric field pulse itself.

11.1. Electrode Arrays with Focusing Elements

Multielectrode electroporation applicators or electrode arrays require complex switching systems that sequentially switch electrode pairs. Electric field focusing can be used to simplify such electrode arrays by including “focusing elements” which are not electrically connected to the system. The case of such modification is shown in Figure 11.1 where the addition of focusing elements (Figure 11.1b) improves the electric field distribution in tissue with respect of an

electrode pair composed of two rows of needles (Figure 11.1a). This application of the technology could be of particular importance in the case of microscopic size systems, such microneedles fabricated with the same techniques as micro electromechanical systems (MEMS). The need to connect all needles to make them electrically active is no longer necessary. In this way, for example, needles that are used to inject therapeutic molecules could serve as “focusing elements” without the need to have an electrical potential applied to them.

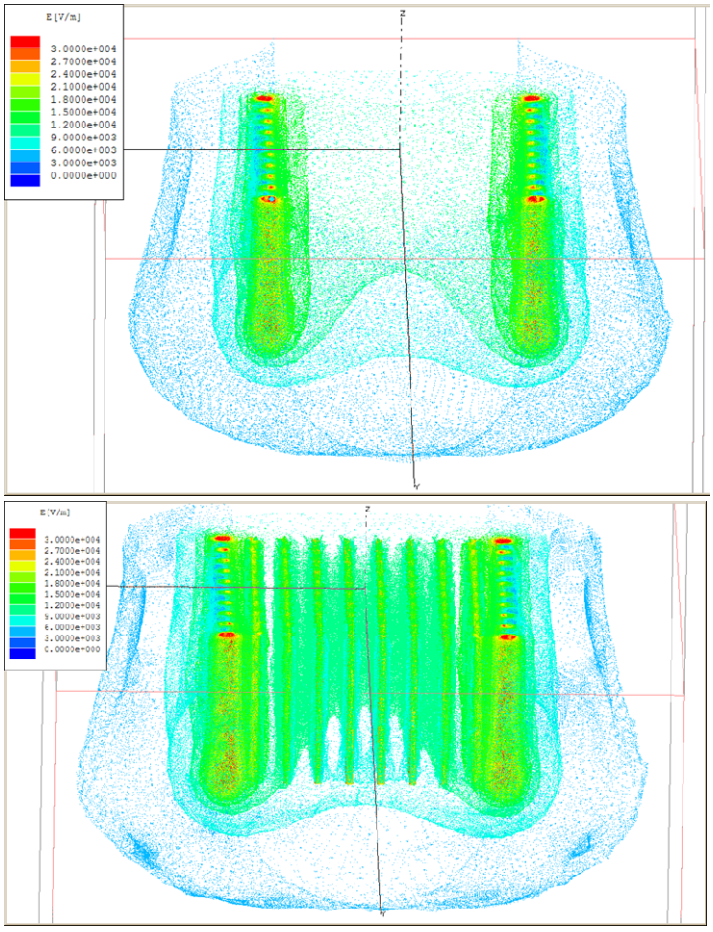

Figure 11.1. Model results. Row needle electrodes and “passive electrodes”.

11.2. Electric Field Focusing for Implants

The use electric field focusing for implantable devices, such as the implantable glucose biosensor presented in this work presents both an opportunity and a challenge. While electric field focusing at the site of a device's sensitive instrumentation is required, the excess of energy at such locations could cause damage to the device. Figure 11.2 shows a particular case in which

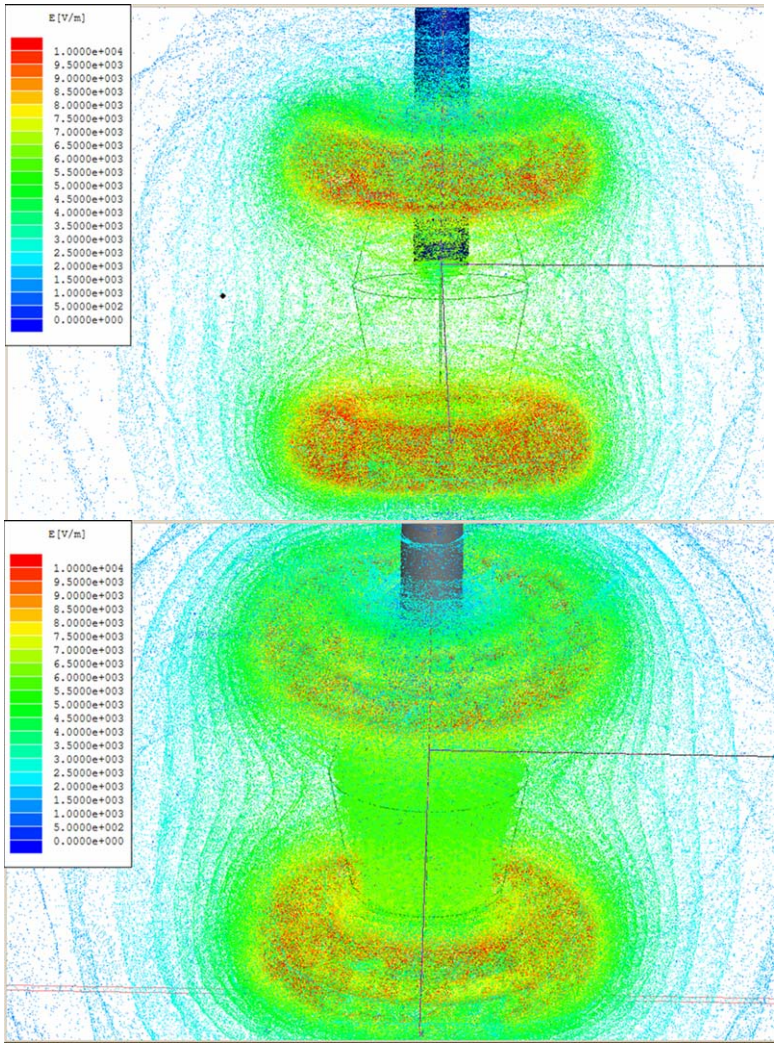

Figure 11.2. Models showing donut electrodes (top) and "focusing elements" (bottom).

two electrodes separated by roughly 500 μm requiring a very low potential applied between them, are embedded in the device. The figure at the top of Figure 11.2 shows two donut shaped electrodes along the sensing element used to apply a nominal field, the image at bottom of the figure shows that charges can be concentrated by “focusing elements” in between the two donut electrodes. These “focusing elements” can be conductive nanoparticles suspended or placed

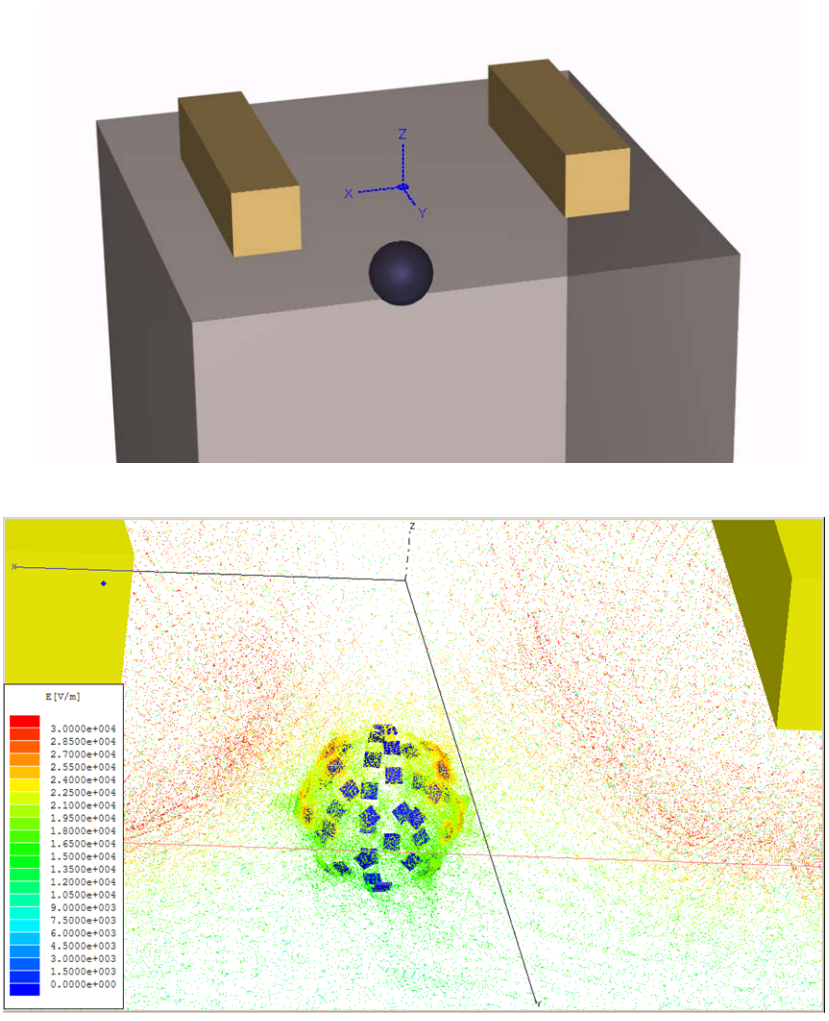

Figure 11.3. Geometry (top), and model results (bottom) of implanted focusing elements.

on a hydrogel for example. They concentrate the intensity of the field in the outer shell of the sensing element, while reducing the impact of the applied electric field in other regions.

Figure 11.3 shows another example applicable to implants, in which a sphere with “focusing elements” is used to focus the electric field applied using superficial electrodes. The top of Figure 11.3 shows the general geometry, while the bottom shows modeling results depicting larger magnitude electric fields at the focusing elements. Examples of materials that could be used are gold conducting elements on a hydrogel (same properties as tissue) or polymer (lower conductivity) sphere. The combination of materials such as those presented in Chapter 7 are not explored in this model but represent a possibility for further improving the focusing capacity of the sytem.

11.3. Electroembolization or Electrochemoembolization

Electroembolization and Electrochemoembolization represent an opportunity to modify an existing procedure to include electroporation using the focusing technology presented in Chapter 9. This new technique uses the existing microspheres that are used for embolization or chemoembolization to deliver higher electric field intensity in tissue near the site of the microspheres. In the unmodified procedure, microspheres are injected into the blood supply of a tumor and due to their size (tens of micrometers) accumulate at branching leading to smaller vesicles. The addition of electric fields is possible using the injection catheter as one electrode and another electrode externally to the

affected organ, or in the vein collecting the blood from the organ. The impact of either embolization or chemoembolization could be improved by delivering focused electric field intensities at microsphere accumulation sites.

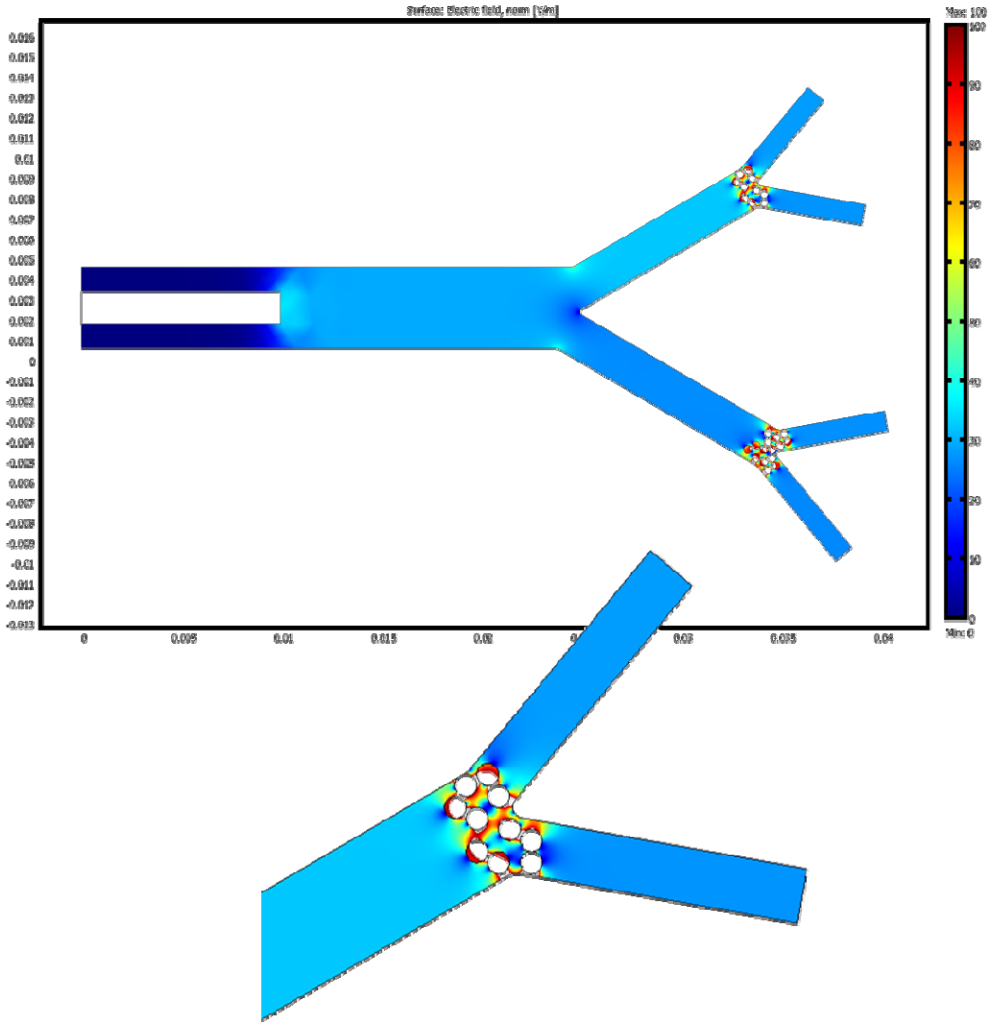

Figure 11.4. Electrochemoembolization or electroembolization procedure.

Figure 11.4 is a 2D representation of an arterial supply to a tumor. Red pseudocoloring represents higher electric field intensities and blue lower fields. The arterial supply branching from left to right in this example. The needle used to inject the microspheres is represented by a white rectangle to the left of the

main vessel. Microspheres have accumulated at the ending branches to the right. When an electric potential is applied using the needle, considerably larger electric field intensities are focused at the site of the microspheres. The image on the bottom of Figure 11.4 represents close-up of a accumulation region.

11.4. Modification of Electroporation Pulse to Improve Electric Field Distribution

Figure 9.4 shows a material that focuses electric field field intensity transversally to the applied field in the form of a donut (in red - Figure 9.4b) when the components of such applied field are of lower frequency than a threshold. The material can also focus fields longitudinally to the applied field when the frequency content is higher than a threshold frequency. In the longitudinal focusing, the focused field volume has the form of two bulbs (in red – Figure 9.4d). The focusing element (shown in gray) material could be selected in conjunction with a designed electroporation pulse that packs the necessary frequency components to maximize the distribution of the focused fields around the element.

The application of this technology provides an additional opportunity when electroporating tissues that not need to include focusing elements. In this application, cells could serve as focusing elements, so that a pulse can be designed to maximize distribution of electric fields in the volume without the need of additional electrodes. Additionally, the contrast needed to focus fields can be increased by injecting a fluid in the interstitial space that differs in electrical characteristics from the cells.

References

[1] B. Yu, Y. Moussy, and F. Moussy, "Coil-type implantable glucose biosensor with excess enzyme loading," *Front Biosci,* vol. 10, pp. 512-520, 2005.

[2] Y. M. Bazhang Yu, Francis Moussy, "Lifetime Improvement of Glucose Biosensor by Epoxy-Enhanced PVC Membrane," *Electroanalysis,* vol. 17, pp. 1771-1779, 2005.

[3] B. Yu, N. Long, Y. Moussy, and F. Moussy, "A long-term flexible minimally-invasive implantable glucose biosensor based on an epoxy-enhanced polyurethane membrane," *Biosensors and Bioelectronics,* vol. 21, pp. 2275-2282, 2006.

[4] M. Gerritsen, J. A. Jansen, A. Kros, R. J. M. Nolte, and J. A. Lutterman, "Performance of Subcutaneously Implanted Glucose Sensors: A Review," *Journal of Investigative Surgery,* vol. 11, pp. 163-174, 1998.

[5] H. E. Koschwanez and W. M. Reichert, "In vitro, in vivo and post explantation testing of glucose-detecting biosensors: Current methods and recommendations," *Biomaterials,* vol. 28, pp. 3687-3703, 2007.

[6] Y. M. Ju, B. Yu, T. J. Koob, Y. Moussy, and F. Moussy, "A novel porous collagen scaffold around an implantable biosensor for improving biocompatibility. I. In vitro/in vivo stability of the scaffold and in vitro sensitivity of the glucose sensor with scaffold," *J Biomed Mater Res A,* 2007.

[7] B. Yu, L. West, Y. Moussy, and F. Moussy, "Transcutaneous Implantation Methods for Improving the Long-Term Performance of Glucose Sensors in Rats," *Sensors Journal, IEEE,* vol. 8, pp. 97-103, 2008.

[8] D. L. Wise, *Biomaterials and Bioengineering Handbook*: Marcel Dekker, 2000.

[9] J. M. Anderson, "Biological Responses to Materials," *Annual Review of Materials Research,* vol. 31, pp. 81-110, 2001.

[10] N. Wisniewski, F. Moussy, and W. M. Reichert, "Characterization of implantable biosensor membrane biofouling," *Fresenius'Journal of Analytical Chemistry,* vol. 366, pp. 611-621, 2000.

[11] F. Moussy, "Implantable glucose sensor: progress and problems," in *Sensors*, pp. 270-273 vol.1, 2002.

[12] M. Gerritsen, A. Kros, J. A. Lutterman, R. J. M. Nolte, and J. A. Jansen, "A percutaneous device as model to study the in vivo performance of implantable amperometric glucose sensors," *Journal of Materials Science: Materials in Medicine,* vol. 12, pp. 129-134, 2001.

[13] P. Dungel, N. Long, B. Yu, Y. Moussy, and F. Moussy, "Study of the effects of tissue reactions on the function of implanted glucose sensors," *Journal of Biomedical Materials Research Part A,* vol. 85A, pp. 699-706, 2008.

[14] B. Yu, Y. Moussy, and F. Moussy, "An investigation of Long-Term Performance of Transcutaneous Glucose Biosensor," in *University of South Florida*, 2006.

[15] A. Ivorra and B. Rubinsky, "Historical Review of Irreversible Electroporation in Medicine," in *Irreversible Electroporation*, B. Rubinsky, Ed., ed: Springer Berlin Heidelberg, pp. 1-21, 2010.

[16] A. J. H. Sale and W. A. Hamilton, "Effects of high electric fields on microorganisms: I. Killing of bacteria and yeasts," *Biochimica et Biophysica Acta (BBA) - General Subjects,* vol. 148, pp. 781-788, 1967.

[17] W. A. Hamilton and A. J. H. Sale, "Effects of high electric fields on microorganisms: II. Mechanism of action of the lethal effect," *Biochimica et Biophysica Acta (BBA) - General Subjects,* vol. 148, pp. 789-800, 1967.

[18] A. J. H. Sale and W. A. Hamilton, "Effects of high electric fields on micro-organisms: III. Lysis of erythrocytes and protoplasts," *Biochimica et Biophysica Acta - Biomembranes,* vol. 163, pp. 37-43, 1968.

[19] E. Neumann and K. Rosenheck, "Permeability changes induced by electric impulses in vesicular membranes," *Journal of Membrane Biology,* vol. 10, pp. 279-290, 1972.

[20] A. Hodgkin and A. Huxley, "A quantitative description of membrane current and its application to conduction and excitation in nerve," *The Journal of physiology,* vol. 117, p. 500, 1952.

[21] T. Heimburg, "Lipid ion channels," *Biophysical Chemistry,* vol. 150, pp. 2-22, 2010.

[22] M. Fromm, L. P. Taylor, and V. Walbot, "Expression of genes transferred into monocot and dicot plant cells by electroporation," *Proc. Natl. Acad. Sci. USA,* vol. 82, pp. 5824-5828, 1985.

[23] M. Hiromichi, I. Asako, M. Chiaki, I. Masato, and Y. Yasuyuki, "Gene transfer into intact plant cells by electroinjection through cell walls and membranes," *Gene,* vol. 41, pp. 121-124, 1986.

[24] R. A. Dekeyser, B. Claes, R. M. U. D. Rycke, M. E. Habets, M. C. V. Montagu, and A. B. Caplan, "Transient Gene Expression in Intact and Organized Rice Tissues," *The Plant Cell,* vol. 2, pp. 591-602, 1990.

[25] B. F. Matthews, A. A. Abdul-Baki, and J. A. Saunders, "Expression of a foreign gene in electroporated pollen grains of tobacco," *Sexual Plant Reproduction,* vol. 3, pp. 147-151, 1990.

[26] S. L. Van Wert and J. A. Saunders, "Electrofusion and electroporation of plants," *Plant physiology,* vol. 99, p. 365, 1992.

[27] J. A. Saunders, B. F. Matthews, and S. L. Van Wert, "Pollen electrotransformation for gene transfer in plants," D. C. Chang, B. M. Chassy, J. A. Saunders, and A. E. Sowers, Eds., ed: Academic Press, pp. 227-247, 1992.

[28] T. K. Wong and E. Neumann, "Electric field mediated gene transfer," *Biochemical and Biophysical Research Communications,* vol. 107, p. 584, 1982.

[29] E. Neumann, M. Schaefer-Ridder, Y. Wang, and P. Hofschneider, "Gene transfer into mouse lyoma cells by electroporation in high electric fields," *The EMBO journal,* vol. 1, p. 841, 1982.

[30] H. Potter, L. Weir, and P. Leder, "Enhancer-dependent expression of human kappa immunoglobulin genes introduced into mouse pre-B lymphocytes by electroporation," *Proceedings of the National Academy of Sciences of the United States of America,* vol. 81, pp. 7161-7165, 1984.

[31] J. M. Crowley, "Electrical breakdown of bimolecular lipid membranes as an electromechanical instability," *Biophys Journal,* vol. 13, pp. 711-24, 1973.

[32] U. Zimmermann, P. Scheurich, G. Pilwat, and R. Benz, "Cells with Manipulated Functions: New Perspectives for Cell Biology, Medicine, and Technology," *Angewandte Chemie International Edition in English,* vol. 20, pp. 325-344, 1981.

[33] J. Teissie and T. Y. Tsong, "Electric field induced transient pores in phospholipid bilayer vesicles," *Biochemistry,* vol. 20, pp. 1548-1554, 1981.

[34] L. Mir, S. Orlowski, J. Belehradek Jr, and C. Paoletti, "Electrochemotherapy potentiation of antitumour effect of bleomycin by local electric pulses," *European journal of cancer (Oxford, England: 1990),* vol. 27, p. 68, 1991.

[35] R. Heller, R. Gilbert, and M. J. Jaroszeski, "Clinical trials for solid tumors using electrochemotherapy," *Electrochemotherapy, electrogenetherapy and transdermal drug delivery.,* pp. 137-156, 2000.

[36] L. Mir, M. Belehradek, C. Domenge, S. Orlowski, B. Poddevin, J. Belehradek Jr, G. Schwaab, B. Luboinski, and C. Paoletti, "Electrochemotherapy, a new antitumor treatment: first clinical trial," *Comptes rendus de l'Académie des sciences. Série III, Sciences de la vie,* vol. 313, p. 613, 1991.

[37] L. F. Glass, M. Jaroszeski, R. Gilbert, D. S. Reintgen, and R. Heller, "Intralesional bleomycin-mediated electrochemotherapy in 20 patients with basal cell carcinoma," *Journal of the American Academy of Dermatology,* vol. 37, pp. 596-599, 1997.

[38] G. Sersa, B. Stabuc, M. Cemazar, B. Jancar, D. Miklavcic, and Z. Rudolf, "Electrochemotherapy with cisplatin: potentiation of local cisplatin antitumour effectiveness by application of electric pulses in cancer patients," *European Journal of Cancer,* vol. 34, pp. 1213-1218, 1998.

[39] R. Heller, M. J. Jaroszeski, D. S. Reintgen, C. A. Puleo, R. C. DeConti, R. A. Gilbert, and L. F. Glass, "Treatment of cutaneous and subcutaneous tumors with electrochemotherapy using intralesional bleomycin," *Cancer,* vol. 83, pp. 148-157, 1998.

[40] R. Heller, M. Jaroszeski, A. Atkin, D. Moradpour, R. Gilbert, J. Wands, and C. Nicolau, "In vivo gene electroinjection and expression in rat liver," *FEBS Letters,* vol. 389, pp. 225-228, 1996.

[41] Y.-i. Yamashita, M. Shimada, H. Hasegawa, R. Minagawa, T. Rikimaru, T. Hamatsu, S. Tanaka, K. Shirabe, J.-i. Miyazaki, and K. Sugimachi, "Electroporation-mediated Interleukin-12 Gene Therapy for Hepatocellular Carcinoma in the Mice Model," *Cancer Research,* vol. 61, pp. 1005-1012, 2001.

[42] G. Sersa, M. Cemazar, and D. Miklavcic, "Antitumor effectiveness of electrochemotherapy with cis-diamminedichloroplatinum (II) in mice," *Cancer research,* vol. 55, p. 3450, 1995.

[43] R. Heller, M. J. Jaroszeski, R. Perrott, J. Messina, and R. Gilbert, "Effective treatment of B16 melanoma by direct delivery of bleomycin using electrochemotherapy," *Melanoma Research,* vol. 7, pp. 10-18, 1997.

[44] M. Lucas, L. Heller, D. Coppola, and R. Heller, "IL-12 plasmid delivery by in vivo electroporation for the successful treatment of established subcutaneous B16. F10 melanoma," *Molecular Therapy,* vol. 5, pp. 668-675, 2002.

[45] A. I. Daud, R. C. DeConti, S. Andrews, P. Urbas, A. I. Riker, V. K. Sondak, P. N. Munster, D. M. Sullivan, K. E. Ugen, J. L. Messina, and R. Heller, "Phase I Trial of Interleukin-12 Plasmid Electroporation in Patients With Metastatic Melanoma," *Journal of Clinical Oncology,* vol. 26, pp. 5896-5903, 2008.

[46] U. Klueh, D. I. Dorsky, and D. L. Kreutzer, "Enhancement of implantable glucose sensor function in vivo using gene transfer-induced neovascularization," in *Biomaterials* vol. 26, ed: Elsevier Science, 2005, pp. 1155-1163.

[47] W. K. Ward, M. J. Quinn, M. D. Wood, K. L. Tiekotter, S. Pidikiti, and J. A. Gallagher, "Vascularizing the tissue surrounding a model biosensor: how localized is the effect of a subcutaneous infusion of vascular endothelial growth factor (VEGF)?," *Biosensors & bioelectronics,* vol. 19, pp. 155-63, 2003.

[48] S. Tuyaerts, A. Michiels, J. Corthals, A. Bonehill, C. Heirman, C. D. Greef, S. M. Noppe, and K. Thielemans, "Induction of Influenza Matrix Protein 1 and MelanA-specific T lymphocytes in vitro using mRNA-electroporated dendritic cells," *Cancer Gene Ther,* vol. 10, pp. 696-706, 2003.

[49] A. T. Prechtel, N. M. Turza, A. A. Theodoridis, M. Kummer, and A. Steinkasserer, "Small interfering RNA (siRNA) delivery into monocyte-derived dendritic cells by electroporation," *Journal of Immunological Methods,* vol. 311, pp. 139-152, 2006.

[50] K. N. Kishimoto, Y. Watanabe, H. Nakamura, and S. Kokubun, "Ectopic bone formation by electroporatic transfer of bone morphogenetic protein-4 gene," *Bone,* vol. 31, pp. 340-347, 2002.

[51] B. Ferraro, Y. L. Cruz, D. Coppola, and R. Heller, "Intradermal Delivery of Plasmid VEGF165 by Electroporation Promotes Wound Healing," *Molecular Therapy,* vol. 17, pp. 651-657, 2009.

[52] A. Honigman, E. Zeira, P. Ohana, R. Abramovitz, E. Tavor, I. Bar, Y. Zilberman, R. Rabinovsky, D. Gazit, and A. Joseph, "Imaging transgene expression in live animals," *Mol. Ther,* vol. 4, pp. 239?249-239?249, 2001.

[53] J. I. Rey, M. J. Jaroszeski, and R. A. Gilbert, "Feasibility study for focusing electric fields to mediate in vitro drug and gene delivery," in *IEEE Engineering and Medicine in Biology Conference Proceedings*, p. 5617, 2006.

[54] B. L. Roth, M. Poot, S. T. Yue, and P. J. Millard, "Bacterial viability and antibiotic susceptibility testing with SYTOX green nucleic acid stain," *Appl. Environ. Microbiol.,* vol. 63, pp. 2421-2431, 1997.

[55] G. Pron, N. Mahrour, S. Orlowski, O. Tounekti, B. Poddevin, J. Belehradek, and L. M. Mir, "Internalisation of the bleomycin molecules responsible for bleomycin toxicity: a receptor-mediated endocytosis mechanism," *Biochemical Pharmacology,* vol. 57, pp. 45-56, 1999.

[56] R. Gilbert, M. Jaroszeski, and R. Heller, "Novel electrode designs for electrochemotherapy," *BBA-General Subjects,* vol. 1334, pp. 9-14, 1997.

[57] M. Okino and H. Mohri, "Effects of a high-voltage electrical impulse and an anticancer drug on in vivo growing tumors," *Japanese journal of cancer research: Gann,* vol. 78, p. 1319, 1987.

[58] L. Heller, M. Jaroszeski, D. Coppola, A. McCray, J. Hickey, and R. Heller, "Optimization of cutaneous electrically mediated plasmid DNA delivery using novel electrode," *Gene therapy,* vol. 14, pp. 275-280, 2006.

[59] R. Heller, Y. Cruz, L. C. Heller, R. A. Gilbert, and M. J. Jaroszeski, "Electrically Mediated Delivery of Plasmid DNA to the Skin, Using a Multielectrode Array," *Human Gene Therapy,* vol. 21, pp. 357-362, 2009.

[60] G. A. Hofmann, "Instrumentation and electrodes for in vivo electroporation," in *Electrochemotherapy, Electrogenetherapy, and Transdermal Drug Delivery: Electrically Mediated Delivery of Molecules to Cells*. vol. 37, M. J. Jaroszeski, R. Heller, and R. A. Gilbert, Eds., ed New Jersey: Humana Press, pp. 37-61, 1999.

[61] Comsol AB, "Comsol Multiphysics AC/DC Module," 3.4 ed, 2008.

[62] D. Miklavcic and T. Kotnik, "Electroporation for electrochemotherapy and gene therapy," in *Bioelectromagnetic medicine*, P. J. Rosch and M. S. Markov, Eds., ed New York: Marcel Dekker Inc, pp. 637-656, 2004.

[63] S. J. Beebe, P. M. Fox, L. J. Rec, K. Somers, R. H. Stark, and K. H. Schoenbach, "Nanosecond pulsed electric field (nsPEF) effects on cells and tissues: apoptosis induction and tumor growth inhibition," *IEEE Transactions on plasma science,* vol. 30, pp. 286-292, 2002.

[64] J. F. Kolb, S. Xiao, J. T. Camp, M. Migliaccio, C. Bajracharya, and K. H. Schoenbach, "Sub-nanosecond electrical pulses for medical therapies and imaging," pp. 1-5, 2010.

[65] J. T. Broch, *Principles of experimental frequency analysis*. New York, NY: Elsevier applied science, 1990.

[66] F. T. Ulaby, *Fundamentals of Applied Electromagnetics*, Media Edition ed. Upper Saddle River, NJ: Prentice Hall, 2001.

[67] S. Grimnes and O. G. Martinsen, *Bioimpedance and Bioelectricity Basics*. San Diego, CA: Academic Press, 2000.

[68] P. Riu, J. Rosell, A. Lozano, and R. Pallà-Areny, "Multi-frequency static imaging in electrical impedance tomography: Part 1 instrumentation requirements," *Medical and Biological Engineering and Computing,* vol. 33, pp. 784-792, 1995.

[69] M. Cheney, D. Isaacson, and J. C. Newell, "Electrical impedance tomography," *SIAM review,* vol. 41, pp. 85-101, 1999.

[70] H. Griffiths and Z. Zhang, "A dual-frequency electrical impedance tomography system," *Physics in Medicine and Biology,* vol. 34, p. 1465, 1989.

[71] S. R. Alexander and et al., "Current source design for electrical impedance tomography," *Physiological measurement,* vol. 24, p. 509, 2003.

[72] R. V. Davalos, B. Rubinsky, and D. M. Otten, "A feasibility study for electrical impedance tomography as a means to monitor tissue electroporation for molecular medicine," *Biomedical Engineering, IEEE Transactions on,* vol. 49, pp. 400-403, 2002.

[73] R. V. Davalos, D. M. Otten, L. M. Mir, and B. Rubinsky, "Electrical impedance tomography for imaging tissue electroporation," *Biomedical Engineering, IEEE Transactions on,* vol. 51, pp. 761-767, 2004.

[74] C. Furse, D. A. Christensen, and C. H. Durney, *Basic Introduction to Bioelectromagnetics*: CRC Press, 2009.

[75] R. P. Feynman, R. B. Leighton, and M. Sands, *The Feynman lectures on Physics* vol. 2. Reading, MA: Addison-Wesley Publishing Company, 1964.

[76] G. K. Batchelor, *An introduction to fluid dynamics*. New York, NY: Cambridge University Press, 2000.

[77] the_tahoe_guy. (2009, *Rock Flow*. Available: http://www.flickr.com/photos/the_tahoe_guy/4183278431/

[78] R. P. Feynman, R. B. Leighton, and M. Sands, *The Feynman lectures on Physics* vol. 1. Reading, MA: Addison-Wesley Publishing Company, 1964.

[79] L. M. Mir and S. Orlowski, "Mechanisms of electrochemotherapy," *Advanced Drug Delivery Reviews,* vol. 35, pp. 107-118, 1999.

[80] J. Bernhardt and H. Pauly, "On the generation of potential differences across the membranes of ellipsoidal cells in an alternating electrical field," *Radiation and Environmental Biophysics,* vol. 10, pp. 89-98, 1973.

[81] E. Neumann, S. Kakorin, and K. Toensing, "Fundamentals of electroporative delivery of drugs and genes," *Bioelectrochemistry and Bioenergetics,* vol. 48, pp. 3-16, 1999.

[82] E. Neumann, S. Kakorin, and K. Toensing, "Principles of Membrane Electroporation and Transport of Macromolecules," in *Electrochemotherapy, Electrogenetherapy, and Transdermal Drug Delivery*. vol. 37, M. J. Jaroszeski, R. Heller, and R. Gilbert, Eds., ed: Humana Press, pp. 1-35, 2000.

[83] J. Teissié and C. Ramos, "Correlation between Electric Field Pulse Induced Long-Lived Permeabilization and Fusogenicity in Cell Membranes," *Biophysical journal,* vol. 74, pp. 1889-1898, 1998.

[84] J. Teissié and M. P. Rols, "An experimental evaluation of the critical potential difference inducing cell membrane electropermeabilization," *Biophysical journal,* vol. 65, pp. 409-413, 1993.

[85] J. D. Hickey, "Simulating the Electric Field Mediated Motion of Ions and Molecules in Diverse Matrices," Ph.D. Chemical Engineering, Chemical Engineering, University of South Florida, Tampa, FL, 2005.

[86] J. Teissie, M. Golzio, and M. P. Rols, "Mechanisms of cell membrane electropermeabilization: A minireview of our present (lack of ?) knowledge," *Biochimica et Biophysica Acta (BBA) - General Subjects,* vol. 1724, pp. 270-280, 2005.

[87] I. Üzün, E. Akyildiz, and M. A. Inanicl, "Histopathological differentiation of skin lesions caused by electrocution, flame burns and abrasion," *Forensic Science International,* vol. 178, pp. 157-161, 2008.

[88] P. Phillip and J. R. Bradley, "Electrostriction of anisotropic tissue," *Physical Review E (Statistical, Nonlinear, and Soft Matter Physics),* vol. 75, p. 021903, 2007.

[89] M. Golzio, J. Teissié, and M.-P. Rols, "Direct visualization at the single-cell level of electrically mediated gene delivery," *Proceedings of the National Academy of Sciences of the United States of America,* vol. 99, pp. 1292-1297, 2002.

[90] E. Phez, C. Faurie, M. Golzio, J. Teissié, and M. Rols, "New insights in the visualization of membrane permeabilization and DNA/membrane interaction of cells submitted to electric pulses," *Biochimica et Biophysica Acta (BBA)-General Subjects,* vol. 1724, pp. 248-254, 2005.

[91] J. I. Rey, J. A. Llewellyn, A. M. Hoff, R. J. Connolly, J. P. Jimenez, and R. A. Gilbert, "Multiphysics Modeling of Cellular Arrays Using Periodic Minimal Surfaces - A Drug and Gene Delivery Applictaion," in *COMSOL Conference 2010*, Boston, MA, 2010.

[92] D. Sel, D. Cukjati, D. Batiuskaite, T. Slivnik, L. M. Mir, and D. Miklavcic, "Sequential finite element model of tissue electropermeabilization," *Biomedical Engineering, IEEE Transactions on,* vol. 52, pp. 816-827, 2005.

[93] N. Pavselj, Z. Bregar, D. Cukjati, D. Batiuskaite, L. M. Mir, and D. Miklavcic, "The course of tissue permeabilization studied on a mathematical model of a subcutaneous tumor in small animals," *Biomedical Engineering, IEEE Transactions on,* vol. 52, pp. 1373-1381, 2005.

[94] A. Ivorra, B. Al-Sakere, and L. M. Mir, "Use of conductive gels for electric field homogenization increases the antitumor efficacy of electroporation therapies," *Physics in Medicine and Biology,* vol. 53, pp. 6605-6618, 2008.

[95] R. J. Hill, "Electric-field-induced force on a charged spherical colloid embedded in an electrolyte-saturated Brinkman medium," *Physics of Fluids,* vol. 18, pp. 043103-7, 2006.

[96] M. A. Matos, L. R. White, and R. D. Tilton, "Enhanced mixing in polyacrylamide gels containing embedded silica nanoparticles as internal electroosmotic pumps," *Colloids and Surfaces B: Biointerfaces,* vol. 61, pp. 262-269, 2008.

[97] T. B. Jones, *Electromechanics of particles*. Cambridge, UK: Cambridge University Prerss, 1995.

[98] T. J. Lewis, "The piezoelectric effect," in *Electrical Insulation and Dielectric Phenomena, 2005. CEIDP '05. 2005 Annual Report Conference on*, pp. 717-720, 2005.

[99] R. Dimova, K. A. Riske, S. Aranda, N. Bezlyepkina, R. L. Knorr, and R. Lipowsky, "Giant vesicles in electric fields," *SoftMatter,* vol. 3, pp. 817-827, 2007.

[100] K. A. Riske and R. Dimova, "Electro-Deformation and Poration of Giant Vesicles Viewed with High Temporal Resolution," *Biophysical Journal,* vol. 88, pp. 1143-1155, 2005.

[101] S. Aranda, K. A. Riske, R. Lipowsky, and R. Dimova, "Morphological Transitions of Vesicles Induced by Alternating Electric Fields," *Biophysical Journal,* vol. 95, pp. L19-L21, 2008.

[102] J. I. Rey, R. J. Connolly, M. J. Jaroszeski, A. M. Hoff, J. A. Llewellyn, and R. A. Gilbert, "Electrostrictive forces on vesicles with compartmentalized permittivity and conductivity conditions," *Dielectrics and Electrical Insulation, IEEE Transactions on,* vol. 16, pp. 1280-1287, 2009.

[103] T. Yamamoto, S. Aranda-Espinoza, R. Dimova, and R. Lipowsky, "Stability of Spherical Vesicles in Electric Fields," *Langmuir,* vol. 26, pp. 12390-12407, 2010.

[104] Comsol AB, *COMSOL Multiphysics Reference Guide*, 2008.

[105] K. B. Colman, W. M. Robert, A. Nabeel, H. N. Petra, W. Antoinette, G. C. Marco, D. D. Mark, and W. H. John, "Electroporation enhances transfection efficiency in murine cutaneous wounds," *Wound Repair and Regeneration,* vol. 12, pp. 397-403, 2004.

[106] M. P. Lin, G. P. Marti, R. Dieb, J. Wang, M. Ferguson, R. Qaiser, P. Bonde, M. D. Duncan, and J. W. Harmon, "Delivery of plasmid DNA expression vector for keratinocyte growth factor-1 using electroporation to improve cutaneous wound healing in a septic rat model," *Wound Repair and Regeneration,* vol. 14, pp. 618-624, 2006.

[107] J. I. Rey, M. J. Jaroszeski, and R. A. Gilbert, "Feasibility study for focusing electric fields to mediate in vitro drug and gene delivery," p. 5617, 2006.

[108] S. Golan, D. Elata, M. Orenstein, and U. Dinnar, "Floating electrode dielectrophoresis," *Electrophoresis,* vol. 27, pp. 4919-4926, 2006.

[109] S. Golan, D. Elata, and U. Dinnar, "Hybrid dielectrophoresis devices that employ electrically floating electrodes," *Sensors and Actuators A: Physical,* vol. 142, pp. 138-146, 2008.

[110] C. Gabriel, S. Gabriel, and E. Corthout, "The dielectric properties of biological tissues: I. Literature survey," *Physics in Medicine and Biology,* vol. 41, p. 2231, 1996.

[111] K. S. Cole, *Membranes, ions, and impulses: a chapter of classical biophysics*. Berkeley, CA: Univ of California Press, 1968.

[112] Automation Creations Inc. MatWeb: The online Materials Information Reference [Online]. Available: http://www.matweb.com

[113] D.-S. Yoo, "The dielectric properties of cancerous tissues in a nude mouse xenograft model," *Bioelectromagnetics,* vol. 25, pp. 492-497, 2004.

[114] P. J. Rankin and D. J. Klingenberg, "The electrorheology of barium titanate suspensions," *Journal of Rheology,* vol. 42, pp. 639-656, 1998.

[115] G. Cardillo. (2010, July 10, 2010). Logrank - Comparing survival curves of two groups using the log rank test. *MATLAB Central File Exchange*. Available: http://www.mathworks.com/matlabcentral/fileexchange/22317-logrank

[116] T. M. Squires and M. Z. Bazant, "Breaking symmetries in induced-charge electro-osmosis and electrophoresis," *Journal of Fluid Mechanics,* vol. 560, pp. 65-101, 2006.

[117] Y. Daghighi and D. Li, "Induced-charge electrokinetic phenomena," *Microfluidics and Nanofluidics,* vol. 9, pp. 593-611, 2010.

About the Author

Jose Ignacio Rey holds a Bachelor of Science degree in Civil Engineering from Universidad Metropolitana (Caracas-Venezuela), a Master of Business Administration from Texas A&M University (Austin-Texas), and a Master of Science degree in Bioengineering from University of South Florida (Tampa-Florida). He has worked in different professional areas, as a Technology Leader in Inelectra S.A. (Caracas Venezuela), as a Project Management Consultant in EPM, LLC (Texas), as an intern in the Kauffman Entrepreneur Internship Program (Florida), and as an intern at the Division of Patents and Licensing, at USF (Florida). Jose is the recipient of numerous awards, such as the Bids & Proposals reengineering project in 1999, the Compareitall Owner-Entrepreneur in 2000, the Mays MBA Program in 2000, the Dolores Auzenne Fellowship in 2003, the National Science Foundation IGERT Graduate Fellowship in 2004, the Alfred P. Sloan Minority Ph.D. Fellowship in 2005, the NIH Minority Research Supplement in 2005, the SKIN-IGERT Fellow of the Year (USF) in 2006, and the Successful Latino Award (USF) in 2008. Jose's Doctoral research work focused on the Guiding of Electric Fields for Electroporation Applications. He conducted his Doctoral work at the USF Center for Molecular Delivery under the supervision of Dr. Richard Gilbert. He successfully defended his doctoral dissertation in March 25th of 2011 at the University of South Florida.